FINAL REPORT
for Period
28 September 1966 to 13 November 1967

INVESTIGATIONS OF ELECTRON EMISSION CHARACTERISTICS OF LOW WORK FUNCTION SURFACES

By

L. W. Swanson
A. E. Bell
L. C. Crouser
B. E. Evans
R. W. Strayer

Prepared for

Headquarters
National Aeronautics and Space Administration
Washington, D. C.

November 1967

CONTRACT NASw-1516

FIELD EMISSION CORPORATION
Melrose Avenue at Linke Street
McMinnville, Oregon 97128

TABLE OF CONTENTS

MEETINGS, PUBLICATIONS AND PRESENTED PAPERS

The following list gives meetings attended, personnel who attended and titles of papers given during contract period:

Meeting	Paper	Given By
Twenty-Seventh Annual Conference on Physical Electronics, March 20-22, 1967, M. I. T.	1) Single-Plane Studies of Oxygen Adsorbed on Tungsten by Probe Field Emission Techniques. 2) Adsorption of Cesium Fluoride on Tungsten.	A. E. Bell
14th Annual Field Emission Symposium, June 26-30, 1967, National Bureau of Standards	Total Energy Distribution of Field Emitted Electrons and Single Crystal Face Work Functions of Mo.	L. W. Swanson

PUBLICATIONS

1. Total Energy Distribution and Single Plane Work Functions of Field Emitted Electrons from Tungsten, Physical Review (in press).
2. Adsorption of Cesium Fluoride on Tungsten, Surface Science (in press).
3. Anomalous Total Energy Distribution for a Molybdenum Field Emitter, Physical Review Letters (in press).

PREFACE

This report describes work performed under support from NASA Headquarters, Washington, D. C., for the period September 27, 1966 to November 13, 1967. The primary purpose of this work has been to gain an improved fundamental understanding of

(1) the phenomena governing the production of low work function surfaces, and

(2) the factors affecting the quality and stability of electron emission characteristics.

It is anticipated that information generated from this investigation will be relevant to various kinds of electron emission (i. e., photo, thermionic and field emission), although the primary emphasis was placed upon field emission.

The formation of low work function surfaces was accomplished by:

(1) adsorption of appropriate electropositive adsorbates, and

(2) coadsorption of appropriate electropositive and electronegative adsorbates.

Various properties of these surfaces investigated in order to obtain a more fundamental understanding of them were the temperature dependency of the emission and work function, the various types of energy exchanges accompanying emission, the energy distribution of the field emitted electron, and various aspects of the surface kinetics of adsorbed layers such as binding energy, surface mobility and effect of external fields.

LIST OF ILLUSTRATIONS

SECTION I

Figure	
1	Sequence of patterns showing migration of a single CsF dose across a W surface. Patterns (c) and (d) are typical Cs on W patterns.
2	Curves show variation of ϕ and log A with CsF dose number. At (a) -200V was applied to the screen during the $1100^{\circ}K$ equilibration.
3	Field emission patterns corresponding to various amounts of F_2 on W.
4	Lower set of curves shows variation of work function with Cs coverage for clean and fluorine coated tungsten. Middle set of curves shows the variation of log A and upper set shows the variation of the equilibration temperature T_e with Cs coverage.
5	Field emission patterns corresponding to increasing amounts of Cs on a F/W surface where $\phi_{FW} = 4.97$ eV.
6	Curves show the variation of ϕ and log A upon heating a fully cesium coated F/W surface at the indicated temperatures for 60 sec intervals. During heating the screen was biased to -185 V (F = 2.0 MV/cm).
7	The upper set of curves shows a plot of ϕ versus log A for a Cs adsorption-desorption sequence, where $\phi_{FW} = 5.14$ eV and a negative voltage of 200 V was applied to the screen during tip heating. The lower set of curves is a similar plot where $\phi_{FW} = 5.07$ eV and a positive voltage of 100 volts was applied to the screen during tip heating. A 200 V positive bias voltage was applied to the screen for the clean W desorption sequence of Cs.
8	Curves show the variation of the relative field emission current with time at various applied field strengths for a Cs/F/W surface of initial work function $\phi = 1.30$ eV and $T \approx 77^{\circ}K$.

LIST OF ILLUSTRATIONS (cont.)

N68-16761

I. ADSORPTION OF CESIUM FLUORIDE ON TUNGSTEN

INTRODUCTION

In the study of low work function adsorbates the favorable properties of the alkali and alkaline earth metals have long been recognized. For cesium adsorbed on tungsten work functions as low as 1.5 eV have been obtained and even lower values were obtained when Cs was deposited upon a chemisorbed layer of oxygen[1,2,3]. In addition, an increase in the binding of Cs to the substrate is effected by the presence of O_2. In view of the enhanced work function lowering $\Delta\phi$ of coadsorbed systems involving highly electropositive and electronegative adsorbates it is of interest to examine the most extreme example of electropositive and electronegative adsorbates, namely the Cs/F/W system. Some of the pertinent physical properties of O_2 and F_2 are summarized in Table 1.

Table I. Physical Properties of Oxygen and Fluorine

	Ionization Potential (Volts)	Atomic Radius (Å)	Electronegativity (Pauling Scale)	Electron Affinity (Volts)
O_2	13.55	0.60	3.5	1.46
F_2	17.34	0.50	4.0	3.45

An earlier field emission study of the Cs/F/W system by Wolf[4] has shown remarkable similarities to the Cs/O/W system. For example, deposition of CsF on W has been observed to yield a work function as low as 1.1 eV. Wolf employed a CsF source which automatically requires the initial deposition to exhibit the stoichiometric ratio of Cs/F. As in the case of the Cs/O/W system, the Cs could be removed by thermal heating leaving a layer of chemisorbed F_2. In this way desired amounts of F_2 up to a coverage commensurate with a work function of 5.1 eV could be attained. In order to allow greater flexibility in the ratio of Cs/F a separate source of Cs was incorporated into the tube employed in this ivestigation; in this way the Cs coverage could be varied independently.

The investigation reported herein was primarily devoted to the measurement of work function-Cs coverage relationships for various underlying coverages of F_2 on W. Surface kinetic studies of diffusion and desorption and the temperature dependency of ϕ for the Cs/F/W system are also reported.

EXPERIMENTAL METHODS AND PROCEDURES

The construction of the field emission microscope for the coadsorption study was standard except for provisions made to measure and control the emitter temperature[5]. Pattern viewing was accomplished by pulse techniques to eliminate field effects due to viewing voltage. The tip temperature was derived from an accurate measurement of the resistance of a small section of the emitter's supporting filament as described elsewhere[5].

The tube also contained a Cs source consisting of a platinum disc onto which Cs was condensed and subsequently sublimed onto the tip by controlled resistive heating of the disc. The CsF source consisted of optical grade crystals which were thoroughly outgassed during tube evacuation by placing them in a resistively heated platinum bucket. After seal-off the tube was placed in a liquid N_2 cryostat; CsF could be deposited onto the emitter in pure form by heating the platinum bucket to $\sim 900^{\circ}K$. The amount of F_2 deposited in a single dosing sequence was probably determined by the size of the Cs atoms of which about one Cs to every four W atoms is enough to constitute a monolayer of adsorbate. A greater concentration of F_2 than one to every four surface W atoms could be achieved by removing the initially dosed Cs from the surface by heating and redepositing more CsF and then heating. Because of the need to heat to $1000^{\circ}K$, it was unlikely that the resultant F_2 layer could have been completely saturated.

The application of the field emission microscope to an investigation of the work function change of various substrates on adsorption is made possible by the well-known and experimentally confirmed Fowler-Nordheim law of field emission. This law may be expressed in terms of the directly measurable field emission current I_e and applied electric field F_a as

$$I_e = \frac{BF_a^2}{\phi t^2(\phi, F_a)} \quad \exp - \left[\frac{b\phi^{3/2} \, v(\phi, F_a)}{F_a} \right], \tag{1}$$

where $t(\phi, F_a)$ and $v(\phi, F_a)$ are tabulated nondimensional functions[6] which take into account the image correction, B is proportional to emitting area, and $b = 6.8 \times 10^7$ where F_a is in V/cm, and the work function ϕ in eV. Although Equation (1) is the zero-degree approximation, it holds reasonably well at higher temperatures provided ϕ is sufficiently large. By defining the field factor $\beta = F_a/V$, where V is the applied voltage, Equation (1) may also be written as

$$\log I/V^2 = \log A + m/V, \tag{2}$$

where A is the intercept and m is the slope of a "Fowler-Nordheim" plot of the I(V) data plotted in the form $\log I/V^2$ vs $1/V$. The slope m may be written as follows:

$$m = \frac{b\phi^{3/2} s(\phi, F_a)}{\beta} \quad , \tag{3}$$

where $s(\phi, F_a)$ is another tabulated function[6]. In the range of F_a and ϕ, encountered in this investigation Equations (1) and (3) may be simplified by the following close approximation:

$$v(\emptyset, F_a) \cong 0.943 - 0.146 \times 10^{-6} F/\emptyset^2 \quad (4)$$

from which it can be easily shown that $s(\emptyset, F) = 0.943$. Using the known work function $\emptyset_s$ of the clean surface as a reference, and assuming β to be unchanged by adsorption, the work function $\emptyset$ at the surface when coated with an adsorbate can then be determined from Equation (3) written as follows:

$$\emptyset = \emptyset_s \left[\frac{m\, s\,(\emptyset, F_a)}{m_s s(\emptyset, F_a)} \right]^{2/3} \quad (5)$$

where m_s and m are the slopes of the corresponding Fowler-Nordheim plots.

The General Behavior of CsF on W

Migration

Upon unilateral deposition onto the emitter at 77°K of a CsF dose considerably less than a monolayer and heating the emitter for 60 second intervals at increasing temperatures, the pattern sequence of Figure 1 was obtained. At temperatures below 142°K the original deposit transformed into what appeared to be a two-phase system corresponding to a two-dimensional dilute and condensed phase system shown in pattern (b). As the emitter temperature was raised to 160°K the high concentration phase receded and the dilute phase migrated across the emitter giving typical Cs on W patterns. It should be mentioned that similar evidence of two-dimensional phase separation was also observed for the Cs/W and Cs/O/W systems[1]. Consistent with the observations of Cs on clean W, the migration of Cs was complete at ~ 250°K and no further pattern change occurred until T $\cong$ 384°K at which temperature the overall pattern began to attain a symmetrical distribution as shown in pattern (f) and, in addition, the overall work function lowered somewhat.

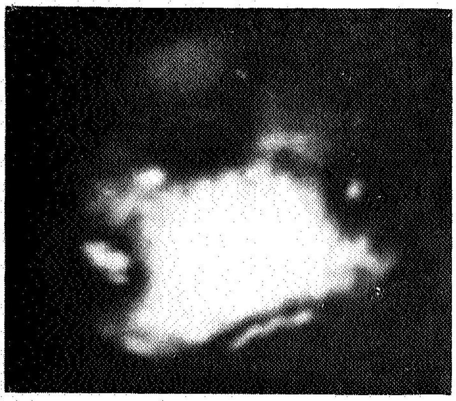

(a)

77°K deposit

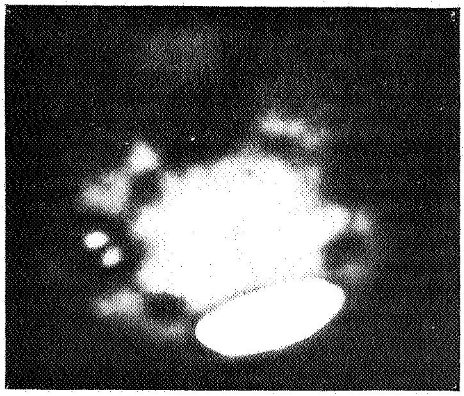

(b)

T=142°K

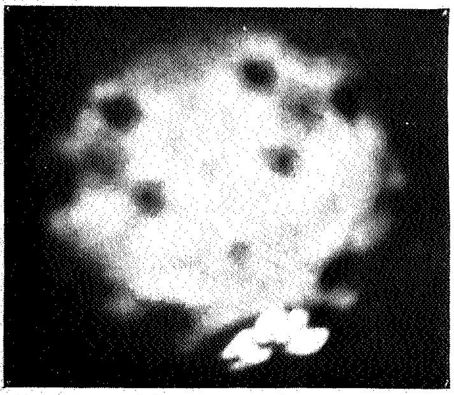

(c)

T=220°K

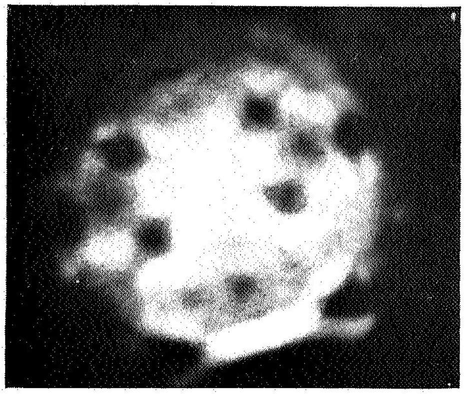

(d)

T=354°K

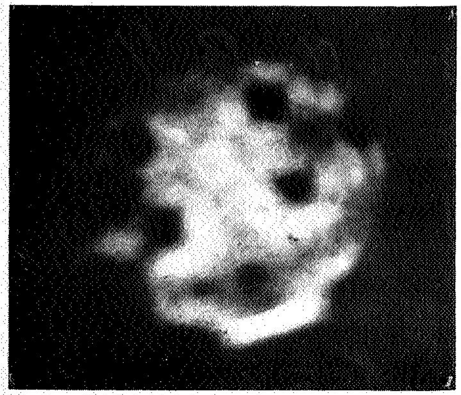

(e)

T=384°K

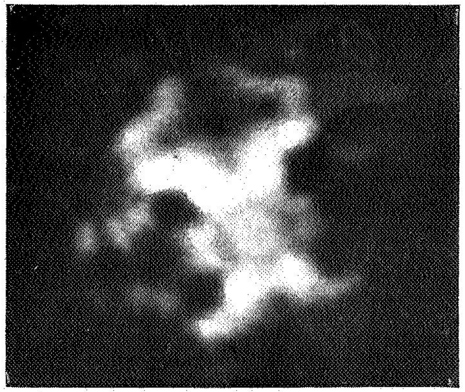

(f)

T=487°K

Figure 1. Sequence of patterns showing migration of a single CsF dose across a W surface. Patterns (c) and (d) are typical Cs on W patterns.

The above behavior can be explained by dissociative adsorption of the CsF and differential migration rates of the Cs and F_2. Apparently the Cs migrates in the usual temperature range of 150-250°K while the F_2 migrates at a higher temperature range of 380-500°K. On the basis that CsF completely dissociates on adsorption one can consider the enthalpy H of the reaction

$$\mathrm{CsF\,(g)} \xrightarrow{H} \mathrm{Cs(a)} + \mathrm{F(a)}, \tag{6}$$

where (g) and (a) refer to gas phase and adsorbed phase respectively. From the thermochemical cycle it can be shown that

$$H = H_{CsW} + H_{FW} - H_{CsF} \tag{7}$$

where H_{CsF} is the heat of dissociation of CsF and H_{CsW} and H_{FW} are the heat of adsorption of Cs and F respectively. Using Wolf's[4] value of $H_{FW} = -6.38$, $H_{CsW} = -3.00$ and $H_{CsF} = -5.7$ eV, one obtains $H = -3.68$ eV. Thus, in view of the highly exothermic nature of reaction (6) it is not surprising to observe complete dissociation of CsF upon adsorption and surface diffusion.

Fluorine Adsorption - Desorption on Tungsten

By impinging a flux of CsF molecules on a W emitter held at 1200°K, Wolf[4] showed that a F/W layer exhibiting a maximum work function value of $\phi_{FW} = 5.8$ eV could be obtained. Figure 2 shows a plot of work function and the Fowler-Nordheim preexponential log A versus the number of CsF doses deposited on the emitter and subsequently equilibrated at 1100°K in order to remove Cs. Figure 3 shows the typical field electron patterns at various degrees of F_2 coverage. Doses 1 through 8 were equilibrated with no electric field applied to the emitter, while doses 9 through 14 were equilibrated with the screen held at -225 V during the heating period.

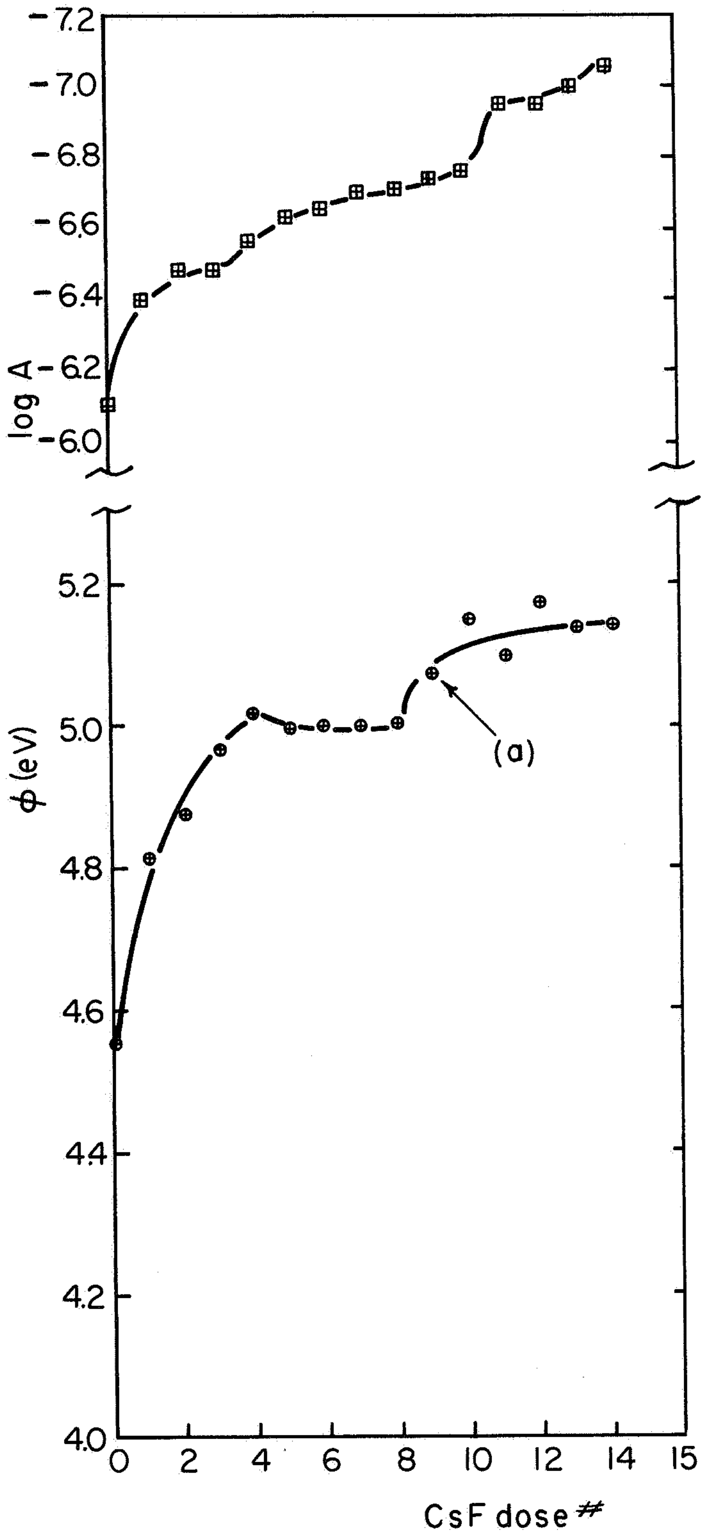

Figure 2. Curves show variation of Ø and log A with CsF dose number. At (a) -200 V was applied to the screen during the 1100°K equilibration.

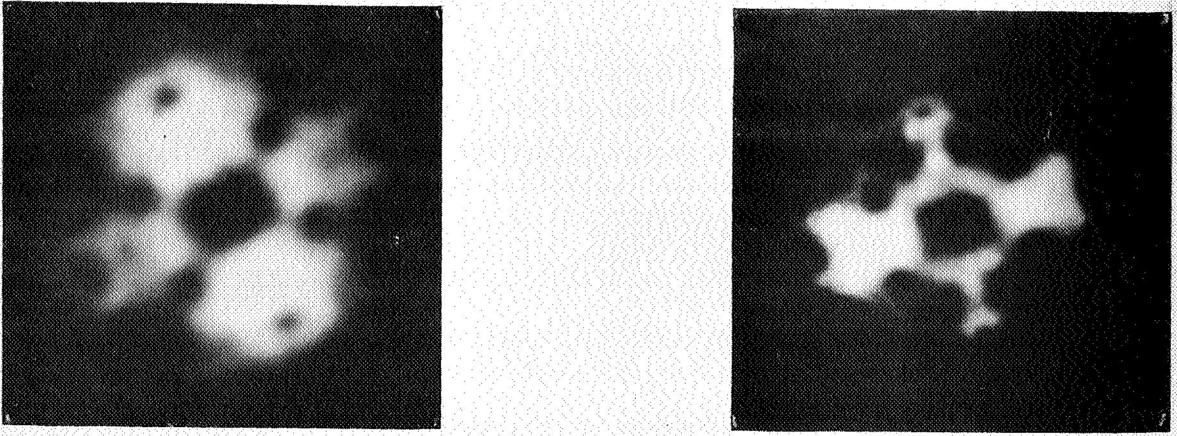

(a)
Clean W

(b)
ϕ =4.65 eV

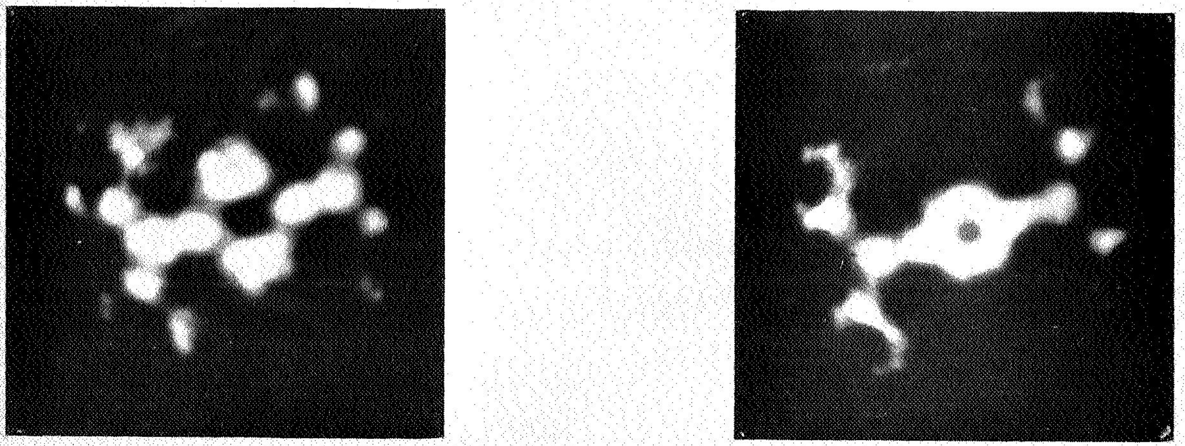

(c)
ϕ =5.05 eV

(d)
ϕ =5.15 eV

Figure 3. Field emission patterns corresponding to various amounts of F_2 on W.

The corresponding field strength was approximately 2.1 x 10^6 V/cm. Following dose 14, the tip was heated to 1100°K for five minutes and the work function remained constant. Temperatures greater than 1400°K were required to initiate removal of the F_2 layer thus formed. However, further exposure to Cs followed by heating at 1100°K with no field applied to the emitter tip reduced the work function from its maximum value of 5.14 to 4.90 eV. It was therefore concluded that the F_2 layer thus formed cannot be removed from W below 1400°K, but it can be thermally removed below 1100°K in the presence of Cs, presumably by evaporating as CsF. Complete thermal desorption of the F_2 layer from W occurred at $\sim$ 1800°K. One interesting contrast between the behavior of F_2 and Cl_2 or O_2 on W is that complete thermal desorption of the latter two adsorbates leads to blunting of the emitter due to removal of WCL_6[7] or WO[8], whereas repeated desorptions of F_2 from W do not cause significant changes in the emitter geometry.

A major discrepancy between our work and that of Wolf[4] is the much lower maximum value of ϕ_{FW}, which in our case was only 5.16 eV as compared to 5.83 eV. Notice, however, that a larger than expected decrease in emission occurs as F_2 is added, owing to a decrease in log A as shown in Figure 2. Upon comparing our patterns with those published by Wolf, we find good agreement; thus, assuming Wolf used the slope method of Equation (5) to obtain ϕ_{FW}, we have no explanation for the lower value of maximum ϕ_{FW} found in the present work.

The near linear decrease in log A with F_2 coverage may be attributed to either a decrease in emitting area and/or the field induced dipole effect discussed elsewhere[9]. There it was shown that $-\log A \propto \sigma_{FW}\alpha$, where σ_{FW} is the F_2 coverage and α its polarizability; hence, one expects log A to decrease with increasing σ_{FW} as observed in Figure 2. In view of the much larger electron affinity of F_2 relative to O_2 one intuitively expects the maximum value of ϕ_{FW} to be at least as large as ϕ_{OW} (which is $\sim$6.2 eV). Thus, it appears that formation of the F_2 layer in this fashion does not lead to complete saturation of adsorption sites.

Adsorption of Cesium on a F/W Layer

During the deposition of Cs on clean W the temperature T_e required to equilibrate (i. e., to migrate the cesium across the emitter surface) each dose was noted. Upon equilibrating each dose, the work function was determined from the slope of a Fowler-Nordheim plot according to Equation (5). From previous knowledge of the ϕ versus Cs coverage σ on clean W, the dose size could be established. A repetition of this procedure at various underlying F_2 coverages yielded the family of curves shown in Figure 4, where the lower set is the ϕ versus σ curves, the middle group shows the variation of log A with σ and the upper curves show the variation of T_e with σ.

From the Figure 4 results it is clear that the presence of an underlying F_2 layer significantly reduces the minimum work function obtainable by Cs adsorption. A comparison of pertinent features of the Cs/O/W and Cs/F/W systems are given in Table II. In contrast to the Cs/O/W system, the value of σ at the minimum work function ϕ_m remains essentially unchanged. We further note that both the F/W and O/W surfaces require an initial work function of 5.0 eV to produce a minimum work function of $\sim$1.1 eV. Thus it appears that an underlying F_2 layer affects the same net work function lowering with Cs as an O_2 layer at corresponding initial work functions.

Table II. Summary of Pertinent Features of the Cs/O/W and Cs/F/W Systems

Cs/F/W			Cs/O/W		
ϕ_{FW}(eV)	ϕ_m(eV)	μ_m(D)	ϕ_{OW}(eV)	ϕ_m(eV)	μ_m(D)
4.52(clean)	1.52	8.4	4.62	1.42	12.6
4.88	1.35	8.9	5.01	1.10	18.6
5.07	1.06	10.1	5.65	1.15	27.0
5.14	1.03	10.4			

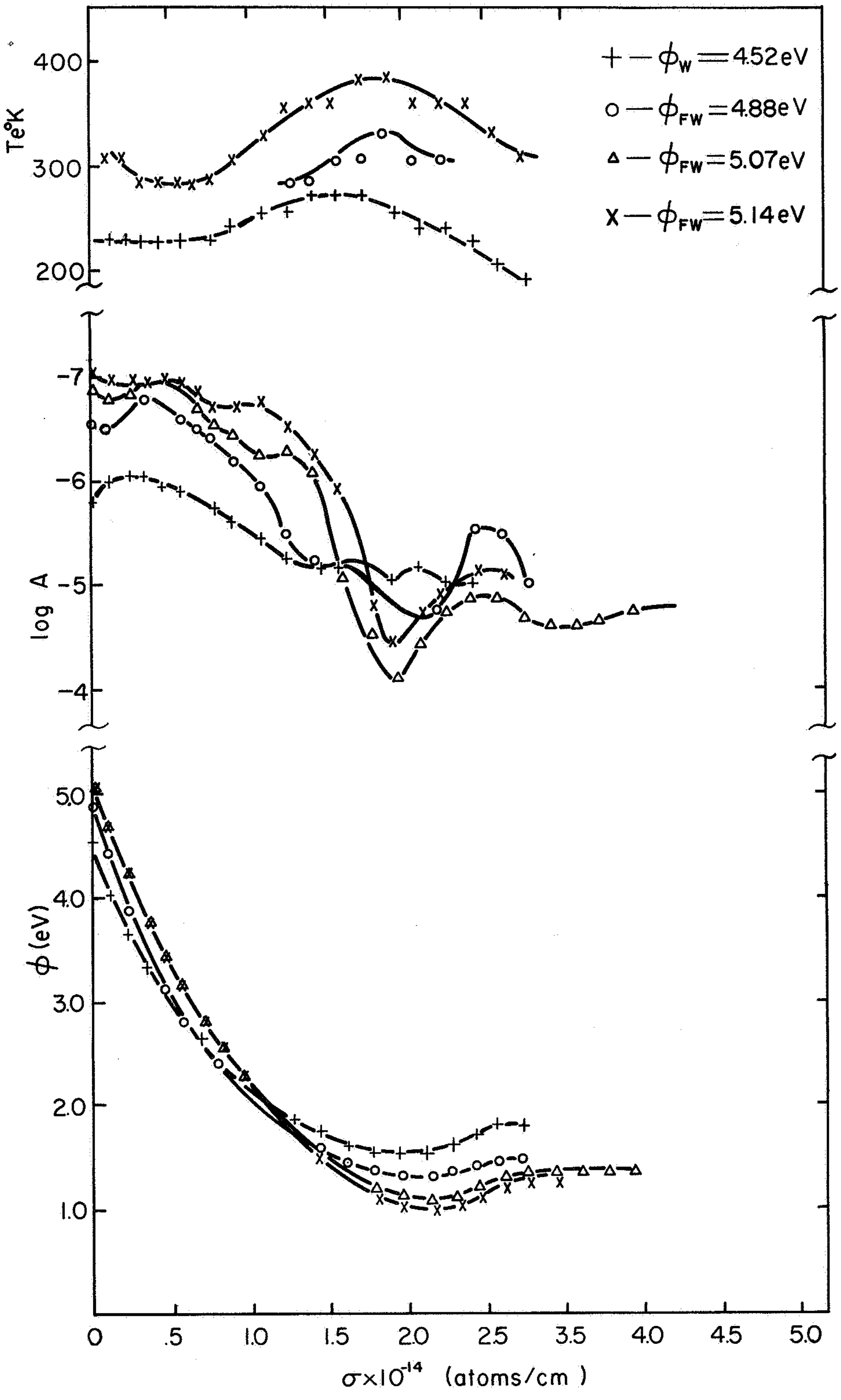

Figure 4. Lower set of curves show variation of work function with Cs coverage for clean and fluorine coated tungsten. Middle set of curves shows the variation of log A and upper set shows the variation of the equilibration temperature T_e with Cs coverage.

The value of log A in Figure 4 exhibits a maximum at the coverage corresponding to $\emptyset_m$. In other words the variation of log A with Cs coverage tends to enhance the maximization of the emission due to the work function lowering. Because of the possibility of variations in the effective emitting area with Cs coverage, which also appears in the log A term, it is not warranted to attempt a detailed interpretation of the log A variations in terms of the induced dipole effect.

The major changes in the emission distribution with Cs coverage on an F/W surface are shown in Figure 5. In contrast to the Cs/O/W system no enhanced emission was observed from the (112) planes at low Cs coverages. On the other hand, at Cs coverages approaching the coverage corresponding to $\emptyset_m$ strong emission from the (112) occurred in agreement with the Cs/O/W system. Also in agreement with the Cs/O/W system at $\emptyset_m$ the emission became rather uniform over the emitting area and at slightly higher Cs coverages the psuedo clean W emission distribution was observed in pattern (f). (Compare with (a) of Figure 3). The latter also occurred at Cs coverages slightly greater than $\emptyset_m$ for both the CsW and Cs/O/W systems.

Clearly F_2, like O_2, greatly enhances the work function lowering of Cs on W. For example, $\emptyset_m = 1.52$ eV for the Cs/W system whereas $\emptyset_m = 1.0$ eV for the Cs/F/W and Cs/O/W systems. Values of the Cs dipole moment μ_m at the work function minimum calculated from

$$\emptyset_m - \emptyset_{FW} = 2\pi\mu\sigma \qquad (8)$$

indicate that underlying O_2 or F_2 enhances the transfer of electronic charge to the substrate (see Table II), thereby greatly increasing the dipole moment formed by the positively charged adsorbed Cs; apparently, from Table II, the O/W is shown to be more effective than the F/W surface in this regard at identical initial work function values.

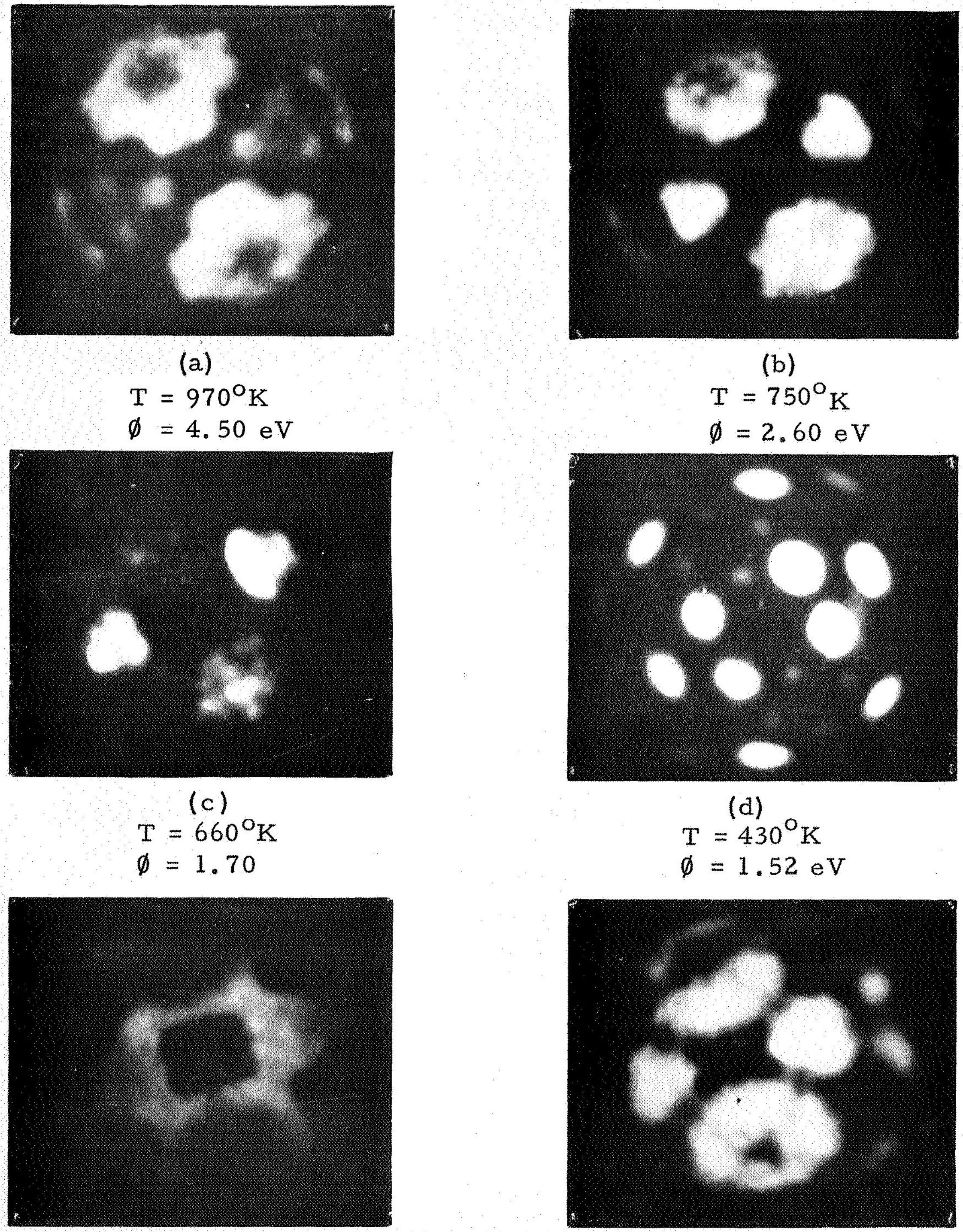

(a)
$T = 970^{\circ}K$
$\phi = 4.50$ eV

(b)
$T = 750^{\circ}K$
$\phi = 2.60$ eV

(c)
$T = 660^{\circ}K$
$\phi = 1.70$

(d)
$T = 430^{\circ}K$
$\phi = 1.52$ eV

(e)
$\phi=0.96$ eV

(f)
$\phi=1.30$ eV

Figure 5. Field emission patterns corresponding to increasing amounts of Cs on a F/W surface where $\phi_{FW} = 4.97$ eV.

Desorption of Cesium From a F/W Layer

That a chemisorbed layer of O_2 on W not only enhances the work function lowering by Cs, but also enhances the binding of Cs to the substrate has been established[1]. As shown in Figure 6, a chemisorbed layer of F_2 produces the same effect. At ϕ_m, for example, thermal desorption of Cs was effected at 560°K for an underlying F_2 chemisorbed layer of $\phi_{FW} = 5.08$ eV, whereas for the Cs/W system a temperature of only 450°K was required. Thus, the thermal stability of the composite system at ϕ_m was markedly increased by addition of F_2. Also the temperature required to completely remove Cs from the F/W layer in ionic form was $\sim$ 1100°K, while for the clean W case only $\sim$ 920°K was required. As the temperature was increased above $\sim$ 1400°K the F_2 began to desorb and the work function approached the clean value of 4.52 eV at $\sim$1800°K. It should be pointed out that removal of Cs should lead to the original F/W work function provided the F_2 layer is unaffected. This, however, was only true for low F_2 coverages or when the screen was held at a negative potential.

By forming the F/W surface in the manner described, one observes that Cs adsorption and desorption is reasonably reversible throughout the coverage range. This can be noted by the similarity in patterns whether obtained by adsorption or desorption; also, the variation of log A shown in the desorption sequence of Figure 6 is nearly identical to that observed in the adsorption sequence of Figure 4. However, the application of a zero or negative electric field during thermal desorption results in a net loss of F_2. This feature is shown more strikingly in Figure 7 where log A is plotted against ϕ for adsorption and desorption sequences on a clean W and F/W surface. Notice that adsorption and desorption points coincide for Cs on clean W indicating complete reversibility. With an underlying F/W layer such that $\phi \cong 5.1$ eV, a region of irreversibility occurs at $\phi \cong 2.0$ eV on both curves and at $\phi \gtrsim 3.5$ eV on the curve with the negative applied field. The cause of the slight irreversibility at $\phi \cong 2.0$ eV is not obvious; however, the irreversibility occurring at $\phi \gtrsim 3.5$ eV for the negative field case (and

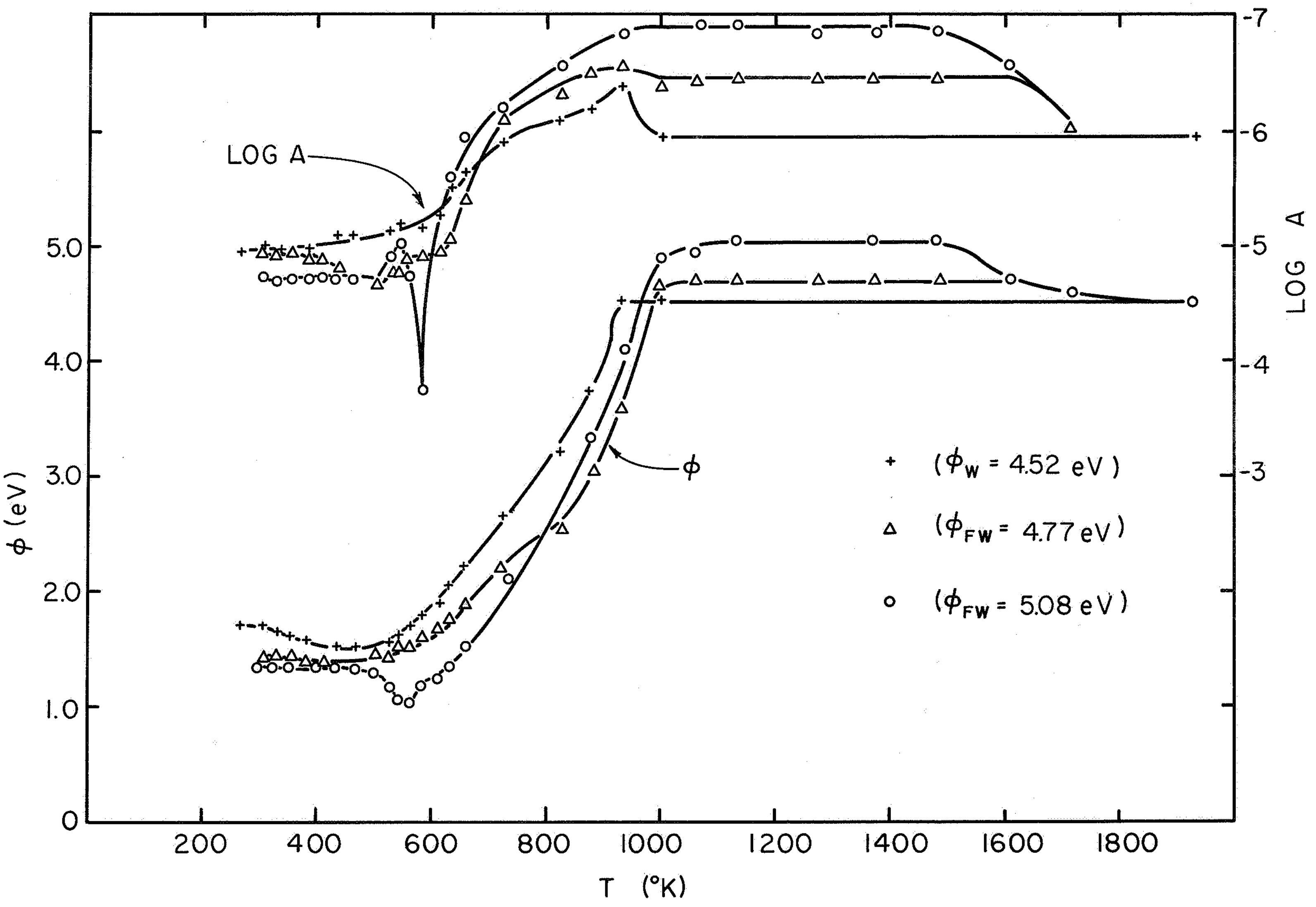

Figure 6. Curves show the variation of Ø and log A upon heating a fully cesium coated F/W surface at the indicated temperatures for 60 sec intervals. During heating the screen was biased to -185 V (F=2.0 MV/cm).

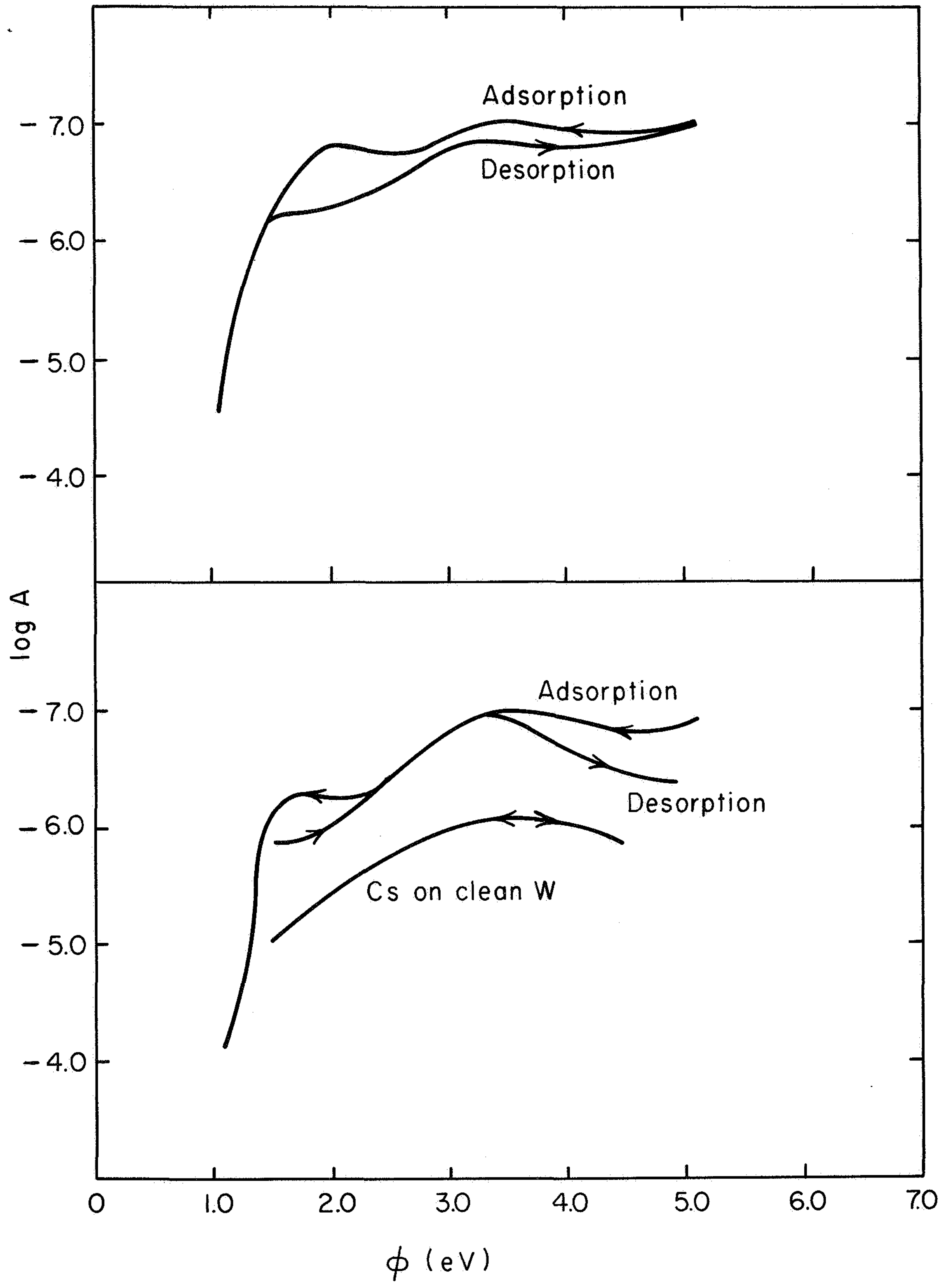

Figure 7. The upper set of curves show a plot of ϕ versus log A for a Cs adsorption desorption sequence, where ϕ_{FW} = 5.14 eV and a negative voltage of 200 V was applied to the screen during tip heating. The lower set of curves is a similar plot where ϕ_{FW} = 5.07 eV and a positive voltage of 100 volts was applied to the screen during tip heating. A 200 V positive bias voltage was applied to the screen for the clean W desorption sequence of Cs.

which also occurs for zero field) is due to F_2 removal. From Figure 6 we observed that $\emptyset \cong 3.5$ eV corresponds to $900^\circ K$, well below the thermal desorption temperature of F_2 alone. Hence, as concluded earlier in connection with the formation of a F_2 layer from CsF, removal of F_2 is enhanced by the presence of Cs above $900^\circ K$.

The explanation of Cs induced F_2 removal can be found by examining the possible desorption paths which are as follows:

$$\mathrm{CsFW} \xrightarrow{E_a} \mathrm{Cs} + \mathrm{FW} \qquad \text{(a)}$$

$$\mathrm{CsFW} \xrightarrow{E_b} \mathrm{CsF} + \mathrm{W} \qquad \text{(b)}$$

$$\mathrm{CsFW} \xrightarrow{E_c} \mathrm{Cs}^+ + \mathrm{FW}^- \qquad \text{(c)}$$

$$\mathrm{FW} \xrightarrow{E_d} \mathrm{F} + \mathrm{W} \qquad \text{(d)}$$

Since a F/W surface is thermally stable up to $1400^\circ K$ when Cs is absent one may conclude that reaction (d) exhibits the highest value of activation energy E_d of the above series. Wolf[4] measured the desorption energy of reaction (d) and obtained $E_d = 6.4$ eV at near zero F_2 coverage. Reaction (a), which represents neutral Cs desorption from a F/W site, can also occur in ionic form according to reaction (c). The energetics of surface ionization readily yield the relation

$$E_c = E_a + I - \emptyset \ , \qquad (9)$$

where I is the ionization potential of Cs. Since $I - \emptyset = 0$ when $\emptyset = 3.87$ eV, the condition $E_c \leqslant E_a$ holds for the coverage range corresponding to $\emptyset > 3.87$ eV. In order for reaction (b) to compete with (c) in this coverage range, we must show that $E_b \lesssim E_c = E_a + I - \emptyset$. Assuming that reaction (a) involves breaking of a CsF bond, the value of E_a is roughly the order of the dissociation energy 5.5 eV, yielding

$$E_c \cong 9.4 - \emptyset. \qquad (10)$$

When $\phi > 3.4$ eV it follows that in order for reaction (b) to compete with (c), the condition $E_b \gtrsim E_c = 6.0$ eV must hold. Although no accurate estimate of E_b can be made, the fact that reaction (b) involves the breaking of a FW bond means the maximum value of E_b must be the order of the measured desorption energy of F_2 from W which is 6.4 eV. Since the value of E_b is likely to be smaller at the larger coverages of F_2, the condition $E_b \lesssim 6.0$ eV can be met and the removal of F_2 via reaction (b) is plausible under zero field conditions.

It now remains to explain why positive applied fields allow desorption of Cs without concomitant desorption of F_2. At sufficiently high positive fields, reaction (c) is enhanced over reaction (b) by positive field desorption[10]; that is, Equation (9) becomes

$$E_c = E_a + I - \phi - e^{3/2} F_a^{1/2} + aF_a + bF_a^2 . \qquad (11)$$

Since at low fields the terms linear and quadratic in F_a are normally small compared to the $F_a^{1/2}$ term, they can be neglected; thus, at a field strength of 1.8×10^6 V/cm, E_c can be reduced by as much as 0.5 eV. Apparently, this reduction in E_c is sufficient to cause reaction (c) to compete favorably with (b) so that F_2 is no longer removed in significant amounts during thermal desorption. Also, since reaction (b) involves a bimolecular reaction between mobile Cs and F_2, the concomitant removal of Cs through reaction (c) reduces the kinetic favorability of (b).

Although the above interpretation is qualitative, its explanation of the experimental observations gives it credence. One may ask why Cs does not enhance removal of O_2 in the analogous Cs/O/W system. This can be explained primarily by the fact that the CsF bond is roughly 2.0 eV stronger than the CsO bond. When reflected through the previous arguments with the further fact that FW and OW bond energies are nearly the same (based on thermal desorption of F_2 and O_2 from W), one finds that reactions (a) and (c) are more favorable than (b) for the Cs/O/W system.

Temperature Dependence of ϕ for a Cs/F/W Surface

The calculation of the work function at elevated temperatures by field emission techniques is given elsewhere[11]. For the Cs/W system the value of the temperature coefficient for the work function was $\Delta\phi/\Delta T \cong -1 \times 10^{-4}$ eV/deg. Similar measurements have been made for the Cs/F/W layer at a coverage where $\phi \cong 1.72$ eV at $T = 77^{\circ}$K. The value of ϕ was found to decrease nearly linearly with T in the range 90 to 180°K. This temperature dependence of ϕ was completely reversible indicating the unlikelihood of desorption or migration of Cs. The value of the temperature coefficient of the Cs/F/W system is $\Delta\phi/\Delta T = -2.4 \times 10^{-3}$ eV/deg, nearly an order of magnitude greater than that observed for the Cs/W system.

The sign of $\Delta\phi/\Delta T$ for the Cs/F/W system is such that the dipole moment per adsorbed Cs must increase with temperature. This implies that either the dipole length and/or the net transfer of electronic charge to the substrate must increase with temperature. The idea that CsF forms a dipolar complex erected by the surface fields of the substrate put forth by Dykman[12] and expanded by others[13] is not supported by our value of $\Delta\phi/\Delta T$. Their model predicts a decreasing value of dipole moment with temperature whereas we observed an increasing value. It appears that a clearer picture of the nature of the adsorbed complex is necessary before the rather large temperature coefficient of work function can be understood.

Field Instability of the Cs/F/W System

Negative Field.- It was observed for the Cs/F/W system in the range of work function values below 2.0 eV, that if the electric field F_a (for emitting electrons) was made sufficiently high, the emission current I_e began to decrease with time. Further, it was noted that the rate of decrease of the field emission current increased with F_a as shown in Figure 8 for $T = 77^{\circ}$K. This phenomenon did not preclude measurement of ϕ by Fowler-Nordheim plots in this range provided values of F_a and, hence, I_e were kept sufficiently

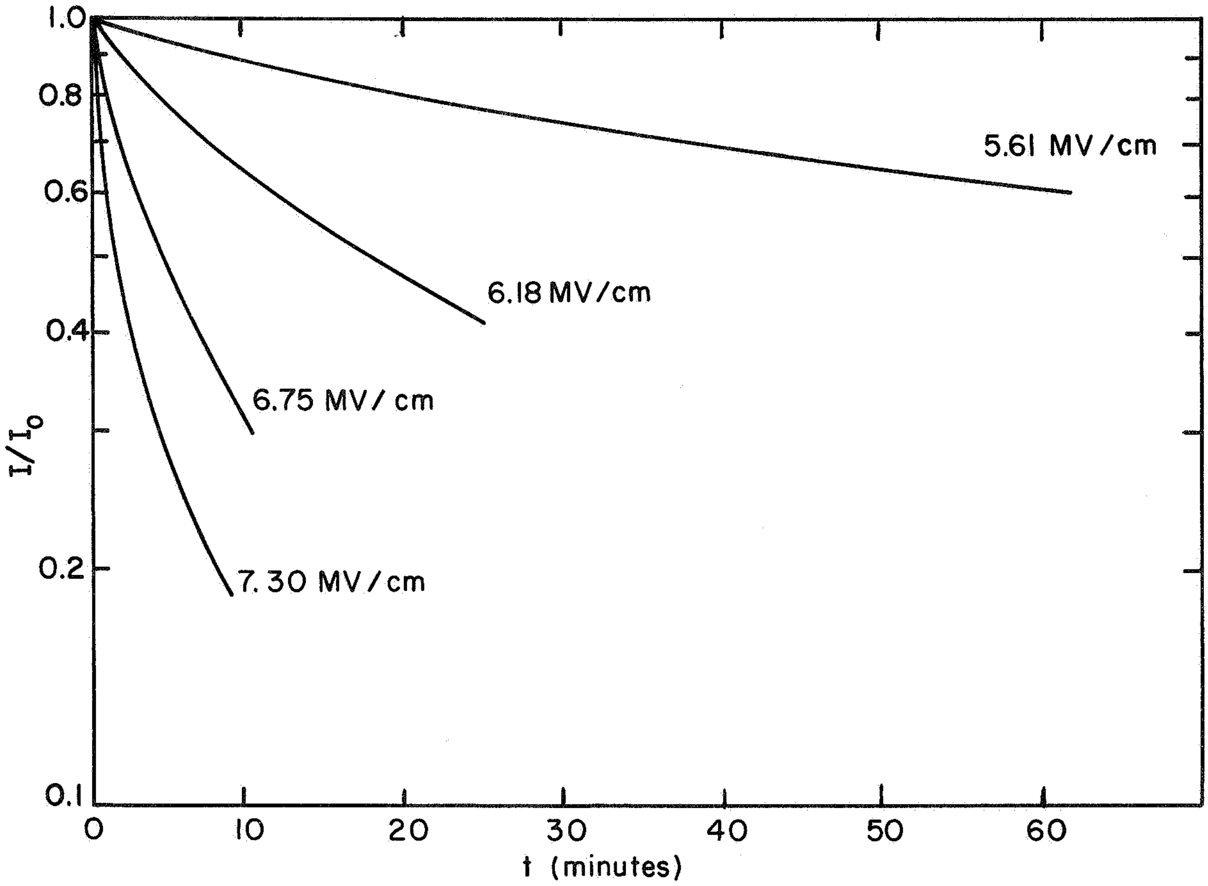

Figure 8. Curves show the variation of the relative field emission current with time at various applied field strengths for a Cs/F/W surface of initial work function $\emptyset$ = 1.30 eV and T = 77°K.

low. The time dependent diminution in I_e with F_a was accompanied by a dimming of the bright emission from the (112) planes as shown in Figure 5(d). Generally, after the current had diminished, the original conditions could be restored by heating to $\sim 115^{\circ}K$, although the temperature required for complete restoration increased as more such cycles were completed. It was also observed that after the emitted current decreased, say at $77^{\circ}K$, no restoration could be effected by reversing the field polarity.

A most interesting study of the temperature dependence of this phenomenon, shown in Figure 9, revealed a decrease in the rate of current change with increasing temperature. At $115^{\circ}K$, as shown in Figure 9, very little net change in I_e occurs with time. We believe that the apparent negative activation energy for the variation in the rate of current change with temperature is due to a concomitant thermally initiated restoration process. This is supported by the fact that even at low temperatures (e. g., $77-90^{\circ}K$) the current slowly returns to its initial value as shown by spot checks of the value of I_e after relaxing the field.

From the experimental observations of this phenomenon obtained thus far we have concluded that field desorption of negative fluoride ions F^- is responsible for the time variation in I_e with constant applied field. We picture the removal of F^- to cause a local net decrease in the dipole moment μ of a CsF complex thereby increasing ϕ. That this is a logical consequence of F^- removal is verified by Figure 4 where removal of F_2 causes ϕ to increase throughout the coverage range of Cs. If we assume an excess of F_2 exists relative to Cs at the coverage at which this phenomenon occurs, the work function is given by

$$\phi = \phi_s - g\pi \left[\mu_{CsF}\, \sigma_{CsF} - \mu_{FW}\, \sigma_{FW} \right], \qquad (12)$$

where σ_{CsF} and σ_{FW} refer to the CsF and F_2 coverage respectively, ϕ_s is the substrate work function and g is 2 or 4 depending on whether image or polarized dipoles are assumed. Clearly, for ϕ to become larger at a given

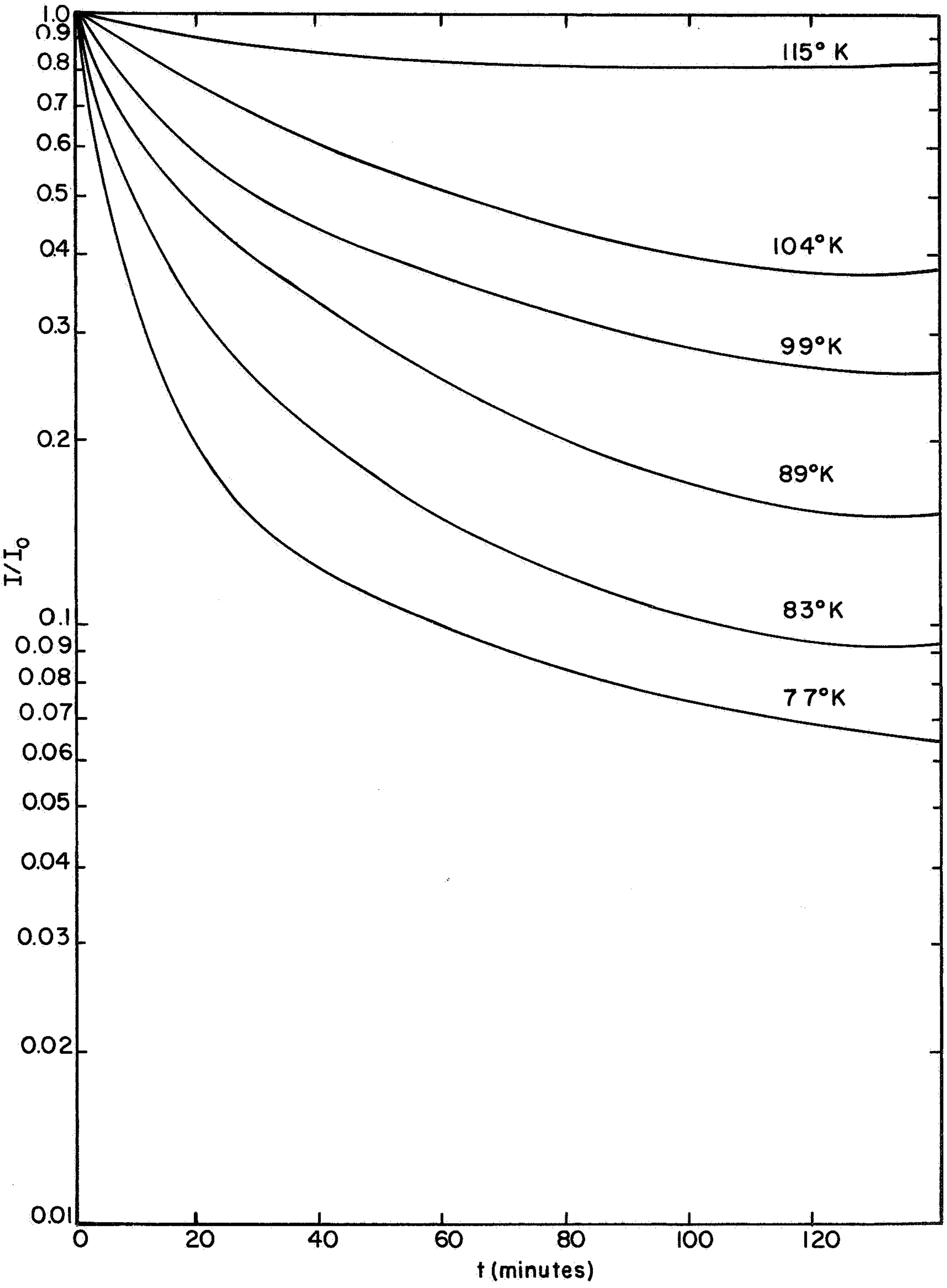

Figure 9. Curves show the variation of relative field emission current with time at various temperatures for a Cs/F/W surface of initial work function 1.25 eV and F = 5.68 MV/cm.

Cs coverage upon removal of F_2, the decrease in μ_{CsF} must override the decrease in the $\mu_{FW}\sigma_{FW}$ term.

The fact that restoration occurs at such low temperature rules out the migration of F_2 from the shank of the emitter where the electric field is too low to promote field desorption of F^-. In fact even Cs is rather immobile at the restoration temperature of 115°K so that gross mobility of either Cs or F may be ruled out of the restoration process. A possible explanation is that F_2 from sites adjacent to adsorbed Cs is removed by field desorption and, provided that F_2 exists in larger concentration than Cs, the Cs need only migrate a few lattice sites to be under the influence of remaining adsorbed F_2 and re-exhibit the original value of μ_{CsF} and, hence, ϕ.

The field desorption of negative halogen ions has also been reported by Kirchner[14] who observed Cl^- desorption from KCL layers on W. An examination of the energetics involved in field desorption of negative ions leads to the following expression for the activation energy E of desorption:

$$E = E_o + \phi - A_e - e^{3/2} F_a^{1/2} + aF_a + bF_a^2 \quad , \qquad (13)$$

where the symbols have the following meaning:

E_o	-	zero field activation energy of the desorption
A_e	-	electron affinity of F_2
e	-	electronic charge
a and b	-	constants

The term linear in F_a comprises the field dipole interactions and field induced work function changes while the term quadratic in F_a involves field induced dipole interactions. The lowering of the Schottky saddle, represented by the $F_a^{1/2}$ term, is the dominate term so that a lowering of E and an increase in rate with applied field is expected as observed in Figure 8. Clearly, the large value of A_e coupled with the small values of ϕ for the Cs/F/W system are conducive to field desorption of negative ions.

In view of the very low temperatures required for restoration it appears difficult to perform a quantitative investigation of the temperature dependence of the rate of F^- field desorption. If temperatures lower than 77°K are employed, the high fields required to initiate desorption would be prohibited because of excessive field emission. By assuming a linear relationship between the change in work function and F_2 coverage, i. e., $\Delta\phi \propto \sigma_{oFW} - \sigma_{FW}$ then Equation (1), at constant F_a, can be written in terms of the ratio of the current I/I_o at ϕ and ϕ_o as follows:

$$\log I/I_o = C_1'(\phi_o^{3/2} - \phi^{3/2}) \cong -C_2' \phi_o^{1/2} \Delta\phi \cong C_3'(\sigma_{FW} - \sigma_{oFW}) \qquad (14)$$

where $\Delta\phi = \phi - \phi_o$. Thus, one can view the variation of $\log I/I_o$ with time in Figure 8 as proportional to the coverage change of F_2 with time. The rapid increase in rate of desorption (i. e., $d(\log I/I_o/dt)$ with electric field is thus expected in view of Equation (13) and the following first order rate equation which normally characterizes field desorption:

$$-d(\log I/I_o)/dt \quad -d\sigma_{FW}/dt = k_o \sigma_{FW} e^{-E/kT} \qquad (15)$$

where k_o is the frequency factor. We therefore conclude that field desorption of F^- is the most likely explanation of the observed emitted current instability.

Positive Field

Upon applying an increasing positive field to a CsF coated tip, the Cs was gradually removed, leaving only a bright ring around the edge of the screen. At moderate Cs coverages, the field desorption process was regenerative and the whole tip was rapidly cleaned to the outer edges. This apparently occurs because the field required for desorption drops sharply with coverage and the process, once initiated, goes rapidly to completion. Since ϕ increases $\sim$4.0 eV while E_a increases only $\sim$ 2 eV with decreasing coverage of Cs, Equation (11) predicts E_p to decrease with decreasing Cs coverage and the field desorption of Cs is therefore regenerative over much of the coverage range. This regenerative feature has been observed both for clean and fluorinated substrates.

At lower coverages, field desorption is slower and the process is observable. In Figure 10 the value of F_a required to initiate field desorption of Cs^+ from a Cs/F/W layer is plotted as a function of Cs coverage. In the temperature range investigated, desorption occurs between 30 and 70 MV/cm. The increase in F_a with Cs coverage stems primarily from the decrease in ϕ. Figure 11 shows a sequence of patterns as the desorption field is increased, starting with a Cs coverage of 0.5×10^{14} atoms/cm^2. That Cs is desorbed leaving an undisturbed F/W layer is established from the sequence of patterns in Figure 11, where the original F/W pattern (photo f) reappears after field desorption of the Cs. The removal of Cs begins near the emitter apex due to the higher electric field, then proceeds outward toward the periphery of the emitter. It can be concluded that positive field desorption does not remove CsF, but rather favors rupture of the Cs-F bond.

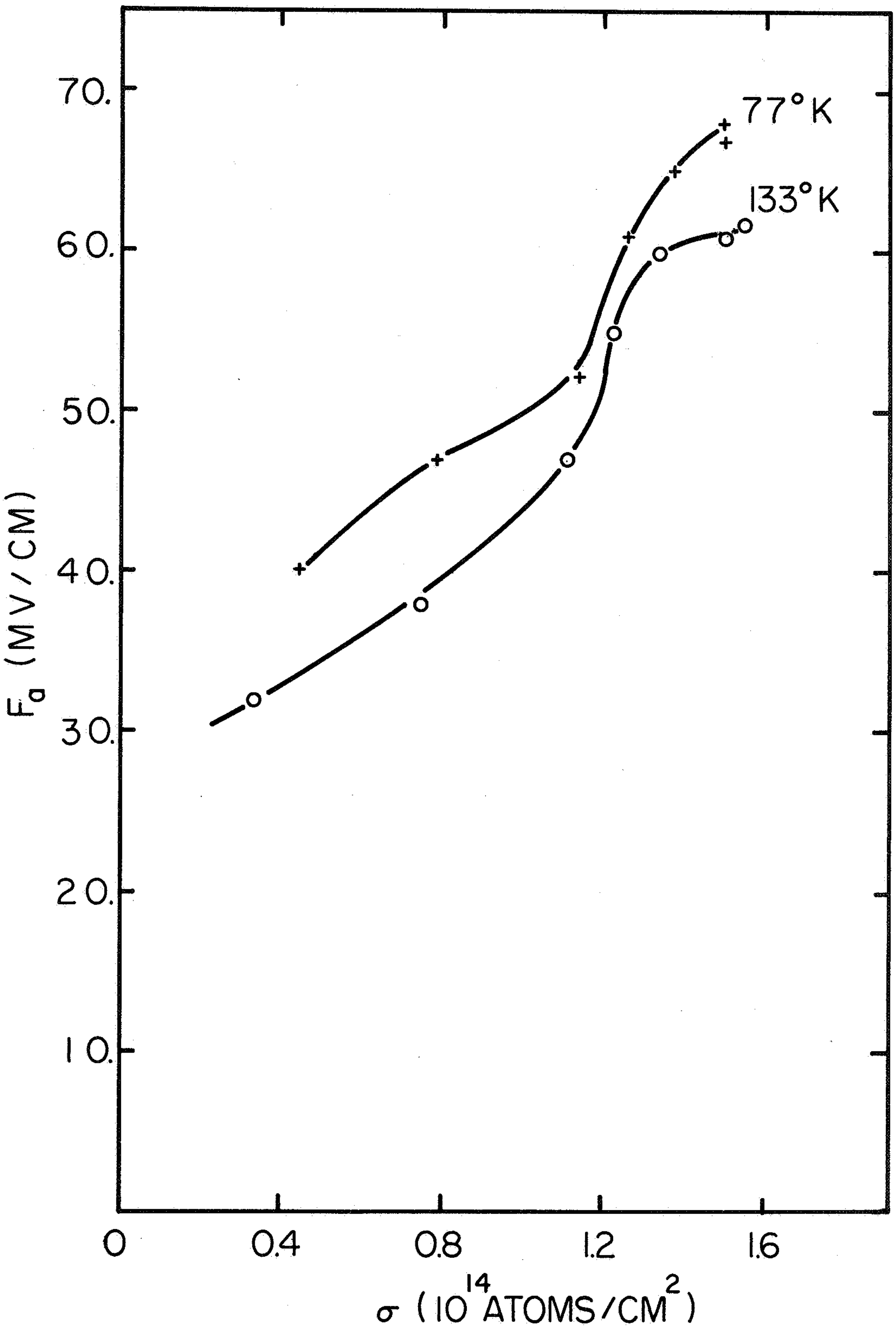

Figure 10. Curves show the positive field required to initiate desorption of Cs as a function of Cs coverage from an F/W surface where $\emptyset_{FW}$ = 5.09 eV.

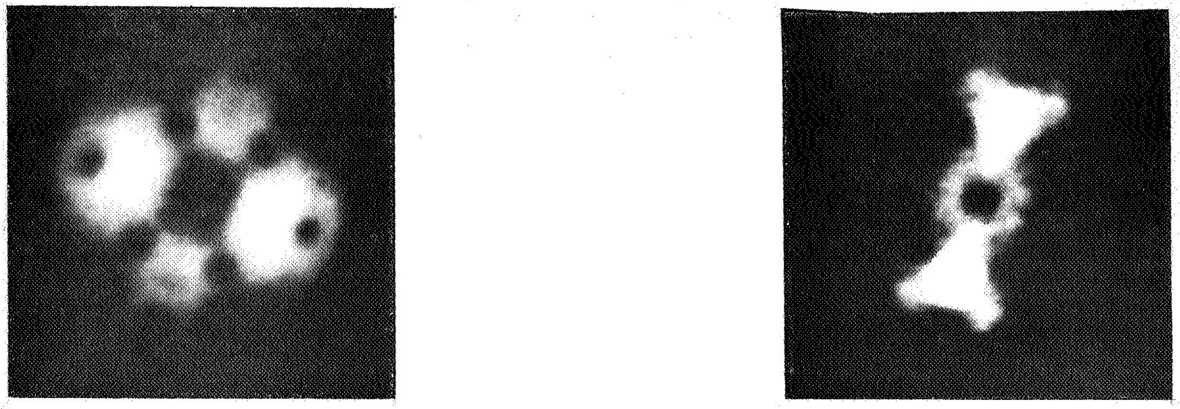

(a)
Clean W

(b)
Initial fluorine deposit;
$\phi_{FW} = 4.81$ eV

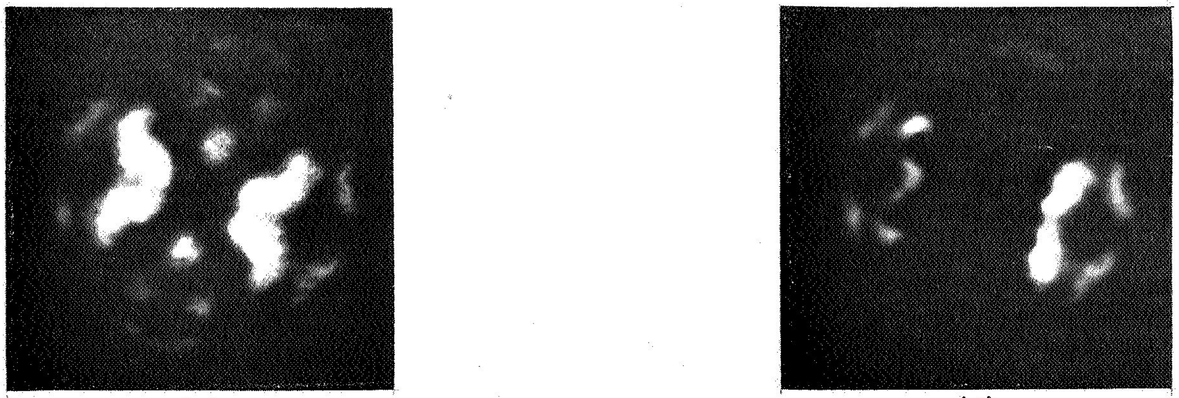

(c)
Initial Cs/F/W layer;
$\phi_{CsFW} = 3.58$ eV

(d)
Field desorption at
F = 41.4 MV/cm

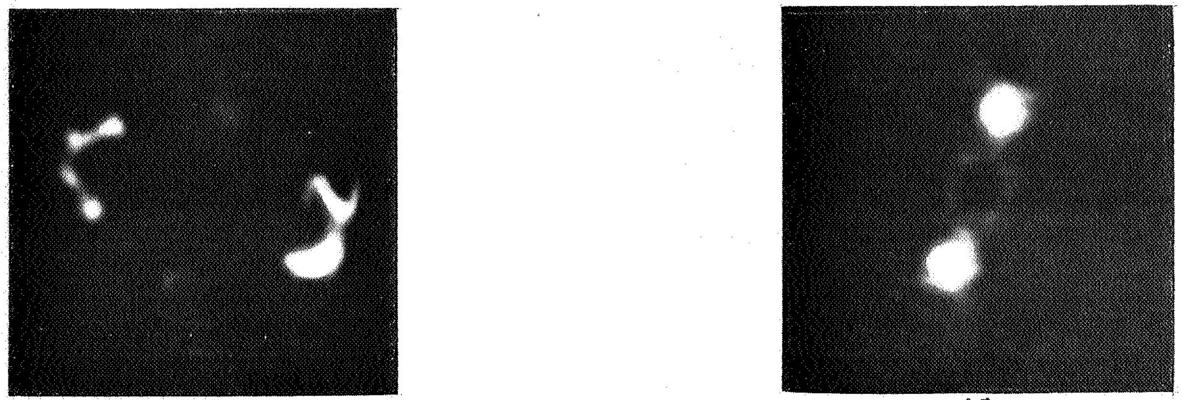

(e)
Field desorption at
F = 46.5 MV/cm

(f)
Field desorption at
F = 56.8 MV/cm;
$\phi_{FW} = 4.8$ eV

Figure 11. Pattern sequence showing progress of field desorption at 77°K. Note pattern (f) is very similar to (b) indicating removal of Cs from the F/W surface.

REFERENCES

1. L. W. Swanson, et al., Final Report, Contract NASw-458, Field Emission Corp. (1963).

2. L. W. Swanson and R. W. Strayer, J. Chem. Phys. (to be published).

3. I. Langmuir and K. H. Kingdon, Phys. Rev. 34, 129 (1929).

4. E. D. Wolf, Twenty-Fifth Ann. Conf. Physical Electronics, Cambridge, Massachusetts (March 1965) and private communication.

5. D. Zimmerman and R. Gomer, Rev. Sci. Instr. 36, 1046 (1965).

6. R. H. Good and E. W. Müller, Handbuch der Physik 21, 176 (1956).

7. M. Silver and R. S. Witte, J. Chem. Phys. 38, 872 (1963).

8. R. Gomer and J. K. Hulm, J. Chem. Phys. 27, 1363 (1957).

9. D. Menzel and R. Gomer, J. Chem. Phys. 41, 3311 (1964).

10. R. Gomer and L. W. Swanson, J. Chem. Phys. 38, 1613 (1963).

11. L. W. Swanson and L. C. Crouser, Phys. Rev. (in press).

12. I. M. Dykman, Ukr. Fiz. Zh. 1, 81 (1956).

13. L. K. Tower, NASA Technical Note, TN D-3223.

14. F. Kirchner and H. A. Ritter, Z. Naturforschg. 11a, 35 (1956).

N68-16762

II. SINGLE PLANE WORK FUNCTION/COVERAGE RELATIONSHIPS FOR CESIUM AND OXYGEN COADSORBED ON TUNGSTEN

Studies of coadsorption from alkali metals and electronegative gases on refractory metal substrates revealed that the minimum work function obtained are lower than those using alkali adsorbates alone.[1-5] Work function lowering of approximately 3.0 is obtained with cesium adsorbed on tungsten; a larger decrease of approximately 3.5 is obtainable with cesium adsorbed on a preadsorbed layer of oxygen.[3] In addition, the cesium becomes more tightly bound to the substrate when oxygen is present.

For the Cs/W and Cs/O/W systems the work function lowering is not the same on all crystallographic planes of the W substrate; marked anisotropies in work function are readily detected in the field electron patterns of field emission microscope studies of the systems. These anisotropies yield information about dipole moments of the adsorbed complex on different planes if assumptions about the adsorbate coverages on these regions can be made.

When cesium is adsorbed on a tungsten field emitter, the (110) planes preferentially adsorb cesium under equilibrium conditions to such an extent that these planes, although initially of very high work function, become the predominant electron emission areas until the coverage of 1.45×10^{14} atoms/cm^2 is reached, at which point the (211) planes are equally bright. Deposition of cesium on top of a chemisorbed layer of oxygen, however, not only results in a lower minimum work function, but alters electron emission anisotropies so that the (211) regions are the predominant electron emission regions when cesium coverage is kept below that required to reach the work function minimum.

A detailed field emission study of the effect of preadsorbed oxygen on the properties of cesium monolayers on tungsten (reported in a paper[3] hereafter designated as paper I) indicated the following:

1. A low work function of 1.15 eV can be attained if the emitter is initially dosed with approximately a monolayer of oxygen ($\Delta\phi$ = 1.25 eV), heated to about 500°K, dosed heavily with cesium and then heated to about 350°K for 60 seconds.
2. The stability of the cesium layer is appreciably enhanced by the presence of an underlying oxygen layer.
3. The temperature required to spread cesium over the substrate is sharply increased by underlying oxygen and cesium coverages of approximately a monolayer.
4. Although the (110) plane emits preferentially over the (100) and (211) planes in the case of cesium on clean tungsten, the reverse apparently is true for cesium adsorbed on oxygenated tungsten if insufficient cesium is present to allow attainment of the work function minimum.

Recently, field emission probe techniques have been applied to studies of the work function variations on different planes of the Cs/W system[3] and O/W system.[6] They have shown, among other things, that a considerable anisotropy in surface coverage of cesium exists on the various planes of a tungsten field emitter when the adsorbate layer of moderate coverage is heated to equilibrate. In view of the remarkable effects of preadsorbed oxygen on cesium layer properties, a probe field emission study of the Cs/O/W system has been undertaken. The effects of small amounts of preadsorbed oxygen on the work function variations due to the adsorption of cesium on the (110), (211), (111) and (100) planes of tungsten are described in this section.

EXPERIMENTAL TECHNIQUES

Experimental Tube

The tube used in this study is suitable both for work function and energy distribution measurements on any plane; moreover, it contains both a cesium and an oxygen source so that the above measurements may be carried out on single or coadsorbed layers of the above adsorbates. Energy distribution measurements of cesium on the (110) plane of tungsten, carried out in this tube, is given elsewhere in this report.

A diagram of the tube is shown in Figure 1. The electron collector design is based on a design of Dr. van Oostrom of the Phillips Laboratory, Eindhoven.[7] It differs from earlier probe tube designs by Müller, et al.,[8] in that it contains a lens electrode E. Electrons passing through the lens are focused near the center of the spherical collector F, and subsequently travel to the spherical electron collector along radius vector paths. This feature of the design enables it to be used successfully in total energy analyzing experiments. The envelope construction enables the main electrode assembly to be removed for inspection or alteration simply by making one crack in the alumino-silicate glass which is conductivized on the inside only in the vicinity of the anode D. In order to minimize the electrical noise pickup by the electron collector lead as it emerges from the tube, the lead is enclosed by a molybdenum cylinder which connects directly to the shield of the coaxial cable leading to the electrometer.

The oxygen and cesium sources are arranged perpendicular to each other and to the emitter axis and each supplies the emitter with adsorbates along a very small glass constriction which points toward the tip.

The oxygen source was a platinum bucket containing small pieces of copper oxide. The copper oxide had been prepared by heating the platinum bucket containing small pieces of well-outgassed copper in a low pressure (approximately 15 torr) of spectroscopically pure oxygen. Dosing of the emitter with oxygen was accomplished by heating the platinum bucket at a constant current for a known time. Although the oxygen beam was directed from one side, the emitter was uniformly dosed with oxygen even when only partial monolayers of oxygen were deposited at 78°K. At this temperature the sticking probability on glass is less than unity so that a dose of oxygen from the source is reflected inside the tube many times before being removed

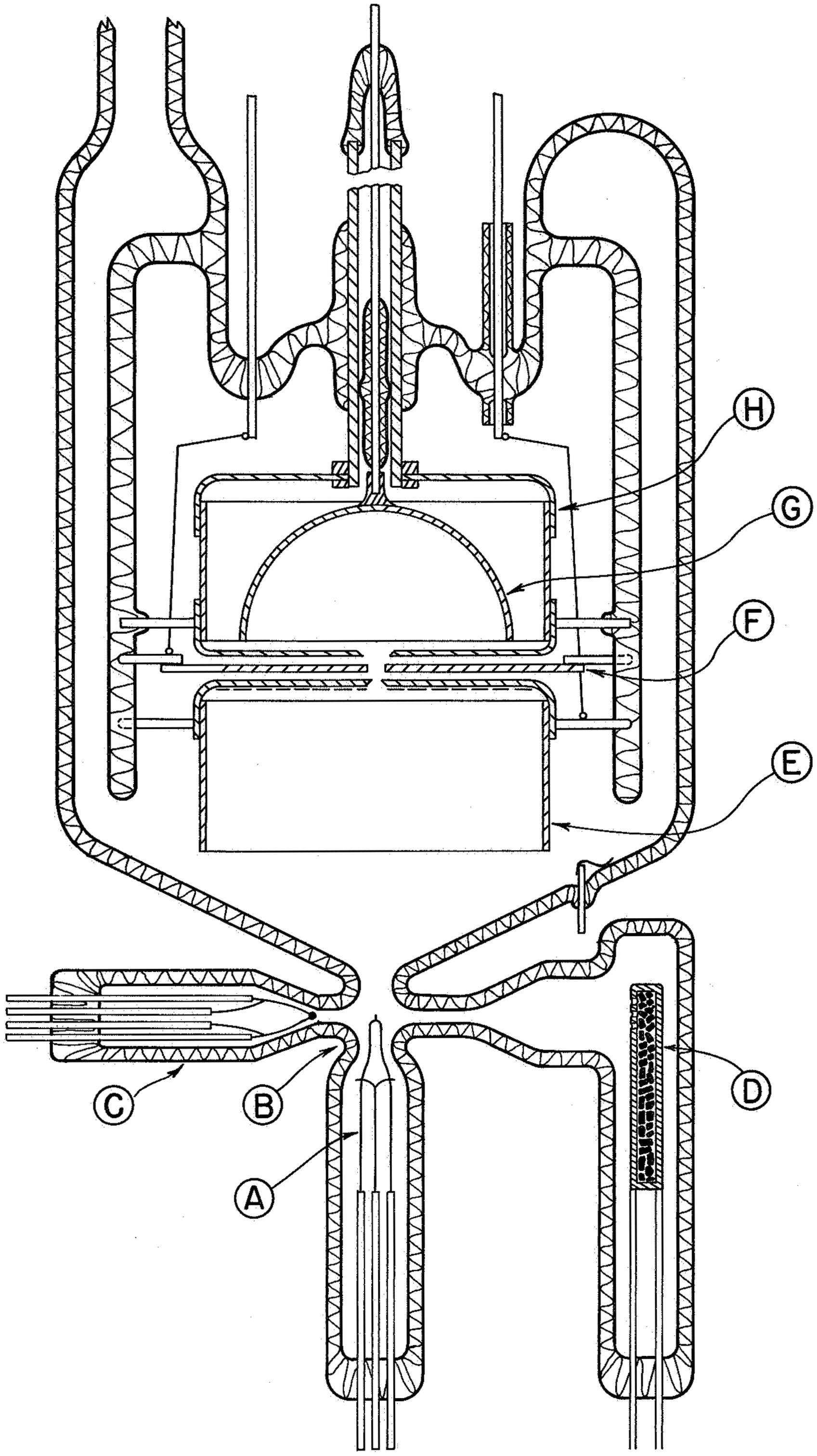

Figure 1. Diagram of co-adsorption magnetic deflection probe tube. Tube contains following components:

(A) emitter assembly;	(E) anode;
(B) space for electromagnet;	(F) lens electrode;
(C) cesium ion source	(G) spherical collector;
(D) oxygen source;	(H) Faraday cage.

by the getter. Before dosing, the getter was activated in order to remove excess oxygen remaining inside the tube after the emitter was saturated.

The cesium source was an ion source consisting of a sodium alumino-silicate molecular sieve powder (Linde Type A Zeolite) which had undergone an ion exchange reaction with cesium.[9] A platinum filament was coated with this material, then heated to 1600°K in vacuum. Subsequent heating to 1100°K caused emission of cesium ions with no neutral content.

A small 1 mm probe hole in the anode D collected emission from a particular plane of the field emission pattern when the pattern was deflected so that the desired plane was centered upon the probe hole. The deflection method employs a small quadrupole electromagnet constructed to fit snugly against the constricted part of the emitter glass envelope so that the horizontal axis through two opposite pole faces bisects that of the other pair at the emitter apex. The electromagnets have carefully annealed Armco cores while all other parts of the magnetic assembly are constructed of non-magnetic materials. This keeps residual magnetic fields to a minimum.

Emitter temperatures are derived from accurate measurement of the resistance of a small section of the emitter's supporting filament C; this makes use of the fact that the resistivity of tungsten is a well-known, monotonic, and nearly linear function of temperature over the range of interest. The resistance of a segment of the loop was determined by passing an accurately known dc current through it and measuring the potential difference across it by means of two small leads attached to the filament. Resistance was calibrated by measuring it at several well-determined temperatures. A servo mechanism developed by Gomer and Zimmerman[10] was used to insure the constancy of emitter resistance and, hence, temperature.

Experimental Procedure

The tube was evacuated and processed by standard UHV procedures and sealed off from the vacuum system at a pressure of 7×10^{-10} torr. Flashing of the titanium-tantalum getter with the tube submersed in liquid nitrogen resulted in a final residual pressure of chemically active gases below 10^{-12} torr as judged by contamination rates of the cleaned field emitter.

Cesium dosing of the tip was accomplished by operating the cesium ion source as an ion gun; the conductivized glass walls around the source were biased -4 volts with respect to the cesium ion source and the emitter was biased -22 1/2 volts in order to maximize the ion current arriving at the emitter assembly. Other investigators [11, 12] have found that the adsorption process gave results dependent upon ion energies if the ion energies were above 5 eV or 8 eV, respectively. At the higher ion energies used here deposition of cesium on clean tungsten held at 77°K and equilibration at 300°K gave variations in surface coverage of approximately 10%. Because of this variation and of the possible desorption of cesium at the higher equilibration temperatures required for cesium on oxygen-covered tungsten, we derived the cesium coverage not from the total charge deposited on the emitter assembly but from data in Paper I, showing the relationship of the work function minimum of the cesium coating to the underlying oxygen coverage.

In earlier field electron microscopy studies of chemisorption of oxygen on tungsten, Gomer and Hulm[13] found adsorption and desorption to be reversible, as judged by pattern and work function change, up to a desorption temperature of 700°K. These results showed that heating a tungsten emitter initially coated with oxygen at low temperatures (22-77°K) above 700°K caused perceptible geometric rearrangement of the tungsten substrate due to incipient oxide formation, whereas below 700°K such arrangement was negligible.

Prior to the successive deposition and thermal equilibration of small amounts of cesium, a small amount of oxygen was deposited onto the tungsten substrate at 77°K and equilibrated at 500°K for 100 seconds. Since this temperature was approximately equal to the highest equilibration temperature required for subsequent cesium depositions[3], further thermal motivated rearrangement of the oxygen layer was unlikely. This, of course, does not rule out chemically-induced rearrangement of the oxide layer due to the presence of cesium.

Work function measurements at a particular cesium coverage was made by focusing attention on a particular plane and obtaining regular Fowler-Nordheim data for a range of voltages and currents, the process then being repeated for other planes of interest. It was found necessary to compensate for the beam deflection resulting from alteration of the anode voltage which takes place when the electron emission currents from single planes were measured.

Work functions are obtained from the Fowler-Nordheim equation:

$$I = \frac{b\,F^2}{\phi(F)\,\left[t(y)\right]^2} \exp\left\{ \frac{-0.687\left[\phi(F)\right]^{3/2} v(y)}{F} , \right\} \qquad (1)$$

where I is the field emission current in amperes, F is the electric field at the emitter surface in V/Å, ϕ is the electron work function in eV and is slightly dependent upon electric field for an adsorbed layer, and b is a constant proportional to the emitting area. The functions t(y) and v(y) are tabulated functions[14] of F and ϕ (note $y^2 = 14.4\ F/\phi^2$) which take into account the image corrections; over the ranges of the variables F and ϕ encountered in the present work, they may be approximated by[15] $t(y) \cong 1.05$ to within $\pm$ 2% and $v(y) \cong 0.951 - 1.026\ y^2$ to within 0.7%. Although the above equation was derived for the case of $0^\circ K$, it holds quite well at $77^\circ K$, the correction for temperature effects being negligible. The electric field F is related to the applied voltage V by $F = \beta V$, where β is a constant dependent on emitter geometry. Equation (1) may also be written as follows:

$$\ln I/V^2 = \ln A + m/V \qquad (2)$$

where A is the intercept and m is the slope of a "Fowler-Nordheim" plot of the I(V) data plotted in the form of $\ln I/V^2$ vs $1/V$. The slope m may be written as follows:

$$m = -0.687\, \phi^{3/2} s(y)/\beta \qquad (3)$$

where s(y) is another tabulated function[14] which may be approximated by s(y) = 0.945 to within ± 3% over the ranges of the variables investigated. If ϕ_o is the work function of the clean surface, then the work function of the surface when coated by an adsorbate may be obtained from

$$\phi = \phi_o \left\{ \frac{m\, s_o(y)\, \beta}{m_o s(y)\, \beta_o} \right\}^{2/3} \qquad (4)$$

and to a good approximation,

$$\phi \simeq \phi_o \left(\frac{m\, \beta}{m_o \beta_o} \right)^{2/3} \qquad (5)$$

Work functions were calculated from Equation (5) and corrected for each plane by using experimentally determined[16] values of (β/β_o) which fall off monotonically with increasing angle away from the apex of the emitter. Variations in s(y) however, are much smaller and can be neglected. Changes in the Fowler-Nordheim preexponential factor A due to adsorption are also of interest. These are conveniently expressed as

$$B = \Delta \log A = \log A/A_o \qquad (6)$$

where A_o is the value of A for the clean emitter plane.

The experimental I(V) data were analyzed by a least squares routine of an IBM 1620 computer according to Equation (2); from the program were obtained m, log A, their probable errors, ϕ and β. The probable errors for both m and log A were generally less than one percent.

EXPERIMENTAL RESULTS

Figures 2 through 5 depict the changes in work function ϕ and pre-exponential term B for the (110), (211), (100), and (111) planes of partially oxygen-coated tungsten as functions of cesium coverage. Since the emitter was heated to equilibrate the cesium coating for these data, the coverage scales are in terms of the average cesium coverage $\bar{\sigma}$ over the emitter surface. In Figures 2 and 3 are graphed ϕ and B, respectively, for an average substrate work function of $\bar{\phi}_{OW} = 4.62$ eV, which corresponds to an average oxygen coverage of 0.5×10^{14} atoms/cm^2, according to the oxygen-on-tungsten $\phi(\sigma)$ data of George and Stier.[17] In Figures 4 and 5 are graphed ϕ and B, respectively, for a substrate work function of $\bar{\phi}_{OW} = 4.85$ eV, which corresponds to an oxygen coverage of 1.7×10^{14} atoms/cm^2. For convenience, the two oxygen-covered substrates will be referred to as O-W-1 and O-W-2, respectively.

In general, the $\phi(\bar{\sigma})$ curves for cesium on the various planes of oxygen-covered tungsten can be directly related to the brightness of the corresponding areas of field emission patterns, which were recorded earlier;[3] i. e., the highly emitting planes have the lower work functions and vice-versa. As expected,[3] of the four major families of planes the $\{211\}$ planes have the lowest work function over most of the cesium coverage range $0 < \bar{\sigma} < \bar{\sigma}_m$ for both oxygen coverages, where σ_m is the cesium coverage for which the average work function $\bar{\phi}$ is a minimum. In contrast, the (110) plane, which has the lowest work function over the cesium coverage range $0 < \bar{\sigma} < \bar{\sigma}_m$ for clean tungsten,[3] has the highest work function over most of the same range for oxygen-covered tungsten (ϕ_{110} is lowest only at $\bar{\sigma}_m$ on O-W-1). For $\bar{\sigma} > \bar{\sigma}_m$, the O-W-2 substrate has a work function sequence $\phi_{110} > \phi_{211} > \phi_{100} > \bar{\phi} > \phi_{111}$, just like the work function sequence of clean tungsten, whereas the O-W-1 substrate has a work function sequence $\phi_{110} > \phi_{211} > \bar{\phi} > \phi_{111} > \phi_{100}$, like the so-called "pseudo-clean" pattern of a near monolayer coverage of cesium on clean tungsten.[3]

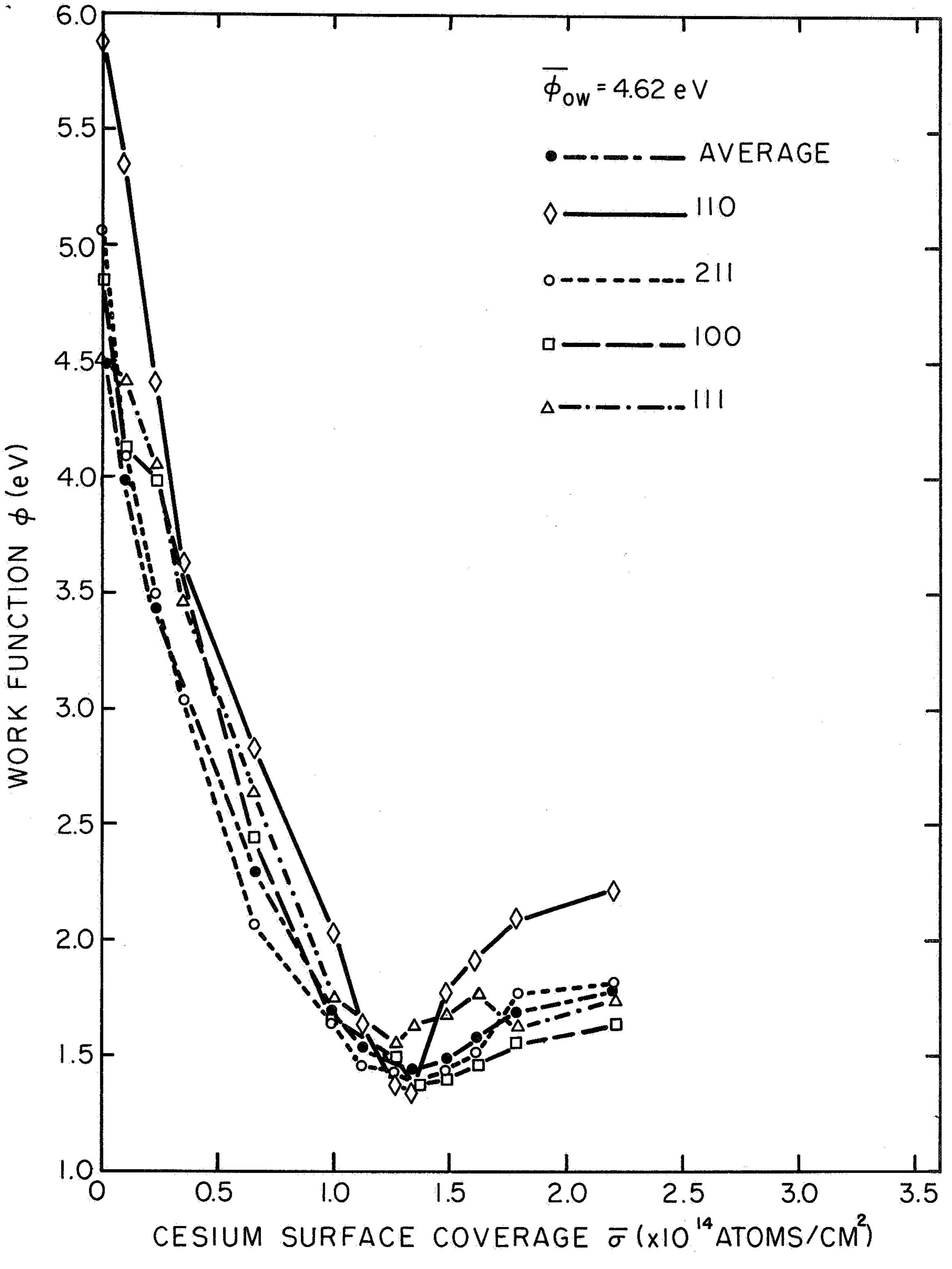

Figure 2. Work function as a function of average cesium coverage for low-index planes of tungsten coated with 0. 5 x 10^{14} atoms/cm^2 average coverage of oxygen.

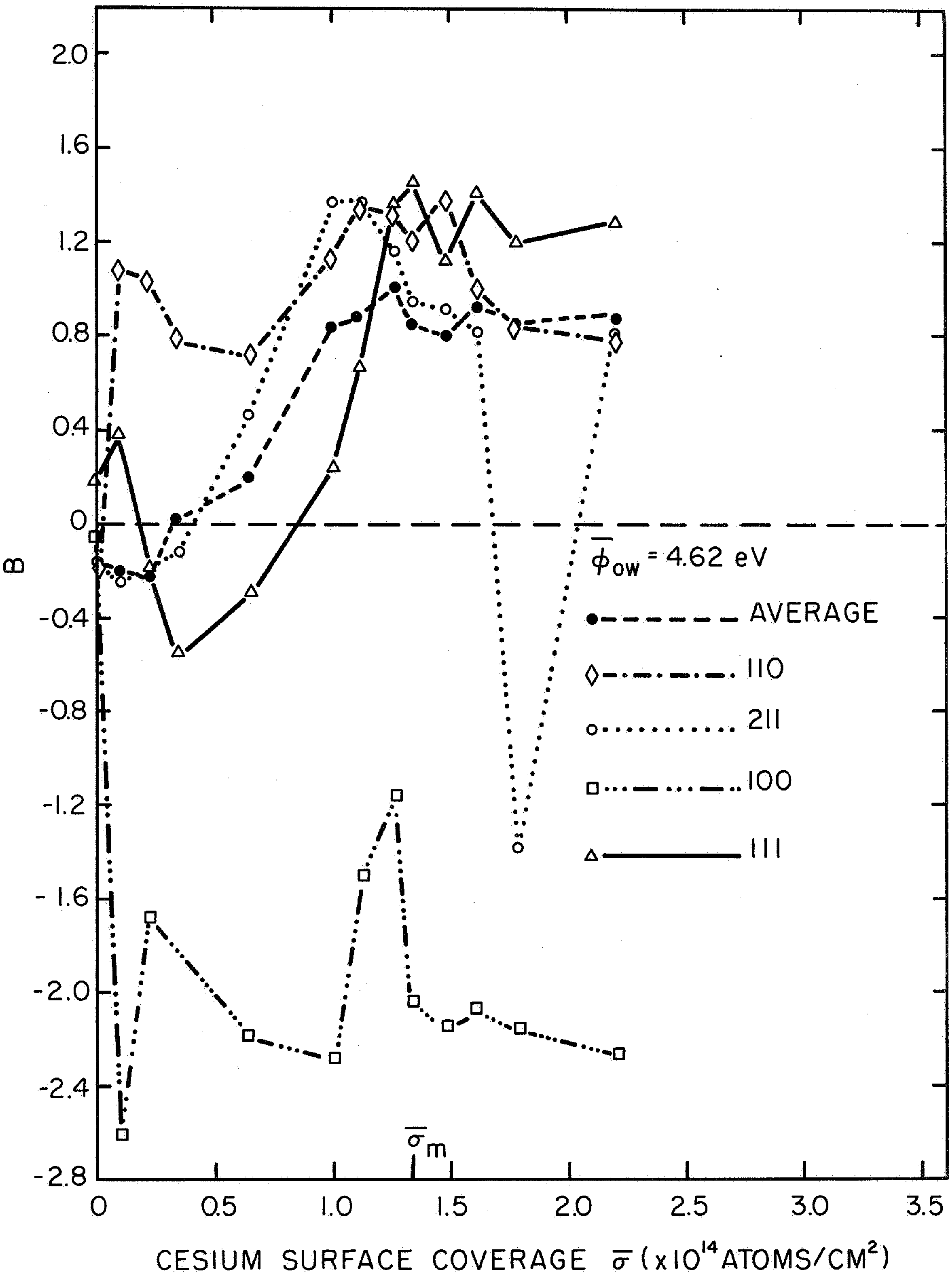

Figure 3. Pre-exponential change B as a function of average cesium coverage for low-index planes of tungsten coated with 0.5 x 10^{14} atoms/cm^2 average coverage of oxygen.

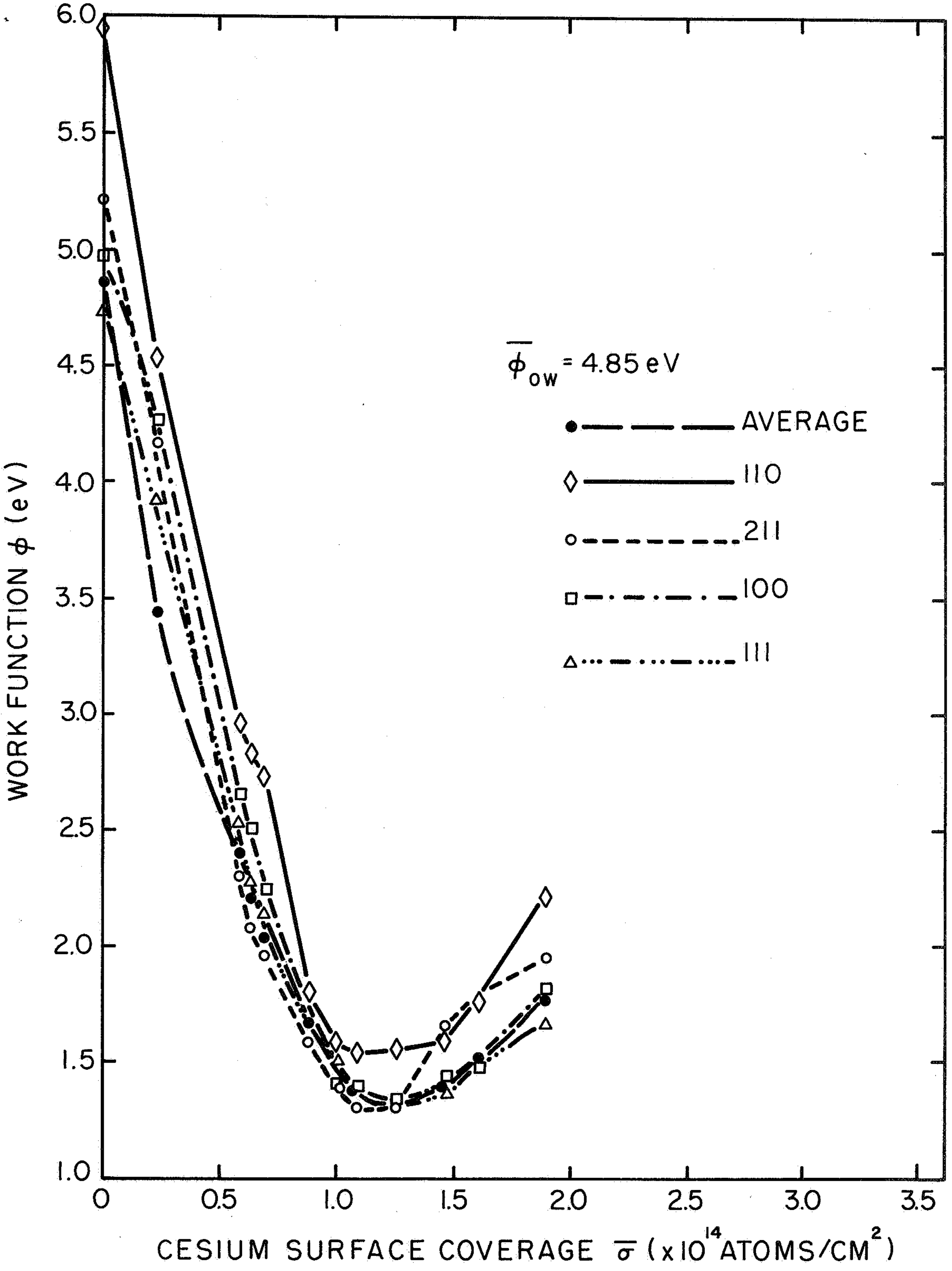

Figure 4. Work function as a function of average cesium coverage for low-index planes of tungsten coated with 1.7 x 10^{14} atoms/cm^2 average coverage of oxygen.

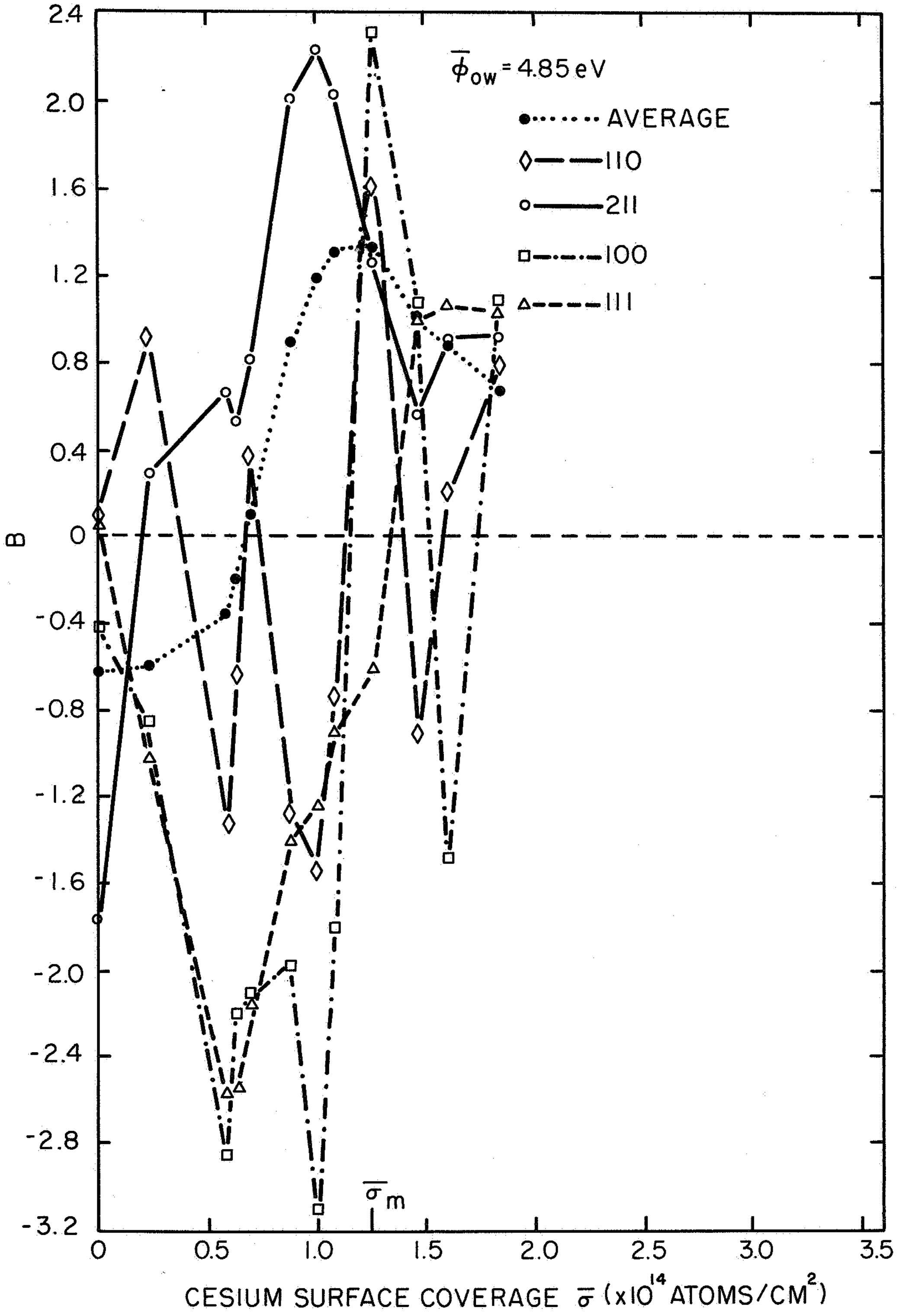

Figure 5. Pre-exponential change B as a function of average cesium coverage for low-index planes of tungsten coated with 1.7 x 10^{14} atoms/cm^2 average coverage of oxygen.

An earlier examination[3] of $\phi(\bar{\sigma})$ for cesium adsorbed on the (110) and (100) planes of clean tungsten showed that $\sigma_m(110) < \bar{\sigma}_m < \sigma_m(100)$, i. e., that $\phi_m(110)$ occurred at a lower coverage than $\bar{\phi}_m$ and that $\phi_m(100)$ occurred at a higher coverage than $\bar{\phi}_m$. The same relationship holds for the initial slopes, $\frac{d\phi}{d\bar{\sigma}}$ $(\bar{\sigma} \rightarrow 0)$, of the corresponding $\phi(\bar{\sigma})$ curves. These relationships were taken[3] to indicate that anisotropies exist in the cesium coverage of clean tungsten such that the (110) plane has a higher than average coverage and the (100) plane has a lower than average coverage. In contrast, for the oxygen-covered surfaces, the minimums in the $\phi(\bar{\sigma})$ curves for the individual planes occur at or very near $\bar{\sigma}_m$ (Figures 2 and 4). Although lack of sufficient low coverage data prevents definite conclusions, it appears that, except for the (111) plane of the O-W-1 substrate, the initial slopes of the $\phi(\bar{\sigma})$ curves for the individual planes have values within a factor of two of the initial slopes of the average curves. This implies that the coverage anisotropies are not as large on oxygen-coated tungsten as they are on clean tungsten.

The $\phi(\bar{\sigma})$ curves for cesium on the (110) and (100) planes of oxygen-coated tungsten are compared with the corresponding curves for clean tungsten in Figures 6 and 7. As oxygen coverage is increased, ϕ_m occurs at lower coverages on both planes, following the trend of the average curves. Like $\bar{\phi}_m$, $\phi_m(100)$ is lowered by increasing oxygen coverage; however, $\phi_m(110)$ has a higher value for the O-W-2 substrate than it does for either the clean or O-W-1 substrate.

The average preexponential terms $\bar{B}$ for cesium on both oxygen coverages behave like $\bar{B}$ for cesium on clean tungsten,[18] in that as coverage increases they are at first slightly negative, then go positive up to a value of about 1 at the higher coverages. For the O-W-1 substrate the B's for the (110), (111) and (211) planes follow the general behavior of $\bar{B}$; the term B_{100} differs considerably from the others by having a value of about -2 over most of the coverage range. The fluctuations in the B's for the various planes of the O-W-2 substrate are considerably larger than for the lesser oxygen coverages.

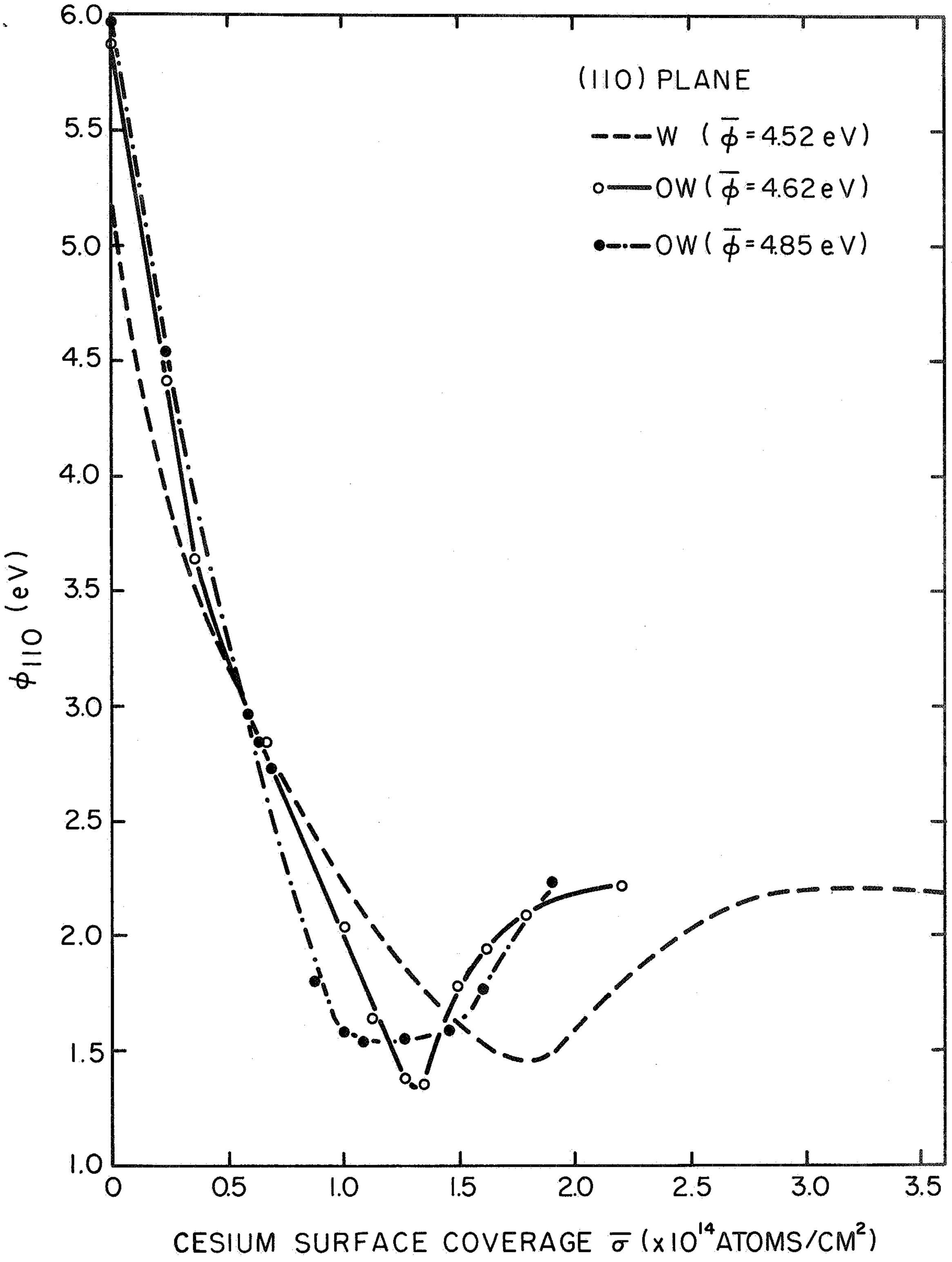

Figure 6. Work function of the (110) plane of tungsten as a function of average cesium coverage for 0, 0.5, and 1.7 x 10^{14} atoms/cm^2 average oxygen coverages.

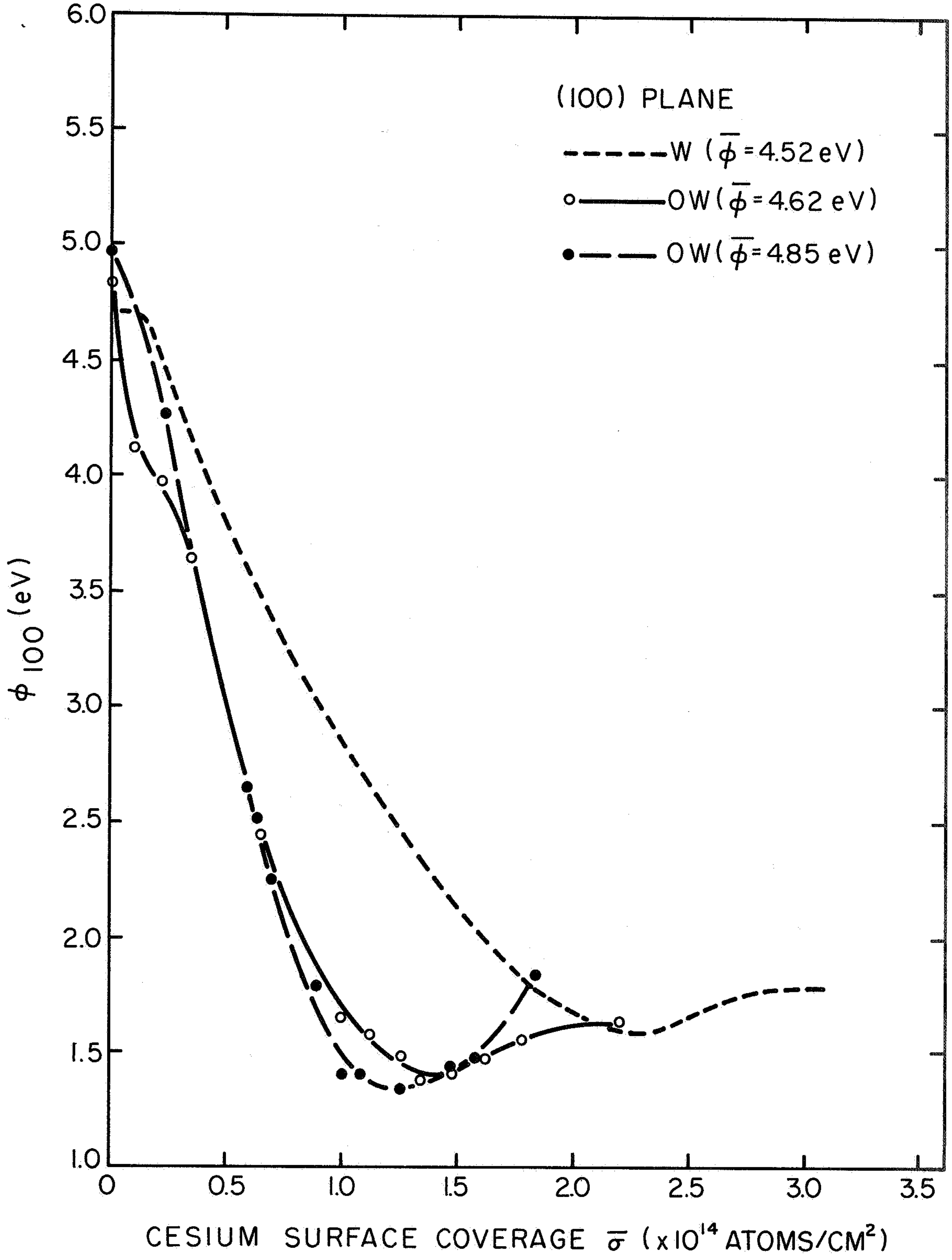

Figure 7. Work function of the (100) plane of tungsten as a function of average cesium coverage for 0, 0.5, and 1.7 x 10^{14} atoms/cm^2 average oxygen coverages.

DISCUSSION

The striking change in the emission distribution of the cesium-coated surface with the addition of small amounts of oxygen can be explained in part by substrate-adsorbate geometric factors, as discussed in Paper I. Reproduced from that paper is Table I, which is a summary, based upon a hard sphere model, of maximum cesium atom density, ratio of oxygen atom density to cesium atom density, and Cs-O bond distances for saturated layers of cesium and oxygen on the various planes of tungsten. As pointed out in Paper I, the hard sphere model permits the oxygen atoms to be partially or completely below the plane of the uppermost tungsten atom layer on the (211), (100), and (111) planes, but not on the (110) plane; furthermore, on the (211) plane each oxygen atom is allowed to contact one overlying cesium atom, thereby maximizing the pair-wise Cs-O interaction. The work function changes measured here, as well as the emission distribution observed earlier[3] in field emission patterns, tend to confirm this model.

TABLE I

Summary of a W monolayer Cs atom densities on various planes of W based on atomic diameter hard sphere model. The ratio σ_{OW}/σ_{Cs} and Cs-O bond distances are based on saturated layers of Cs and O.

Plane	Cs Monolayer Density (Atoms/cm^2 x 10^{-14})	σ_{OW}/σ_{Cs}	Cs - O Distance (Å)
110	3.53	3	3.7
100	2.50	2	4.4
112	4.08	1	3.2
111	1.92	2	5.4

Both of the oxygen coverages investigated here, 0.5 and 1.7 x 10^{14} atoms/cm^2, were well below the theoretical maximum according to Table I; thus the work function changes on any plane with cesium adsorption depend significantly upon the cesium equilibrium coverage distribution. If there were no anisotropies in the coverage distribution, values of the zero coverage dipole moment μ_o could be determined from the initial slopes of the $\phi(\bar{\sigma})$ plots for the various planes by the equation[3]

$$\mu_o = - \frac{1}{g\pi} \left(\frac{d\phi}{d\sigma} \right)_{\sigma \to 0} \tag{7}$$

where g is equal to 4 or 2 depending upon whether or not μ is wholly contained in the adlayer. Although what coverage anisotropies exist at low coverage cannot be ascertained from this data (the low value of the initial slope for the (111) plane of the O-W-1 substrate suggests that its cesium coverage may be lower than average at first; pattern detail also suggest this), the small variation in initial slopes for most planes suggest that the differences in dipole moment on the various planes are small compared to the changes in dipole moment with increasing coverage of either cesium or oxygen.

The dipole moment μ of a cesium layer adsorbed on any plane may be obtained from[3]

$$\phi_{OW} - \phi = g\,\pi\,\mu\,\sigma \tag{8}$$

where $g = 2$ for an induced dipole centered on the plane of electric neutrality, and σ is the local cesium coverage on the plane. At $\bar{\phi}_m$, coverage anisotropies are small compared to the average coverage, and therefore $\sigma_m \cong \bar{\sigma}_m$. Thus for any plane, Equation (8) may be rewritten

$$\phi_{OW} - \phi_m \cong 2\,\pi\,\mu_m\,\bar{\sigma}_m \tag{9}$$

where μ_m is the dipole moment of the adsorbed cesium layer at the minimum work function. In Figure 8, both $\phi_{OW} - \phi_m$, obtained from Figures 2 and 4,

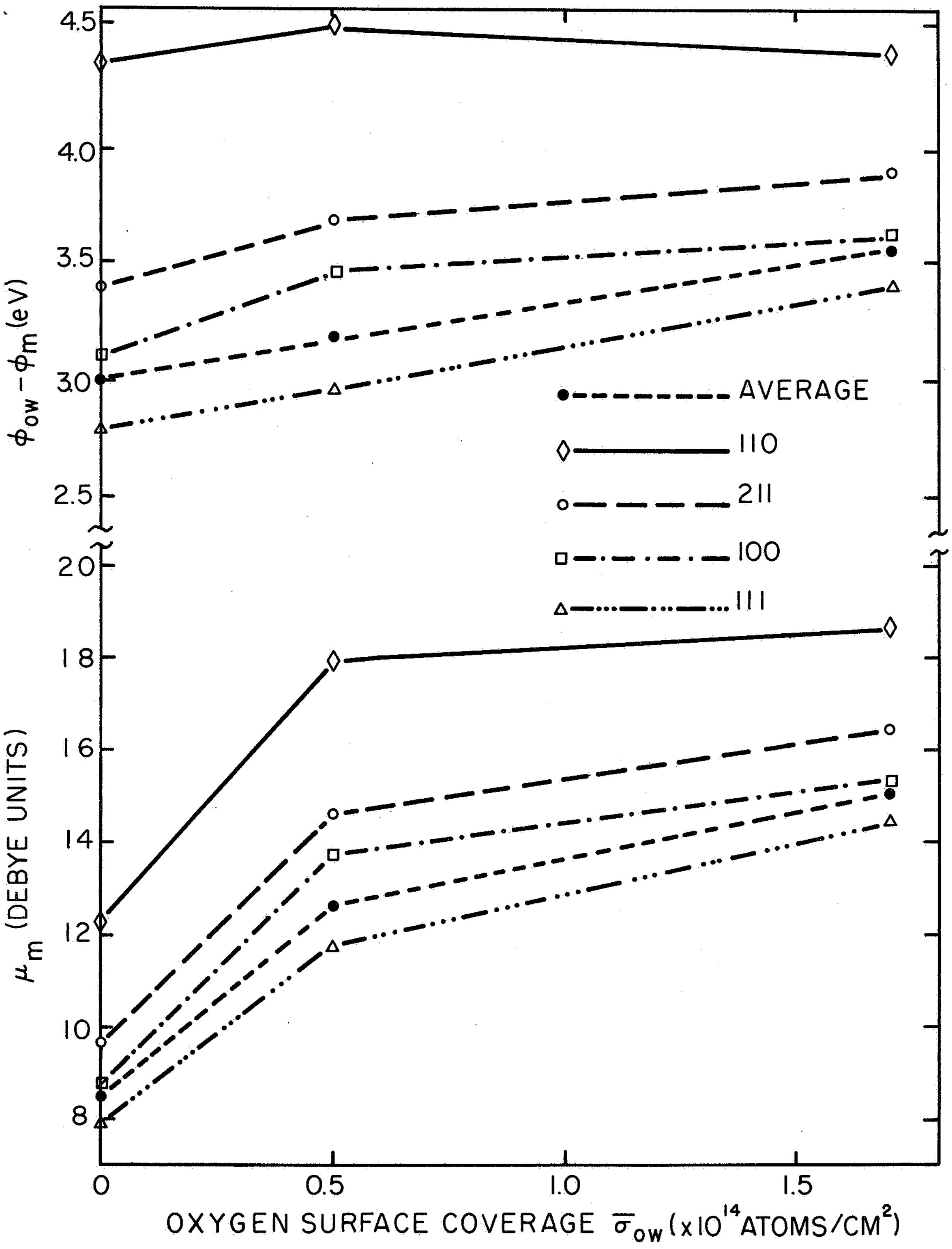

Figure 8. Maximum work function change $\phi_{OW} - \phi_m$ and the corresponding dipole moment μ_m as functions of average oxygen coverage for cesium adsorbed on low-index planes of oxygen-coated tungsten.

and μ_m, calculated from Equation (9), are plotted as functions of average oxygen coverage. Two main observations from these results are: (1) the values of μ_m increase with increasing oxygen coverage on all planes, in agreement with the behavior of $\bar{\mu}_m$ observed earlier;[3] and (2) the curves of $\mu_m(\bar{\sigma}_{OW})$ for the different planes follow the trends of $\bar{\mu}_m(\bar{\sigma}_{OW})$, so that the relative charge distribution about the adsorbed cesium on the various planes is not changed much by the addition of small amounts of oxygen.

As outlined in Paper I, the adsorbate polarizability α may be determined as a function of cesium coverage from measurements of B, ϕ and σ, and by use of the following equation,

$$\frac{\alpha}{\epsilon} = \frac{\log \dfrac{\phi_o t^2(\phi_o, F_o)}{\phi t^2(\phi, F)} - B + 4.42\left(\dfrac{1}{\phi^{1/2}} - \dfrac{1}{\phi_o^{1/2}}\right)}{4.20 \times 10^7 \phi^{1/2} g \pi \sigma}, \qquad (10)$$

where the dielectric constant ϵ is given by

$$\epsilon = 1 + 9 \alpha \sigma^{3/2} \qquad (11)$$

for a Topping array of field induced point dipoles centered on the image plane, and g = 2 for an induced dipole centered on the plane of electric neutrality. The resulting α's for low-index planes of the O-W-1 substrate are given in Table II. When compared to the α's of the (110) and (100) planes of clean tungsten,[3] it is observed that the α's of Table II have more variation with coverage and seem to be more systematic in their variations, e. g., $\alpha(110)$ changes radically at $\bar{\sigma}_m$, and α (211) goes through a maximum at $\bar{\sigma}_m$. It is interesting to note that: (1) the average α's for the (110) and (100) planes of O-W-1 substrate are close to corresponding α's for clean tungsten; and (2) α is the highest on the (211) plane and lowest on the (100) plane. In general, the α's are closer to the atomic value (40 to 60 A^3) than to the ionic value (2.8 A^3). For the O-W-2 substrate, the variations in

B are so large that application of Equation (10) to the data does not give meaningful results; some other as yet unknown mechanism must be in operation.

TABLE II

Calculation of adsorbate polarizability for Cs co-adsorbed on W with an O coverage of 0.5 x 10^{14} atoms/cm^2, according to Equation (10).

$\bar{\sigma} \times 10^{-14}$ (atoms/cm^2)	α (110) (Å^3)	α (211) (Å^3)	α (111) (Å^3)	α (100) (Å^3)
2.20	12.0	24.0	5.9	
1.78	16.5		13.6	
1.61	18.8	60.4	4.0	0.8
1.48	14.6	64.1	15.8	1.7
1.34 ($\bar{\sigma}_m$)	65.4	72.5	8.0	6.3
1.26	52.8	44.2	15.3	33.6
1.12	27.6	31.3	34.4	14.5
1.00	17.9	16.4	52.2	
0.65	13.9	41.8	46.8	
0.35		59.3	58.1	
0.22		66.8	26.8	
0.10			25.0	
Average	26.6	48.1	25.5	9.5
Average (clean W)	23.0			13.0

REFERENCES

1. I. Langmuir and K. H. Kingdom, Phys. Rev. 34, 129 (1929).
2. D. S. Villars and I. Langmuir, J. Am. Chem. Soc. 53, 486 (1931).
3. L. W. Swanson and R. W. Strayer, J. Chem. Phys. (in press).
4. E. D. Wolf, Rep. on the 25th Ann. Conf. on Physical Electronics, M. I. T. (1965), p. 57.
5. B. E. Evans, L. W. Swanson, and A. E. Bell (submitted to Surf. Sci.)
6. A. E. Bell, L. W. Swanson, and L. C. Crouser, Surf. Sci. (in press).
7. A. van Oostrom, Philips Res. Rep. Suppl. , Netherlands, N. 11 102 (1966).
8. E. W. Müller and R. D. Young, J. Appl. Phys. 33, 91 (1962).
9. R. E. Weber and L. F. Cordes, J. Sci. Instr. 37, 112 (1966).
10. R. Gomer and D. Zimmerman, Rev. Sci. Instr. 36, 1046 (1965).
11. D. L. Fehrs and R. E. Stickney, Surf. Sci. 8, 267 (1967).
12. L. F. Cordes, Rep. on the 26th Ann. Conf. on Physical Electronics, M. I. T. (1966), p. 213.
13. R. Gomer and J. K. Hulm, J. Chem. Phys. 27, 1363 (1957).
14. R. H. Good, Jr. , and E. W. Müller, Handbuch der Physik 21, 176 (1956).
15. F. M. Charbonnier and E. E. Martin, J. Appl. Phys. 33, 1897 (1962).
16. L. W. Swanson and L. C. Crouser, Phys. Rev. (in press).
17. T. H. George and P. M. Stier, J. Chem. Phys. 37, 1935 (1962).
18. L. W. Swanson, et al. , Final Report, Contract NAS3-2596, Field Emission Corp. (1964), p. 28.

LIST OF ILLUSTRATIONS

SECTION II

III. STUDIES OF THE ADSORPTION AND DESORPTION OF MERCURY ON CLEAN AND OXYGENATED TUNGSTEN

Mercury as an adsorbate is somewhat unique since it represents the special case of metallic adsorption by a monatomic adsorbate in which the ionization potential (I_a = 10.2 V) is considerably greater than that of most metallic adsorbates studied thus far. A study of the surface kinetics of mercury adsorption and coadsorption with oxygen on tungsten is of interest because of its similarity to electronegative adsorbates.[1] Thus a study of the mercury-tungsten system extends the experimental base upon which to formulate empirical and theoretical models of metallic adsorption.

FIELD DESORPTION OF MERCURY ON TUNGSTEN

Ionic desorption of an adsorbate occurs under the influence of a sufficiently high positive field. This process, known as field desorption, is of considerable interest because a quantitative study of field desorption rates offers a fairly direct approach to the determination of the shape of the potential-energy profile for the interaction between adsorbate and substrate.[2]

One of the primary requirements for performing quantitative rate studies of field desorption is the necessity of operating at temperatures below which the adsorbate is mobile; otherwise, the region from which the adsorbate is field desorbed can be replenished from the emitter shank. The mercury-tungsten system is particularly suitable for field desorption studies because the ratio of diffusion energy to desorption energy E_d/E_p is large throughout the coverage range.

Results of preliminary studies[1] established the values of electric field required to initiate field desorption of mercury as a function of coverage at 200°K. These results showed that the field required to initiate field desorption increased from 100 MV/cm at monolayer coverage to 190 MV/cm at zero coverage.

Experimental Procedures and Results

Field desorption rates are a very sensitive function of the applied voltage, therefore it was necessary to design the field emission microscope used for these studies in such a way that a field of greater than 200 MV/cm at the tip of the cleaned field emitter could be obtained with an applied dc voltage of less than 13 kV, the maximum stable voltage obtainable with existing equipment. Accordingly, a small (.200 in.) diameter ring was positioned .250 in. from the emitter. With this field defining ring and careful thermal cleaning of the emitter, the ratio of electric field at the tip to applied voltage F/V was $1.7 \times 10^{4} \text{cm}^{-1}$, thus, at 13 kV the field at the tip (220 MV/cm) was sufficient to do the experiment.

A provision for depositing reproducible amounts of mercury onto the emitter was made by condensing high purity mercury onto a thin heatable platinum disk that was held at 77°K by either immersing the entire tube or the small appendage containing the platinum disk in liquid nitrogen. Mercury could be vaporized onto the emitter by resistively heating the platinum disk by means of a well-controlled electronic servo-circuit.

Before mercury was allowed into the main body of the tube, it was established that a negative screen potential of 13 kV across the tube had negligible effect. However, after dosing several times at 77°K with large doses of mercury, a negative voltage of only 8 kV applied to the screen caused an arc in the tube. Subsequent experiment showed that the source of the arc was the mercury covered emitter assembly. In previous work,[1] it was observed that a dc field of only 25 MV/cm applied to a heavily mercury covered surface ($\theta \gtrsim 1.5$) caused small protuberances to be pulled out. The conclusion to be drawn from the above experiment is that these arcs are associated with the actual fracture of these small protuberances that are drawn out by the applied field.

The arcs in the experimental tube terminated the experiment before sufficient data was obtained. However, it was found that at relative coverages of less than 0.5 a field of 220 MV/cm could be applied without causing an arc. Termination of the contract period disallowed the securing of further results.

COADSORPTION OF MERCURY AND OXYGEN ON TUNGSTEN

The study of the adsorption, desorption, surface diffusion and work function change of mercury on clean tungsten showed that in many ways the surface bonding of mercury was similar to that of electronegative adsorbates. In order to secure additional information on coadsorbed systems involving electronegative and electropositive coadsorbates, the Hg/O/W system was studied. Combining the data obtained from this study with that obtained from the Cs/F/W and Cs/O/W systems, it was anticipated that the basic interactions involved in the dipole moment enhancement could be established.

Experimental Procedures

This study was performed using a standard field emission microscope with a mercury source such as that described in preceding field desorption section and an oxygen source. The oxygen source consisted of the well-known in situ formed copper oxide, which yields a pure source of oxygen when heated above $500^{\circ}K$. The average work function change was measured using standard "Fowler-Nordheim" plots in the usual method.

Results and Discussion

In the present study we have investigated Hg adsorption on a W surface containing a small amount of preadsorbed oxygen which was equilibrated at $500^{\circ}K$ prior to Hg deposition. The results are summarized in Figure 1(b) for $\phi_{OW} = 4.63$ eV which corresponds to an O coverage of $\sim 1 \times 10^{14}$ atoms/cm^2.

Comparing these results with Hg adsorption on clean W, shown in Figure 1(b) we note that the primary influence of O is to reduce the maximum of ϕ from

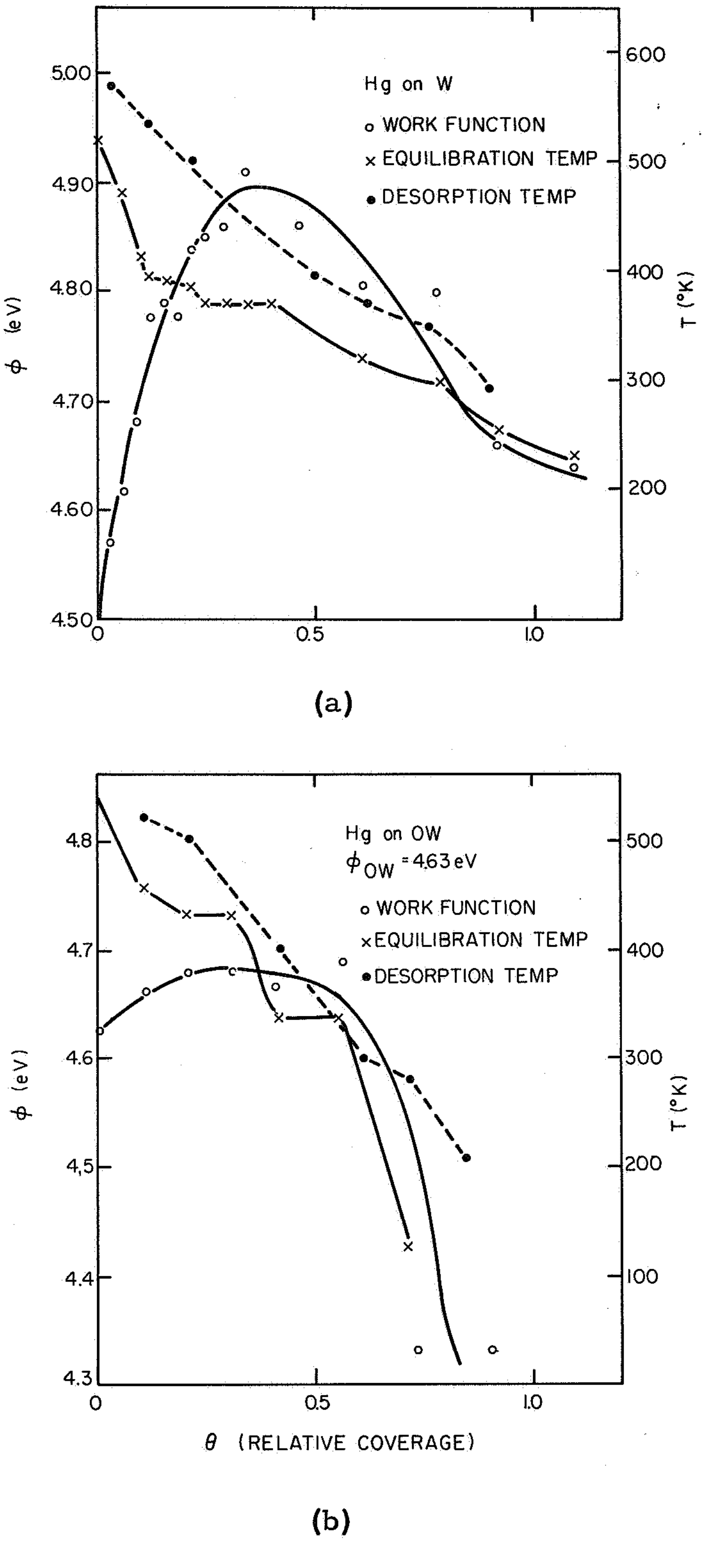

Figure 1. Curves show the dependence of work function, equilibration and thermal desorption temperature upon Hg coverage on W (a) and OW (b).

4.9 eV for clean W to 4.68 eV. The terminal desorption temperature of Hg from clean W is approximately 590°K, whereas from the oxygenated surface Hg is removed at a slightly lower temperature, i. e., ~ 530°K. On the other hand, the equilibration temperature, which is a measure of the surface mobility of Hg, is essentially unchanged by the presence of this amount of O.

Before a definitive picture of the Hg/O/W system can be obtained, the above work should be carried out at higher oxygen coverages. It appears, however, from this initial work that O reduces the magnitude of the negative dipole moment for adsorbed Hg. This is in agreement with the general observation from the more electropositive adsorbates, e. g., Cs. Namely, the chemisorbed O layer causes a shift in electronic charge density from the adsorbed atom toward the substrate, either by chemical interaction or local polarization, thereby increasing positive or decreasing negative dipole moments of the admetal atom.

REFERENCES

1. L. W. Swanson, R. W. Strayer, L. E. Davis, Surf. Sci. (to be published).

2. L. W. Swanson and R. Gomer, J. Chem. Phys. <u>39,</u> 2813 (1963).

N68-16764

IV. STABILITY STUDIES OF FIELD EMISSION CATHODES

INTRODUCTION

It has been observed that the emission properties of zirconium and oxygen coadsorbed on tungsten field emission cathodes at room temperature are quite stable during low current density operation, but the low work function coating seems to deteriorate as the current density is raised to practical levels. It has also been found that operation of these cathodes at elevated temperatures (1000-1200°K) seems to inhibit this deterioration, and therfore enhance the stability and practicality of such a cathode. Operation at elevated temperatures requires relatively large expenditures of power in resistive heating of filaments, and transformers, necessary for heating, add weight to any practical device thereby reducing its attractiveness as a small package, lightweight device. Also, operation at elevated temperatures dictates a large energy spread in electron energy distribution which for some applications is not acceptable. A cathode life study of zirconium and oxygen coadsorbed on tungsten field emission cathodes was initiated in order to gain insight into the life and stability of low work function coated tungsten field emission cathodes. The main interest lay in the determination of mechanisms involved in cathode emission current deterioration during operation and the possibility of increasing the stability and life of such a cathode by minimizing effects contributing to coating deterioration. The attractive feature of the zirconium-oxygen coating on tungsten is the confinement of emission to the (100) plane which improves the electron optical features of the cathode.

There are two physical processes by which field emitted current from a clean surface may vary with time. One is geometric change in the emitter surface caused by bombardment of high energy positive ions formed in the gas phase or at the anode surface. The other process involves work function change due to adsorption of neutral gas molecules on the emitter surface. Since ionic bombardment roughens the surface, microscopic protrusions are usually formed which enhance the local electric field and, hence, current. Gas adsorption, on the other hand, nearly always increases the work function, thereby decreasing the field emission current. In the case of an adsorbate coated emitter which lowers the work function, ionic bombardment may not only roughen the surface, but also sputter the low work function adsorbate, thus leading to a current decrease with time.

In view of the fact that current instability occurs even in high vacuum field emission tubes and is generally proportional to the emitted current, it appears plausible that both ionic and neutral bombardment of the emitter is caused by the now well-known process of electron induced desorption of ions and neutrals from the anode surfaces. The specific purpose of this study is to examine the origin of these ions by attempting to suppress ionic bombardment of the emitter by creating potential saddles for ions in front of the emitter surface and by reducing the collected electron energy below the threshold for electron induced desorption.

EXPERIMENTAL TUBE

A schematic diagram of the first tube used in this experiment is shown in Figure 1. By operating the tube in an axial magnetic field, the emitted electrons could be confined to a small diameter beam and collected in a Faraday cup at various voltages . By placing a screen grid in front of the Faraday cup, all secondary electrons created at the Faraday cup could be suppressed from returning to high voltage electrodes where ions could be created. A circular resistively heatable zirconium source was placed in front of the emitter such that direct interception with the electron beam was impossible. The anode consisted of a tungsten disc, phosphor-coated for pattern viewing purposes with a 1/4 inch diameter aperture in the center. The beam could be focused through the aperture and collected in the Faraday cage when the tube was immersed in the magnetic field.

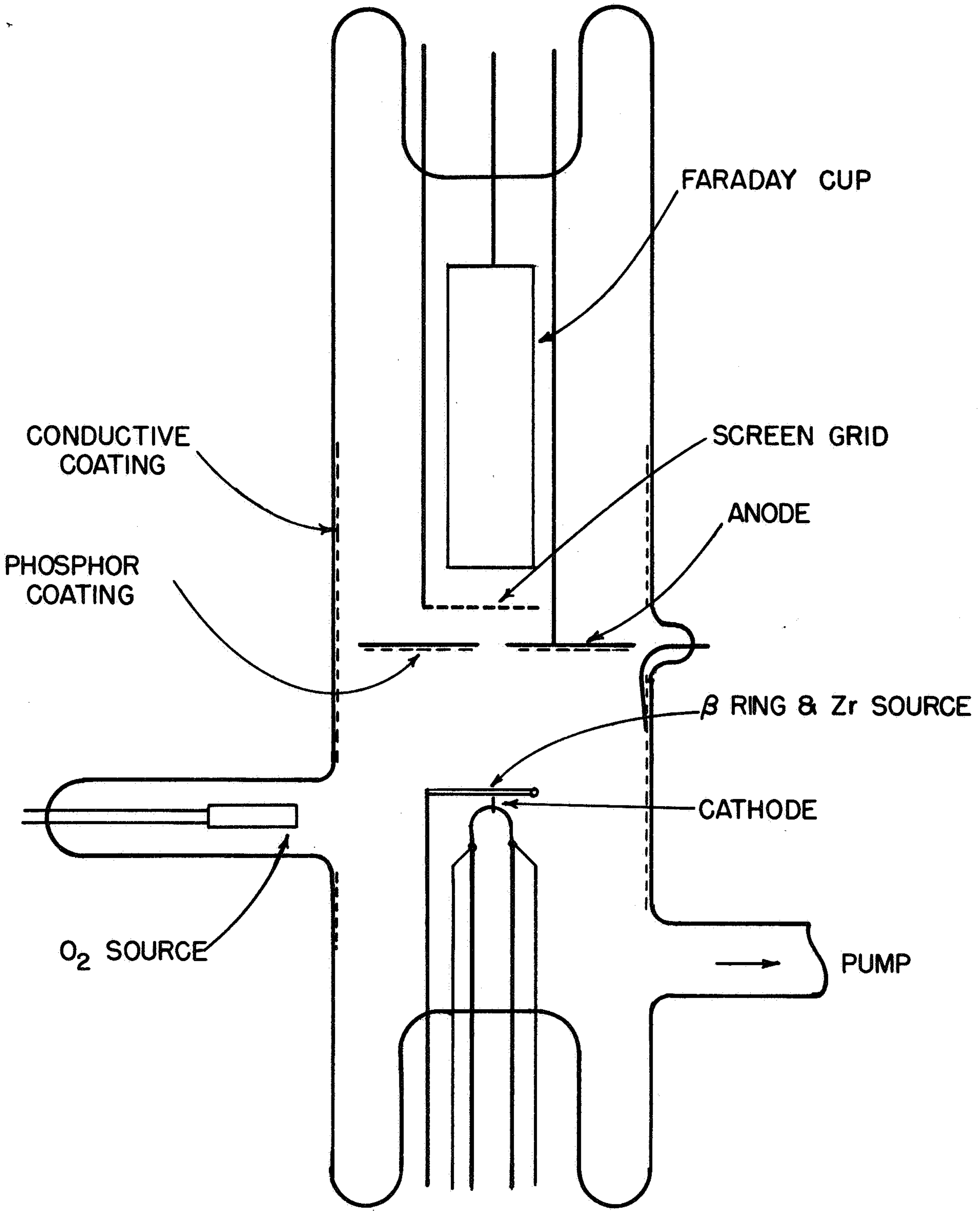

Figure 1. Diagram of first tube designed to eliminate ion bombardment of the cathode.

The tube was operated in two basic modes. One mode was as a simple diode in which all elements, except the tip assembly, were tied electrically to the anode voltage. In this mode of operation ions and neutrals formed at the anode could return to the negative emitter assembly. In the second mode of operation the zirconium source was employed as the most positive element, the phosphor-coated electrode and suppressor electrode were operated in the voltage range 20-50 V so as to maximize current collection at the Faraday cup and minimize current collection elsewhere. The primary reason for operating the phosphor-coated electrode at low voltages was to maximize beam transmission through the aperture. In this operational mode a positive potential hump formed by the β ring prevented ions formed on other electrode elements from returning to the emitter. Also the collector voltage was varied continuously to examine the effect of collected electron energy on emitter stability.

It was found that the magnet the tube had been designed to fit did not have a large enough axial field to completely confine the beam as it was decelerated causing a loss in transmission as the voltage of the collector electrode was lowered.

A second tube was designed and constructed which more effectively utilized an axial magnetic field for confining the electron beam. A schematic diagram of the tube employed in this experiment is shown in Figure 2 and is quite similar in design to the first tube. The basic difference is in the envelope design which permits the tube to be immersed in the magnetic field of a horseshoe-type magnet to achieve better beam confinement. Another change to achieve more effective shielding of the cathode with respect to ions formed at the collector electrode was construction of electrode A from a 5/8 inch diameter molybdenum cup with a 150 mil aperture in the center for passage of the electron beam. This design was expected to yield good collection of the electron beam in the Faraday cage D at electron energies below electron impact desorption values and essentially eliminate ion and neutral production by electron impact. It was found however, that the screen

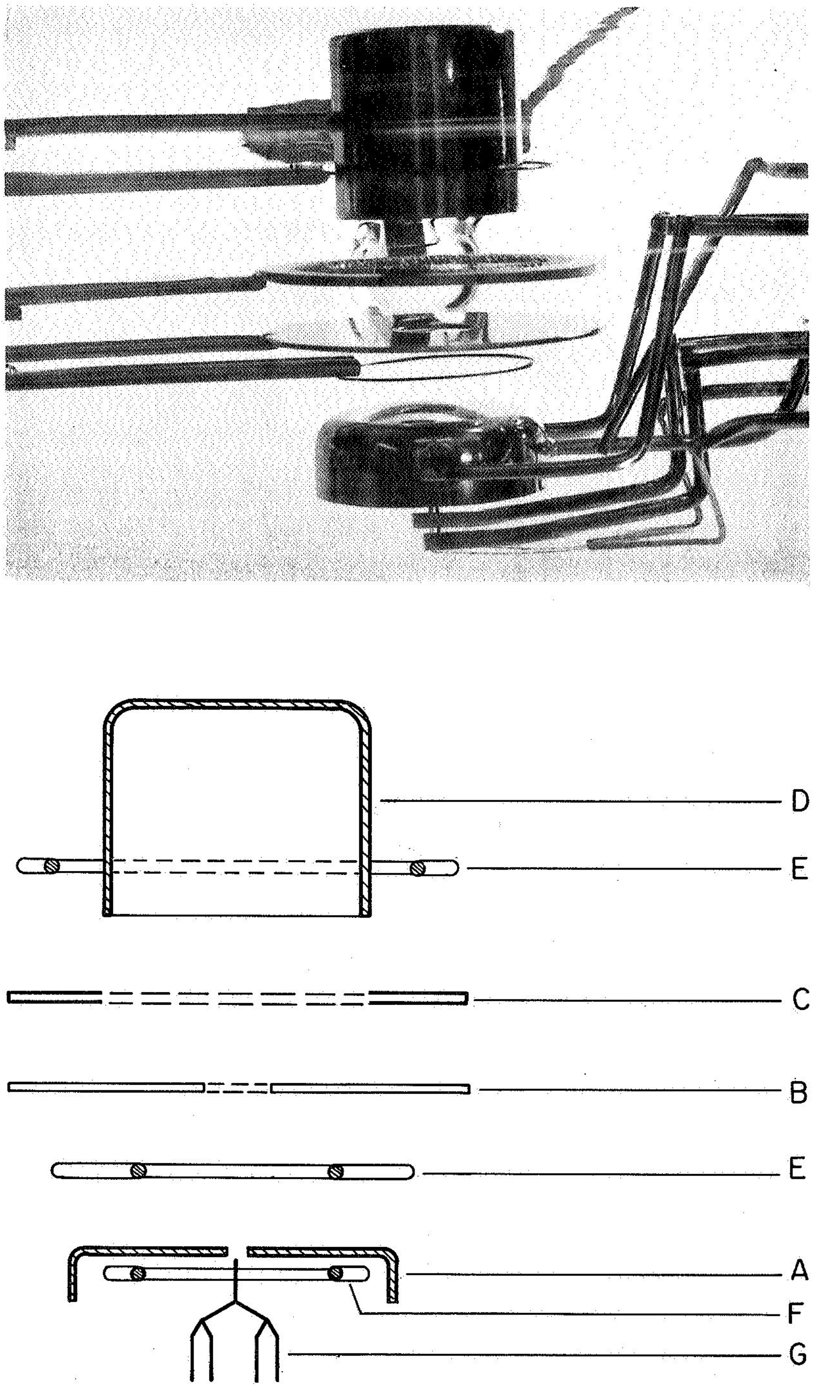

Figure 2. Schematic diagram and photograph internal components of the second life test tube showing: A - first electrode, B - second electrode, C - screen grid, D - Faraday cup, E - outgasing filaments, F - zirconium source, and G - cathode.

grid C, placed in front of the Faraday cage to suppress secondaries and reflected electrons, was a source of secondary or reflected electrons itself. Even though the suppressor screen was highly transparent, it was found nearly impossible to prevent the secondary electrons formed at the screen from returning to electrode A (which was the anode) where they were collected at high energy. This effect occurred even though the electrode B was held at cathode potential and seemed to be the result of field lines from the electrode A bulging through the aperture of electrode B, thereby causing electrons from the screen to be accelerated back to electrode A.

EXPERIMENTAL RESULTS

The emitter of the first tube was coated with a low work function Zr/O coating by heating the poorly outgassed Zr source after which the tube was operated at $\sim 1.5\ \mu A$ for 10 to 15 minute periods with various collection voltages on the Faraday cup. The current was monitored continuously for each voltage so that a plot could be made of current vs time. From this graph an average value of the rate of change of current dI/dt could be obtained for each voltage on the Faraday cup. It was then possible to plot dI/dt vs collector voltage in order to measure the stability of the emitted current as a function of voltage at which the electrons were collected. The tube was also operated as a simple diode at the same current as previously mentioned without any attempt to suppress electron ion tip bombardment. A value of $(dI/dt)_o$ could be found for this mode of operation and compared with each dI/dt data point found previously to obtain a percentage of improvement of stability (i. e. , $1 - (dI/dt) / (dI/dt)_o$) with respect to diode operation as shown in Figure 3. The points in excess of 100% represent a reversal in sign of dI/dt. Also shown in Figure 3 is the fraction of total current I_t being collected at the zirconium source I_β. The current I_β originates from reflected primaries or secondaries from the phosphor-coated electrode.

For the second experimental tube it was found that for good collection of the primary beam current I_t in the Faraday cage (>99% of the emitted electrons)

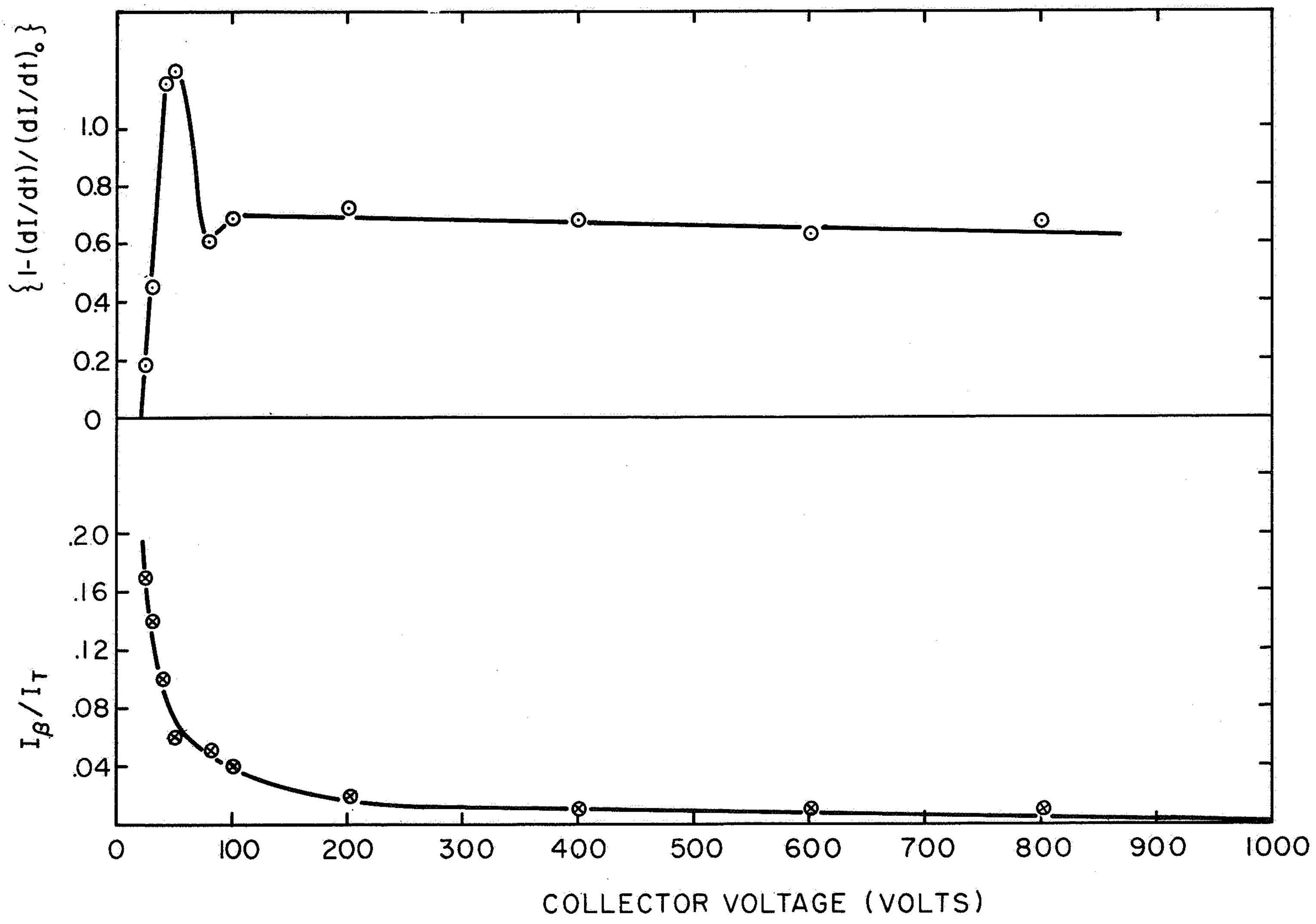

Figure 3. The upper curve shows the percent increase in time stability of the field emission current over straight diode operation when the current is collected at the various indicated voltages. The lower curve shows the ratio of current collected at the β-ring to total current as the collector voltage is increased. The value of I_t was 1.5 μA throughout the voltage range.

it was necessary to operate the Faraday cage at voltages of the order of the electrode A. In so doing, it was found that secondaries created at the screen grid were then attracted to the positive Faraday cage. Collection of electrons at the higher energies resulted in electron impact desorption of ions and neutrals at the cage and acceleration of these ions back toward the cathode. However, since the first electrode was normally the highest positive element in the tube, a positive potential hump was formed and thus prevented ions created on all but the first electrode from returning to the cathode G. By operating the tube in this manner, it was possible to achieve excellent collection at the Faraday cage, suppress ions from bombarding the cathode and prevent secondaries from returning to the electrode A where more ions might be created. Table I gives the operating voltages and the current ratios measured at the various elements of the tube shown in Figure 2.

Operation of the second tube in the mode described above was carried out for a Zr/O coated and clean tungsten cathode and was compared with operation of the tube in a simple diode configuration. Figure 4 shows the results of operation in the two modes for both clean and coated tungsten cathodes.

TABLE I

Electrode Potentials and Current Ratios for Figure 4 Data

Run	V_A(kV)	V_B(Volts)	V_C(Volts)	V_D(kV)	I_D/I_t	I_A/I_t
A	3. 9	490	98	3. 8	. 99	. 01
B	6. 4	0	99	6. 3	. 99	. 01
C	3. 8	3. 8	3. 8	3. 8	---	---
D	6. 1	6. 1	6. 1	6. 1	---	---

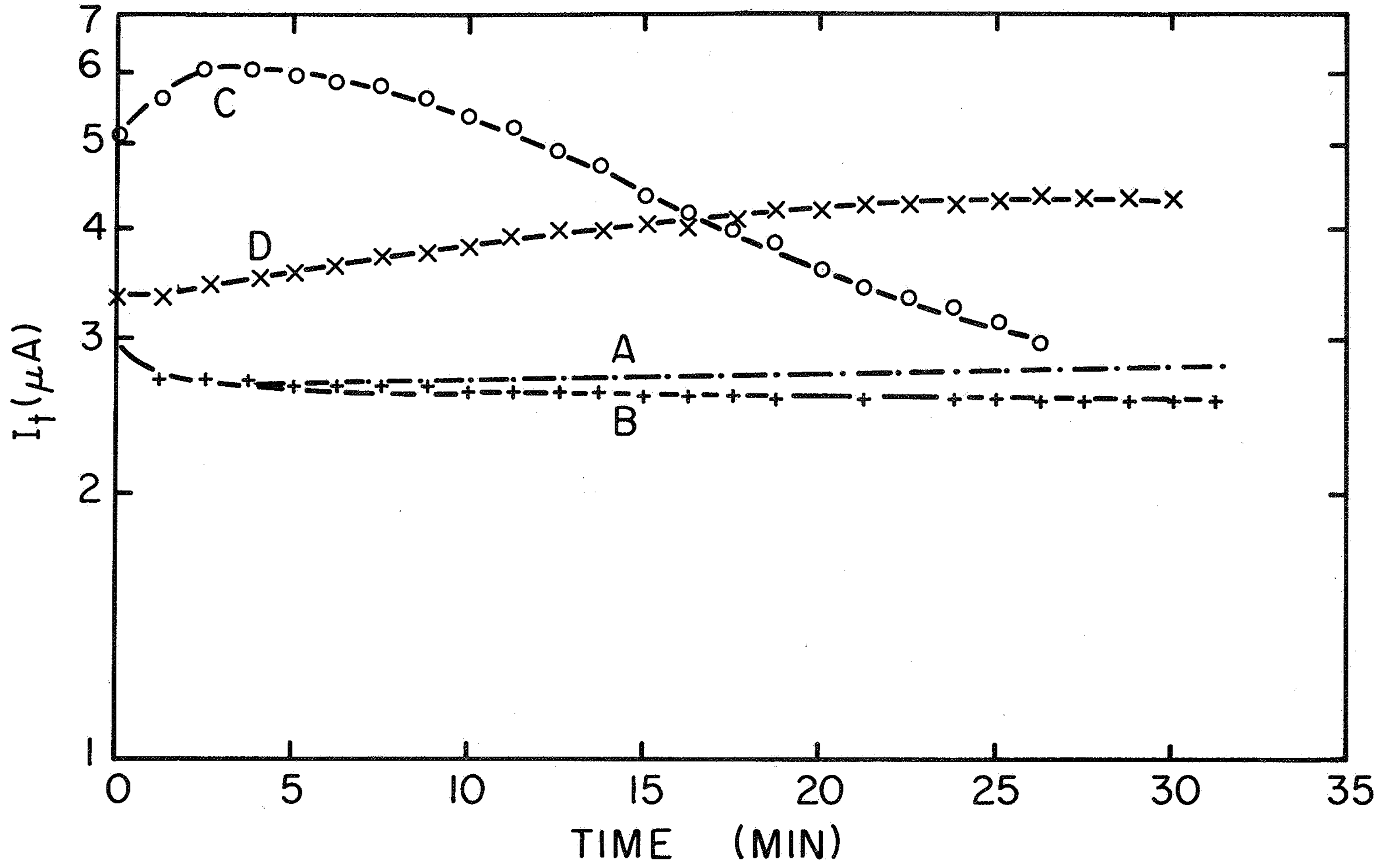

Figure 4. Stability tests taken with (A, B) and without (C, D) ion and secondary trapping for both clean (B, D) and zirconium coated (A, C) tungsten. Electrode operating parameters given in Table I.

CONCLUSIONS

The data obtained in these experiments yields some interesting evidence of the effects of the stability of zirconium-oxygen surface coatings on tungsten field emitters. First, it must be pointed out that the relationship between operating conditions of the ion suppression mode and the simple diode mode are quite different. When operated in the ion suppression mode nearly all electrons are collected in a Faraday cup on clean metal surfaces, whereas operation in the diode mode did not limit electron collection to any one surface. Metal, phosphor-coated metal and tin oxide-coated glass were all bombarded by high-voltage electrons in the diode mode, so it is not surprising that a 60 to 70% improvement in current stability is observed between the two modes of operation, due to the difference in cleanliness of the surfaces bombarded.

In the first tube it was found that very little improvement in cathode deterioration rate was observed between collection voltages of 800 and 100 volts. This is probably a result of the fact that ion bombardment has been practically eliminated, and the effect of neutral capture by the tip results in a constant rate of coating deterioration in this voltage range. It is also shown in Figure 3 that a small fraction of the total current is not collected in the Faraday cup and is either reflected or creates secondaries which return to the zirconium source where ions and neutrals can be created by electron bombardment, neither of which can be prevented from striking the tip. Between 100 and 50 volts the coating deterioration rate improves rapidly and the rate of change of dI/dt becomes positive. This effect appears to be the result of approaching the threshold for electron induced desorption of gas atoms from the bombarded surface, resulting in a rapid decrease in the neutrals returning to the tip. Ion bombardment of the tip is not changed however, since ions originating at the β ring can continue to bombard the emitter. Apparently there is a balancing of effects--- on one hand, ion bombardment, which causes an increase in current due to surface roughening, and on the other, neutral adsorption, which causes a decrease in current due to an increase in work function. The rapid change of direction of the cathode deterioration rate between 0 and 50 volts seems to be the result of the effect of space charge enlarging the electron beam, and thereby increasing I_β/I_t such that the deterioration rate approaches that of diode operation. The close proximity of the zirconium source to the emitter probably enhances the deterioration rate.

Operation of the second tube in the ion and secondary suppression mode shows marked improvement in cathode performance. The fact that ion bombardment of the cathode causes the current from the Zr/O coated cathode to decrease and from the clean tungsten cathode to increase with time is a demonstration of the different effects of ion bombardment on the two surfaces. A deterioration of the coating leads to an increase in the work function toward that of the clean substrate. On the other hand, ion bombardment of the clean surface results primarily in a roughening of the surface, which in turn leads to field enhancement and a resulting rise in current.

Elimination of ions from striking the cathode greatly improves the stability for both cases of clean and Zr/O coated tungsten cathodes. For the Zr/O surface, a rapid drop during diode operation is changed to a slow increase in current when the cathode is operated in the ion suppression mode. The same behavior is observed in the clean tungsten case, only the effects are reversed; a fairly rapid increase in current during diode operation is changed to a slow decrease in current during ion suppression operation. Since collection of the electrons at the collector surface was well above the threshold for electron induced desorption of ions and neutrals, it is probable that the small changes in current with time observed during the ion suppression mode of operation was caused by neutral species desorbed from the collector surface which readsorbed on the emitter during operation.

It seems reasonable to assume that two effects involved in the current instability of Zr/O/W coated field emitters are neutral and ion bombardment of the tip during operation. Neutral adsorption apparently causes a negative dI/dt whereas ionic bombardment causes a positive dI/dt. More stable operation of this type of cathode coating results from collecting electrons on low voltage, clean surfaces which reduces the probability of electron desorption of adsorbed gases. The presence of a positive potential hump in front of the cathode also greatly aids in increasing the stability of the Zr/O/W surface.

LIST OF ILLUSTRATIONS

SECTION IV

Figure

1 Diagram of first tube designed to eliminate ion bombardment of the cathode.

2 Schematic diagram and photograph internal components of the second life test tube showing: A - first electrode, B - second electrode, C - screen grid, D - Faraday cup, E - outgasing filaments, F - zirconium source, and G - cathode.

3 The upper curve shows the percent increase in time stability of the field emission current over straight diode operation when the current is collected at the various indicated voltages. The lower curve shows the ratio of current collected at the β - ring to total current as the collector voltage is increased. The value of I_t was 1.5 μA throughout the voltage range.

4 Stability tests taken with (A, B) and without (C, D) ion and secondary trapping for both clean (B, D) and zirconium coated (A, C) tungsten. Electrode operating parameters given in Table I.

V. TOTAL ENERGY DISTRIBUTION STUDIES OF FIELD EMITTED ELECTRONS FROM CLEAN MOLYBDENUM

INTRODUCTION

The measurement of the total energy distribution (TED) and current voltage characteristics from field emitters has provided information concerning the surface work function and more recently certain details of the bulk electronic band structure.[1]

The TED measurements reported earlier[1] for the $\langle 310 \rangle$, $\langle 111 \rangle$, $\langle 116 \rangle$, $\langle 112 \rangle$, $\langle 100 \rangle$ and $\langle 110 \rangle$ directions of W have shown adequate agreement with theory along all but the $\langle 110 \rangle$ and $\langle 100 \rangle$ directions. The $\langle 110 \rangle$ data yielded an unusually large value of ϕ_e ranging from 6.4 to 8.8 eV, whereas (using $\bar{\phi}_o = 4.52$ eV) values of ϕ_f ranged from 5.7 to 6.0 eV. Both of these measurements compare unfavorably with thermionic values which are reported in the range 5.0 to 5.3 eV. Young showed that patch field corrections can be important for the $\langle 110 \rangle$ direction of W[2]; however, the correction leads to even larger values of ϕ_e and thereby enhances the discrepancy between field emission and thermionically measured work function values of the $\langle 110 \rangle$. Recently, an explanation of the large values of ϕ_e in terms of electron pair emission was rejected by experimentation[3]. Thus, it is not clear at the moment why TED measurements lead to unusually large values of ϕ_e. Some possible alternative explanations are (1) band structure effects or (2) failure of the one-dimensional WKB approximations.

It is along the $\langle 100 \rangle$ direction that band structure effects are clearly manifested as shown in Figure 1. The "hump" which occurs 0.35 eV below E_f is attributed to a separation of the Δ_7 band along the $\langle 100 \rangle$ direction as shown in Figure 2 and which leads to a band splitting whose magnitude depends upon the degree of spin-orbit coupling[4]. For W the spin-orbit coupling is believed sufficient to raise the upper Δ_7 band above the Fermi level as shown in Figure 2 e. In contrast, for Mo the spin-orbit coupling is believed to be

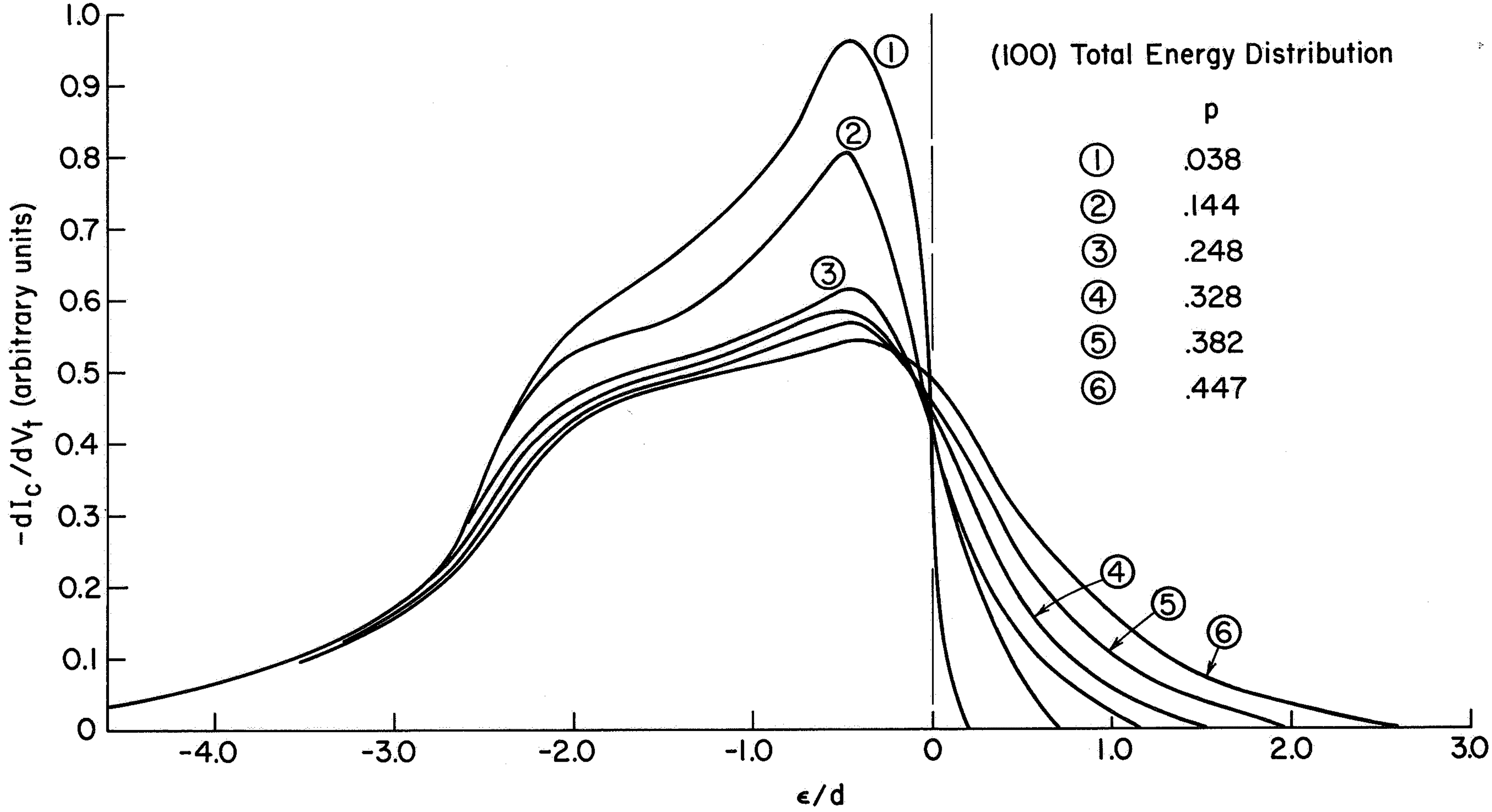

Figure 1. Experimental total energy distribution plots along the ⟨100⟩ direction of a W emitter as a function of p where d = 0.174 eV and F = 4.08 x 10^7 V/cm.

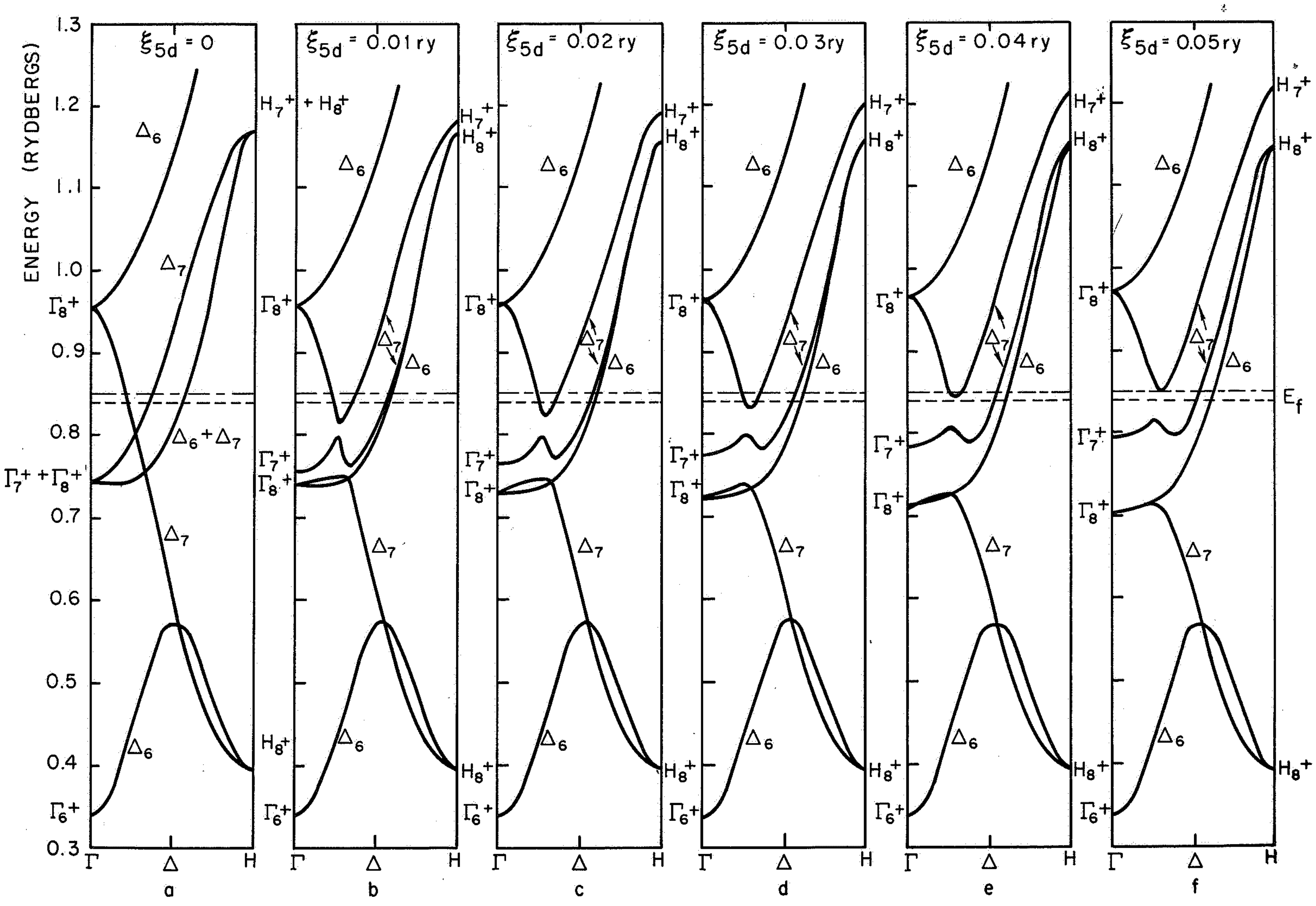

Figure 2. Theoretical plots of the electronic band structure of W along the ⟨100⟩ direction as a function of the spin-orbit parameter ξ_{5d} (see ref. 4).

insufficient to raise the upper Δ_7 band above E_f. A cross section of the Fermi surface in the (100) plane shown in Figure 3 illustrates the consequence of the spin-orbit splitting on the Fermi surface along the $\langle 100 \rangle$ direction ΓH. The dipping of the Δ_7 band below E_f for Mo leads to an electron "lens" along ΓH which has been detected for Mo but not for W[5].

Thus, an investigation of the TED along the $\langle 100 \rangle$ of Mo should exhibit definite structure owing to the band gap near E_f. Such a result assumes that bulk band structure is not significantly altered by the presence of the physical surface.

THEORETICAL CONSIDERATIONS

For the strictly Sommerfeld model upon which the Fowler-Nordheim (FN) theory of field emission is based, the current density per unit total energy $J(\epsilon)$ (where ϵ is the energy relative to the Fermi energy E_f) is given by:

$$J(\epsilon) = J_o e^{\epsilon/d} / d\,(1 + e^{\epsilon/pd}) \ , \tag{1}$$

where $p = kT/d$ and J_o is the total current density at $0^{\circ}K$. As shown elsewhere,[1] the difference between the integral current I_p of a retarding potential measurement and the maximum current I_o is related to the collector work function ϕ_c and the tip-to-collector bias voltage V_t as follows:

$$\log\,(I_o - I_p) / I_o = -\phi_c/2.3\,d + V_t/2.3\,d\ , \tag{2}$$

where

$$d = \hbar eF/2\,(2m\phi)^{1/2}t(y). \tag{3}$$

In Equation (3) F is the field strength, ϕ the emitter work function and $t(y)$ is the tabulated image correction term[6] which is a function of the slowly

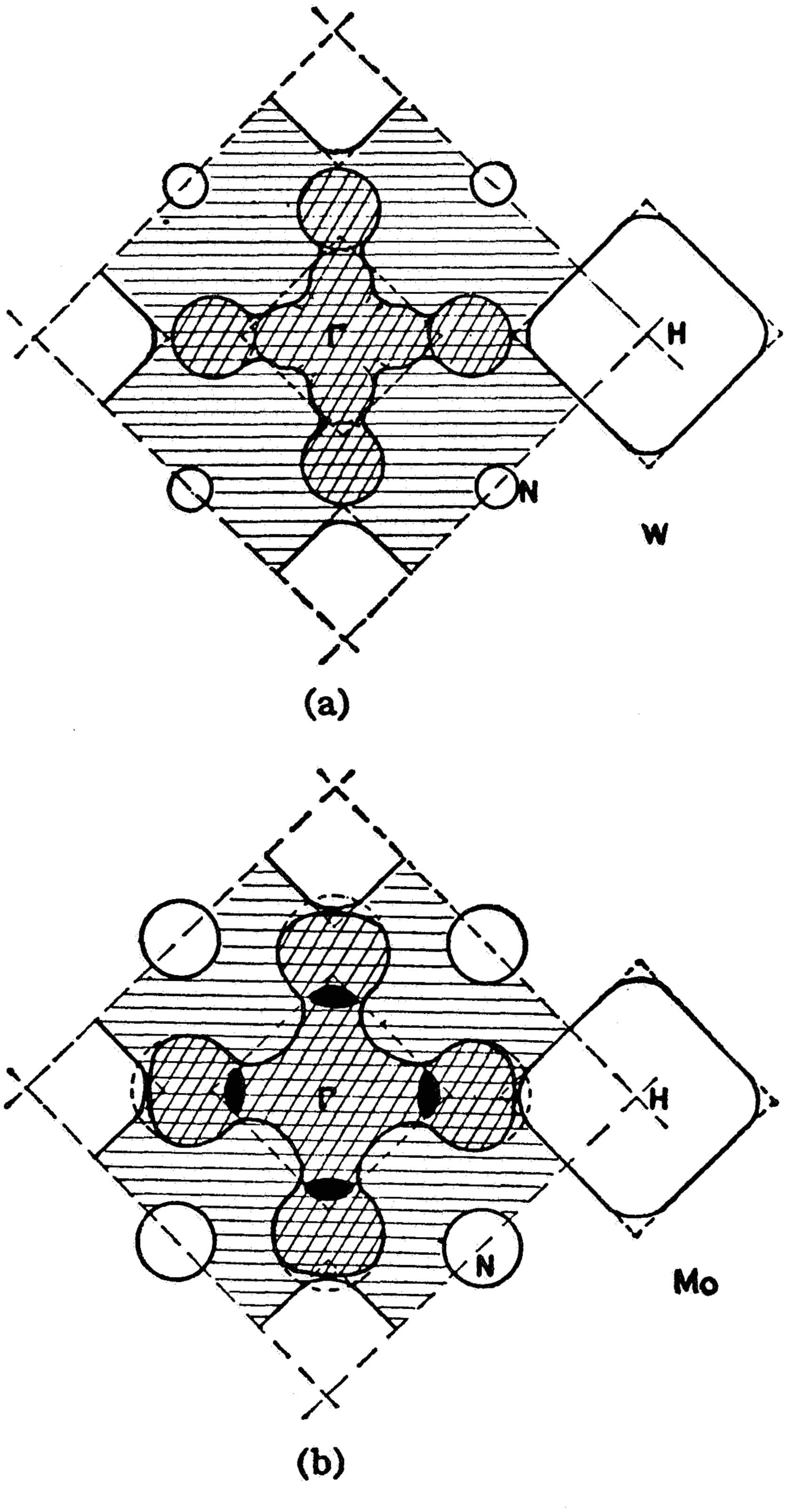

Figure 3. Diagram of the Fermi surface of a (100) section W (a) and Mo (b). The dashed lines represent experimental figures to fit the data, while solid lines are artist's conception. This figure is reproduced from ref. 5.

varying auxilliary variable $y = (e^3F)^{1/2}/\phi$. The values of d and ϕ_c can be obtained respectively from the slope m_e and the intercept of a plot of $\log (I_o - I_t) / I_o$ vs V_t. Experimental values of d so obtained can be compared with that obtained by Equation (3) in order to provide a rough check on the energy distribution theory.

It is further observed that a "Fowler-Nordheim plot" of $\log I_o/V^2$ vs $1/V$ yields a slope m_f which is related to the emitter work function ϕ_f and the geometric factor $\beta = F/V$ as follows:

$$m_f = -2.96 \times 10^7 \phi_f^{3/2} s(y)/\beta \text{ (cm)} , \qquad (4)$$

where s(y) is a slowly varying tabulated function[6] arising from the image potential. The values of ϕ_f relative to a reference value ϕ_o can readily be established as shown by rewriting Equation (4) as follows:

$$\phi_f = \phi_o (m_f/m_{fo})^{2/3} , \qquad (5)$$

where m_{fo} is the FN plot slope for the reference surface and the value β is assumed unchanged. Because of the difficulty in determining accurate values of β, Equation (4) cannot be employed for precise work function calculation. However, as pointed out by Young[7], the expression for m_e and m_f can be combined to give

$$\phi_e = - 3 m_f t(y) / 2 m_e V s(y), \qquad (6)$$

where V is the anode voltage. Accordingly, an accurate value of work function can be ascertained from combined TED and FN measurements.

EXPERIMENTAL PROCEDURE

The experimental energy analyzer tube and procedure has been described in an earlier report.[1] Briefly, the tube designed by van Oostrom[8], is a retarding potential analyzer equipped with magnetic deflection to align emission from a particular direction with a small aperture in the anode plate.

The alignment of a specified crystal direction along the emitter tip axis was accomplished by zone melting orientation of a molybdenum rod from which the emitter was subsequently formed.

RESULTS

The results of the TED from four different directions of Mo plotted according to Equation (1) are shown in Figure 4. Clearly, these data exhibit the predicted exponential relationship between $I_o - I_p = \Delta I_p$ and V_t. As a further test of the reasonableness of the TED data, values of ϕ_f and ϕ_e were determined according to Equations (4) and (5) and compared in Table I. The results depicted in Table I are average values of two or more runs at different values of the anode potential. No value of ϕ_e for the (111) direction is given because the large deflection angle is known to influence values of m_e.[1] In Table I, M represents the linear magnification obtained from the relation

$$M = (A_p/A_f)^{1/2} \qquad (7)$$

where A_f is the emitting area obtained from the "FN" plot intercept and A_p is the area of the probe aperture.

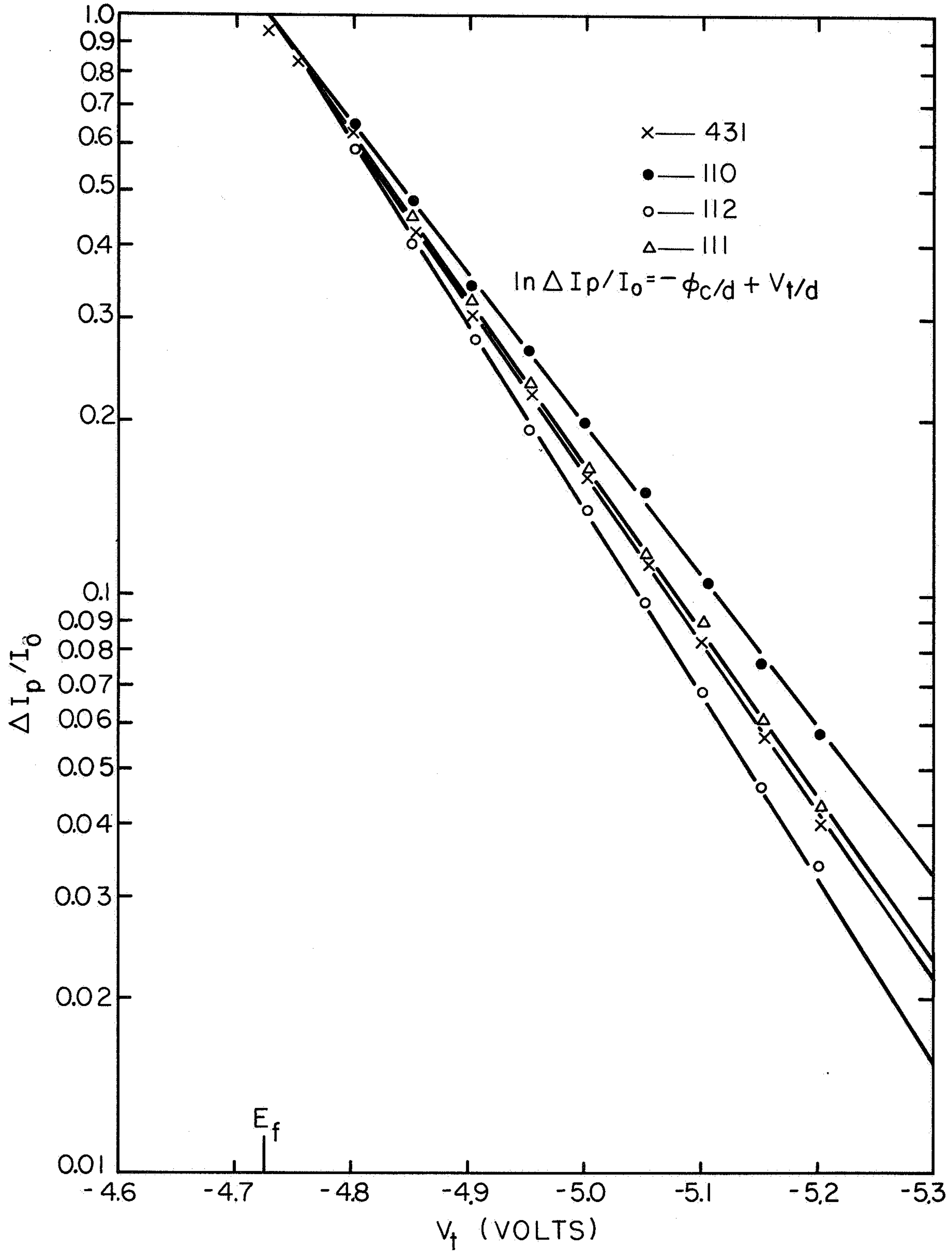

Figure 4. Typical results of retarding plots of the integral field emission current plotted according to Equation (2) from various directions of a clean Mo emitter at 77°K.

TABLE I

Summary of Results from Clean Mo

Plane	ϕ_f^*(eV)	ϕ_e(eV)	M (x10^4)	θ (deg)
(100)	4.35 ± 0.02	---	0.93 ± 0.10	38
(431)	4.02 ± 0.06	4.32 ± 0.14	2.65 ± 0.26	0
(112)	4.51 ± 0.07	4.45 ± 0.07	2.03 ± 0.02	10
(111)	4.00 ± 0.08	---	2.29 ± 0.17	35
(110)	4.81 ± 0.09	5.12 ± 0.16	13.5 ± 4.8	0

* corrected for variations in β with θ

The TED curves for the crystallographic directions shown in Figure 5 were obtained by graphical differentation of the I_p vs V_t curves according to

$$J(\epsilon) = n\, dI_p/dV_t \tag{7}$$

where n is an arbitrary constant of normalization. Calculated half-width values Δ(calc) were obtained from the theoretical curve of Figure 6. The values of d used in Figure 6 to obtain Δ were determined from the slopes of the Figure 4 type plots, since

$$d = -1/m_e \tag{8}$$

The TED data from the $\langle 100 \rangle$ direction would not obey Equation (2). Upon obtaining the differentiated curves shown in Figure 7 the cause of the unreasonable values of ϕ_e becomes obvious. Clearly, the Sommerfeld model does not adequately describe the TED along the $\langle 100 \rangle$ direction as a separate peak occurs 0.15 eV below E_f. Figure 7 shows the TED from Mo $\langle 100 \rangle$ as a function of F and Figure 8 illustrates the effect of temperature.

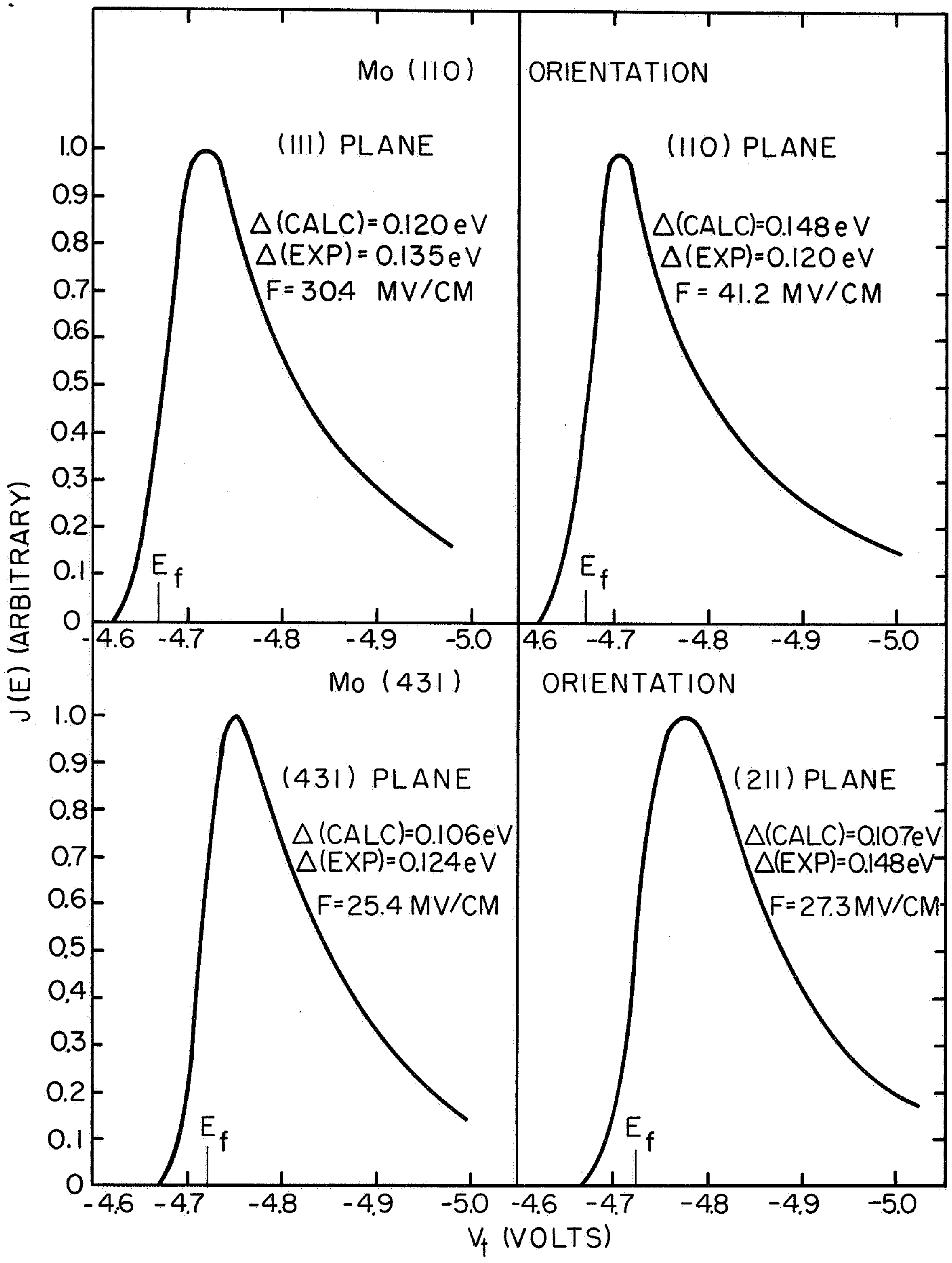

Figure 5. Experimental total energy distribution plots along various directions of a clean Mo emitter at 77°K. Experimental and calculated half-widths are indicated.

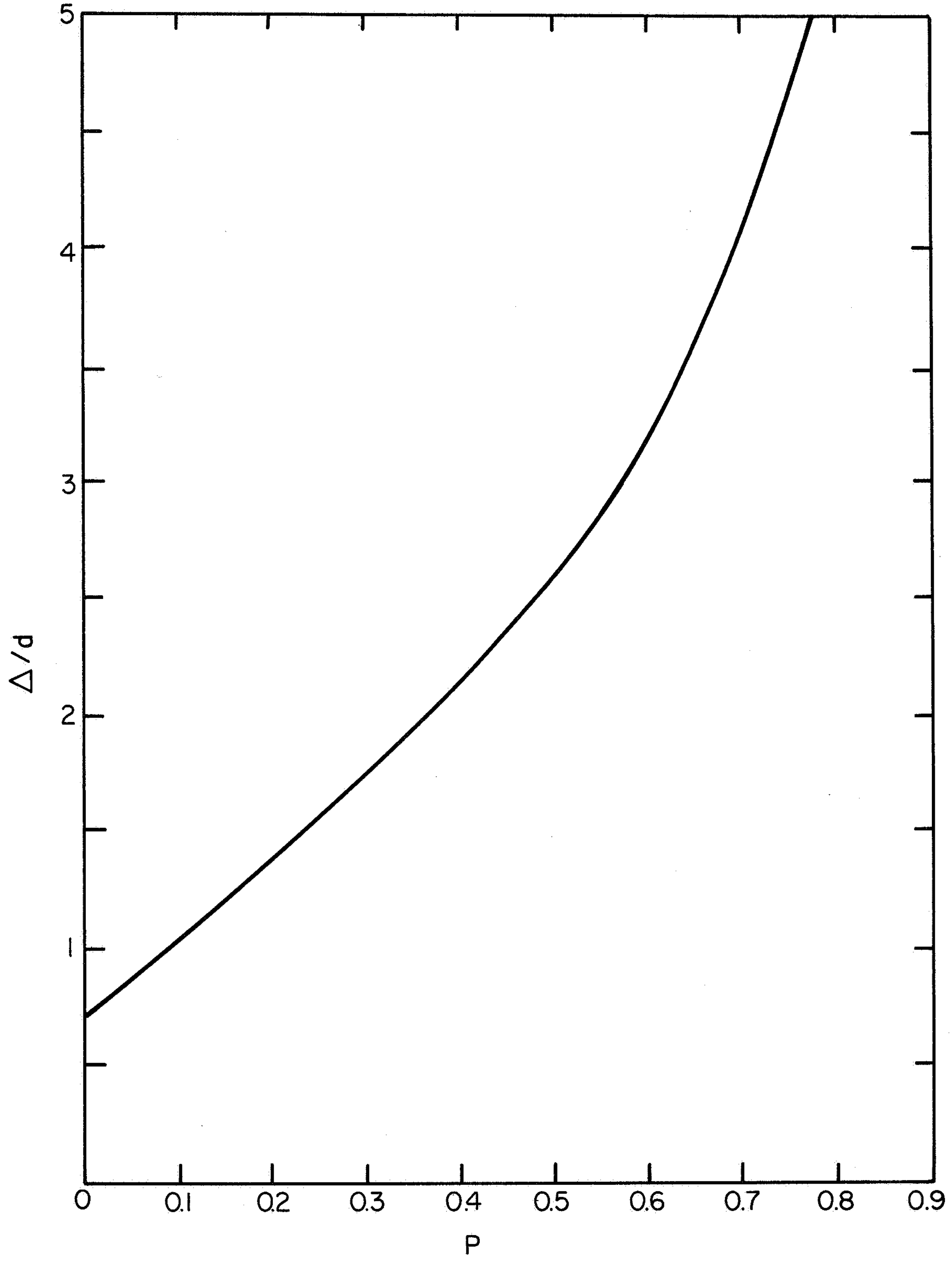

Figure 6. Theoretical plot based on the Sommerfeld model of the variation of half widths of the total energy distribution curves with the parameter p = kT/d.

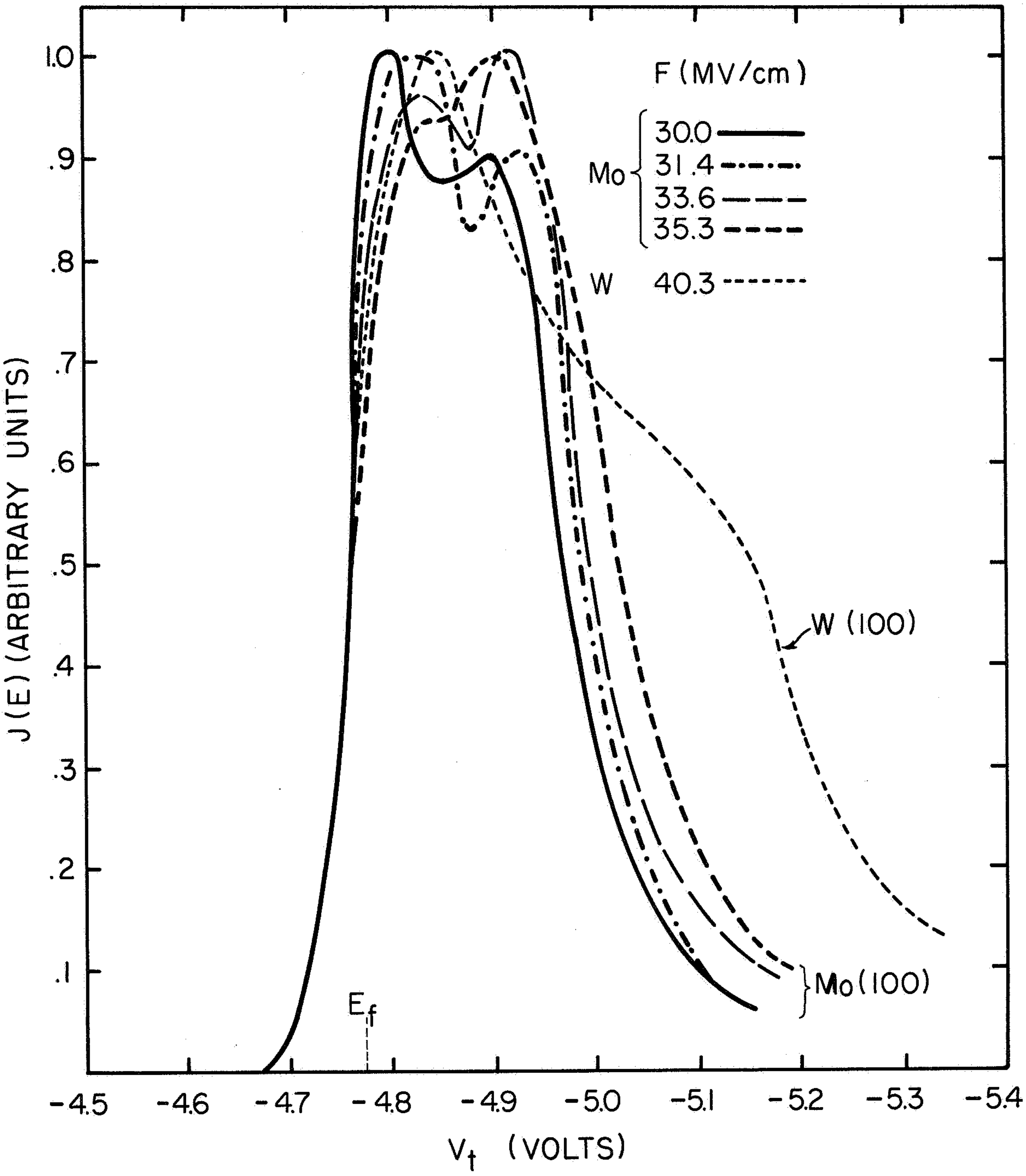

Figure 7. Experimental total energy distribution plots along the ⟨100⟩ direction of clean Mo and W at 77°K.

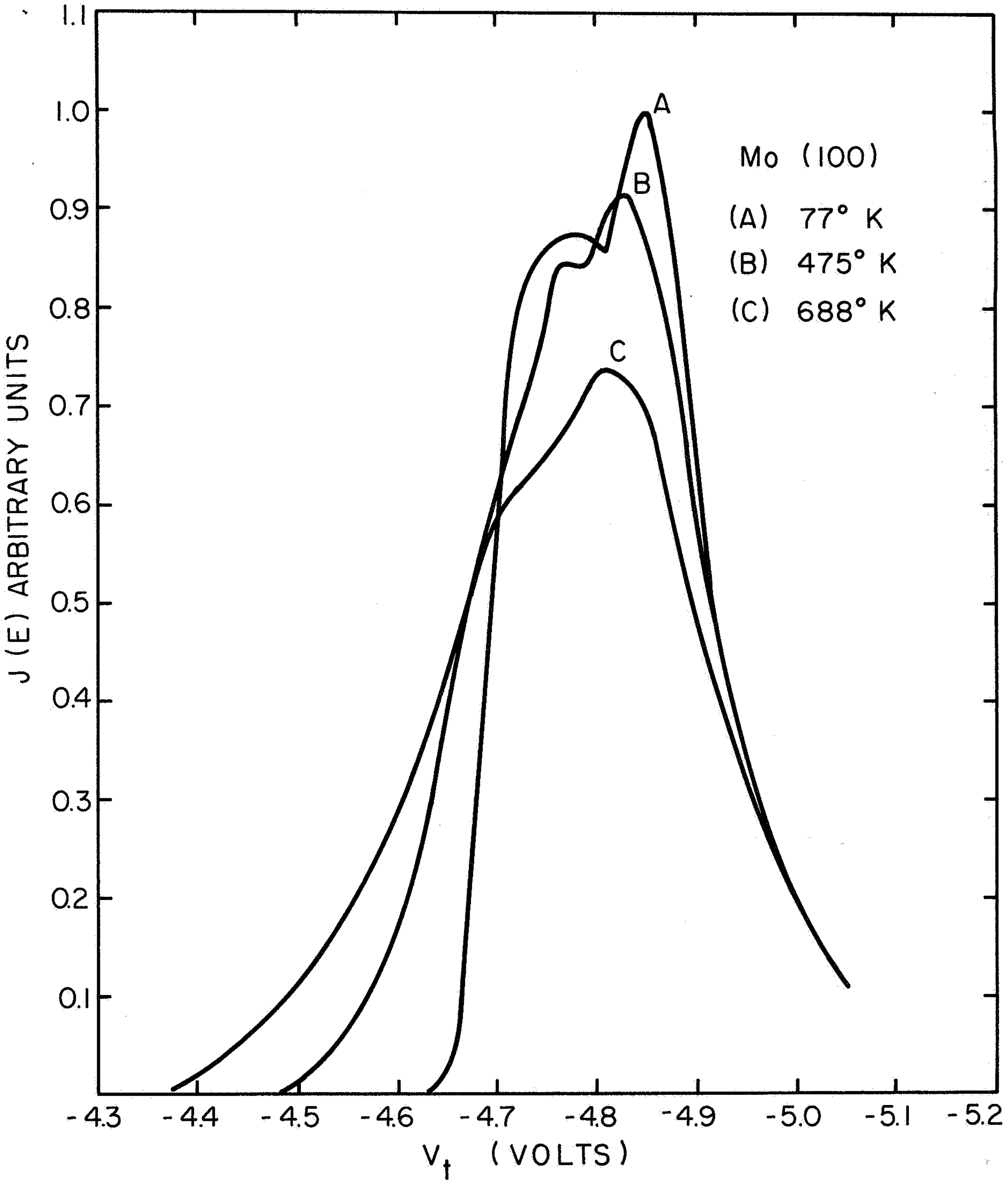

Figure 8. Experimental total energy distribution plots along the ⟨100⟩ direction of clean Mo at the indicated temperatures.

In the former case the largest peak has been normalized to unity while in the latter case the TED's have been normalized to cause the low energy tails to overlap. These results show that increasing the field causes a relative increase in the lower energy peak, while increasing the temperature mainly shifts both peaks to the left and eliminates the distinct valley separating them.

Shown in Figure 9 is the temperature variation of the work function for the $\langle 112 \rangle$, $\langle 100 \rangle$ and $\langle 116 \rangle$ directions of Mo. The calculation of the work function at elevated temperatures by the Fowler-Nordheim equation is outlined in a previous report;[1] there, the experimental values of $d\phi/dT$ for the $\langle 112 \rangle$, $\langle 100 \rangle$ and $\langle 116 \rangle$ directions of tungsten were -14.3, -10.9 and 5.0 ($\times 10^{-5}$ eV/deg.) respectively and were reasonably constant between 77 and 700°K. The molybdenum results agree in sign with the tungsten data, but not in magnitude for the $\langle 112 \rangle$ and $\langle 116 \rangle$. Further, the $\langle 116 \rangle$ of molybdenum exhibits a relationship of the form

$$\phi = 3.95 + 4.5 \times 10^{-10}\, T^{3} \text{ (eV)}, \tag{9}$$

rather than the linear (i.e., $\phi = \phi_o \pm aT$) form observed for tungsten and the other measured directions of molybdenum.

DISCUSSION OF RESULTS

The most striking feature of the reported TED results is the band structure effects noted along the $\langle 100 \rangle$ as shown in Figure 7. This seems to correlate with the theoretical band structure picture of Figure 2 if we attribute the two peaks to electron emission from the upper and lower Δ_7 bands. Superimposed upon the emission is an additional contribution from the Δ_7 band, which crosses the gap, and the hole surface at H. In view of the solid state studies which predict the existence of an electron "lens" along ΓH for Mo, but not for W (see Figure 2), we view the W and Mo (100) TED results as exhibiting amazingly close correlation to the bulk band structure expectations; the existence of the lens is a consequence of the

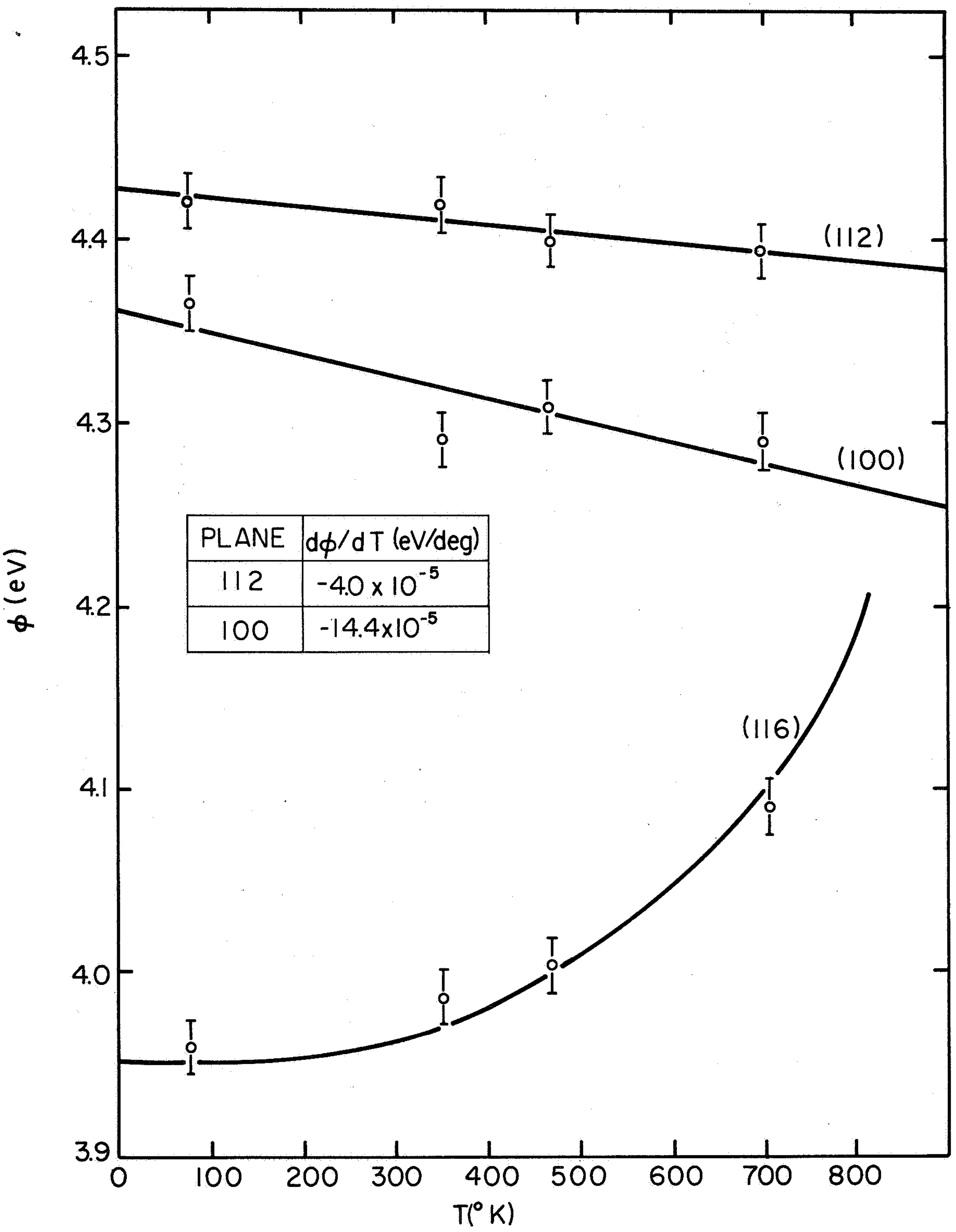

PLANE	$d\phi/dT$ (eV/deg)
112	-4.0×10^{-5}
100	-14.4×10^{-5}

Figure 9. Variation of work function with temperature for the indicated planes of Mo.

Δ_7 band dipping below the Fermi level for Mo which, in turn, leads to the existence of an emission peak near E_f in the Figure 7 results. Also, the peak attributed to the lower portion of the split Δ_7 band is 0.35 and 0.15 eV below E_f for W and Mo respectively according to our results. This is in agreement with the larger spin-orbit splitting expected for W and which accounts for the absence of an electron lens for W along ΓH and the larger band gap.

By arbitrarily normalizing the peaks to unity in Figure 7, we note relatively larger emission from the lower peak as the field strength increases. Although the values of Δ (exp) given in Table III increase as expected with F, they are much larger than Δ (calc). These observations are also in accord with a band gap model in which the relative emission from the lower band increases with F.

TABLE III

Summary of Experimental and Theoretical Half-Widths
of the Mo $\langle 100 \rangle$ TED (see Figure 7)

F (MV/cm)	Δ (exp) (eV)	Δ (calc) (eV)	d (eV)	p
30.0	0.203	0.114	0.133	0.050
31.4	0.219	0.118	0.139	0.048
33.6	0.227	0.125	0.148	0.045
35.3	0.257	0.130	0.156	0.042

A further important consequence of these results is the implication that bulk band structure for metals is not significantly altered in the region of the physical surface from which field emission occurs. Hence, bulk band structure data appears to adequately describe electron emission processes at the surface.

As expected, the TED from other directions of Mo obey Equations (1) and (2) which are based on the Sommerfeld model. This was also the case for W and can be anticipated from the bulk band structure calculations which show relatively large Fermi surfaces and no band crossing near E_f for other major crystallographic directions.[4] Evidence of the adequate description of the TED measurements by the Sommerfeld model is also given by reasonable agreement between ϕ_e and ϕ_f for the $\langle 431 \rangle$, $\langle 112 \rangle$ and $\langle 110 \rangle$ directions. Presumably the $\langle 111 \rangle$ direction also obeys Equation (1) as suggested by the TED results shown in Figure 5, although ϕ_e was not calculated due to electron optical effects on m_e stemming from the large deflection angle.

Of further interest is the good agreement between ϕ_f and thermionic values of work function tabulated in Table IV for Mo. This strengthens the validity of field emission probe work functions and the correction to ϕ_f due to the variation of β with angular deflection.[1]

TABLE IV

Thermionic Values of Mo Work Functions

Plane	ϕ (eV)
(110)	5.10 ± 0.05^a, 4.90 ± 0.07^b
(111)	4.15 ± 0.05^a
(100)	4.35 ± 0.07^b
(112)	4.53 ± 0.10^c

(a) U. V. Azizov, et al., Soviet Physics - Solid State 7, 2232 (1966).

(b) E. M. Savitskii, et al., Soviet Physics - Technical Physics 11, 974 (1967).

(c) E. A. Coomes and W. L. Girard, Thermionic Specialists Conference, San Diego, California (1965).

A notable feature of the Table I results is the close agreement between ϕ_f and ϕ_e for the $\langle 110 \rangle$ direction of Mo. Such agreement is lacking for W[1,7] and has been the subject of much speculation as to its cause.[2,3] The relatively large value of M for the $\langle 110 \rangle$ of Mo given in Table I is evidence that complete agreement with the classical Fowler-Nordheim model may be lacking for Mo along the $\langle 110 \rangle$. Examination of the Fermi surface of Mo (see Figure 3) shows a hole surface at N that is twice as large as corresponding ones for W. The extent to which the hole surface at N affects the emission along the $\langle 110 \rangle$ must await further theoretical evaluation.

Finally, the temperature dependence of the work function may be partly due to band structure effects as was discussed in an earlier report.[1] The cube law dependence of ϕ on temperature for the $\langle 116 \rangle$ agrees with a Young's[9] formulation of Gelberg's[10] thermionic data on the temperature coefficient of polycrystalline Mo. Because the (116) is a low ϕ plane the polycrystalline results should be weighted heavily by the (116) planes; thus we conclude our measurements of the temperature coefficient of the (116) work function are supported by Gelberg's data. Further theoretical studies of the origin of the different temperature coefficients of ϕ from different crystallographic directions are needed.

REFERENCES

1. L. W. Swanson, et al., Final Report, Contract NASw-1082, (Field Emission Corporation, McMinnville, Oregon, Nov. 1966).
2. R. D. Young and H. E. Clark, Phys. Rev. Letters 17, 351 (1966).
3. R. D. Young, 14th Annual Field Emission Symposium, National Bureau of Standards, (1967).
4. L. F. Mattheiss, Phys. Rev. 139, 1893 (1965).
5. D. M. Sparlin and J. A. Marcus, Phys. Rev. 144, 484 (1966).
6. R. H. Good and E. W. Müller, Handbuch der Physik 21, 176 (1956).
7. R. D. Young and H. E. Clark, Appl. Phys. Letters 9, 265 (1966).
8. A. van Oostrom, Philips Res. Rept. Supplement, (Netherlands) No. 11, 102 (1966).
9. R. D. Young and E. W. Müller, J. Appl. Phys. 33, 91 (1962).
10. A. Gel'berg, et al., Radiotekn. i Electron. 3, 1000 (1958).

LIST OF ILLUSTRATIONS

SECTION V

VI. THE EFFECT OF ADSORBED CESIUM ON THE TOTAL ENERGY DISTRIBUTION OF FIELD EMITTED ELECTRONS

INTRODUCTION

One of the motivations for total energy distribution (TED) measurements of adsorbate-coated substrates stems from the possibility that the interaction potential of the adsorbate may alter the transmission probability and, hence, the TED. This expectation has been given a theoretical basis by Duke and Alferieff[1] (D and A), who treated field emission through adsorbed atoms by an atomistic one-dimensional psuedo-potential model. In the case of metallic adsorption, their results predict an increase in transmission apart from the usual work function lowering. This approach is in contrast to other treatments which assume the adsorbed layer modifies the Fowler-Nordheim equation either through the work function term[2] or the image potential term.[3] In each of these cases including the D and A theory a change in both the pre-exponential and exponential terms of the Fowler-Nordheim (FN) equation is predicted. The D and A theory is unique in that it also predicts an additional hump or shoulder on the total energy distribution in the case of metallic adsorption when the valence level of the adsorbate falls below the substrate Fermi level.

In this section we describe preliminary results of the influence of adsorbed cesium layers on the total energy distribution and emission characteristics and we further attempt to ascertain the appropriate theoretical description of the effect of adsorbed layers.

EXPERIMENTAL METHOD

The experimental approach and procedures were similar to those outlined in Section V. Both molybdenum and tungsten substrates were employed in this investigation. Attention was mainly given to those planes perpendicular to the wire axis owing to the slight alteration of the TED's when magnetic deflection was employed. Zone-oriented wire was employed to fabricate tips with the desired crystal direction along the wire axis.

Deposition of cesium onto the substrate was accomplished by resistively heating to $\sim 1100^{\circ}$K a small bead of cesium zeolite fused onto a platinum wire.[4] This method has proven to give a pure flux of cesium ions which can be focused onto the emitter. The results on the tungsten (110) plane reported herein were plagued with some oxygen contamination due to the fact that an oxygen source was incorporated into the tube for previous coadsorption studies. For the molybdenum results reported in this study the cesium adsorbate appeared to be pure as judged by the pattern sequences and the absence of oxygen traces after thermal desorption of the cesium layers.

RESULTS AND DISCUSSION

In the results reported herein we have examined the energy distributions and current voltage I(V) data from various planes of molybdenum and tungsten coated with cesium. The I(V) data has been analyzed according to the well-known Fowler-Nordheim equation as described in Section II, Equation (1-6). Of primary interest is the quantity B, which is the logarithm of the ratio of the adsorbate coated to clean Fowler-Nordheim equation pre-exponential. Also average $\overline{\phi}_f$ or single plane ϕ_f work functions can be calculated according to Equation (5) of Section II provided a reference work function value is chosen. The retarding potential analysis of the current from various planes has been analyzed by Equations (2) and (5) of Section V so that Fowler-Nordheim work functions ϕ_f and assumption-free values of work function ϕ_e could be determined.

An investigation of the effect of Cs on the TED from the $\langle 110 \rangle$, $\langle 112 \rangle$ and $\langle 100 \rangle$ planes of Mo has been initiated with preliminary results reported here. Results obtained for Mo $\langle 110 \rangle$ are given in Table I, along with comparison between ϕ_e and ϕ_f at different values of Cs coverage. The total surface average work function $\overline{\phi}$ is also given along with the ratio of the apparent emitting area A_f to the clean value A_o. The coverage range is approximately 0.15 to 0.20 monolayer. Figures 1 and 2 show the differentiated curves for

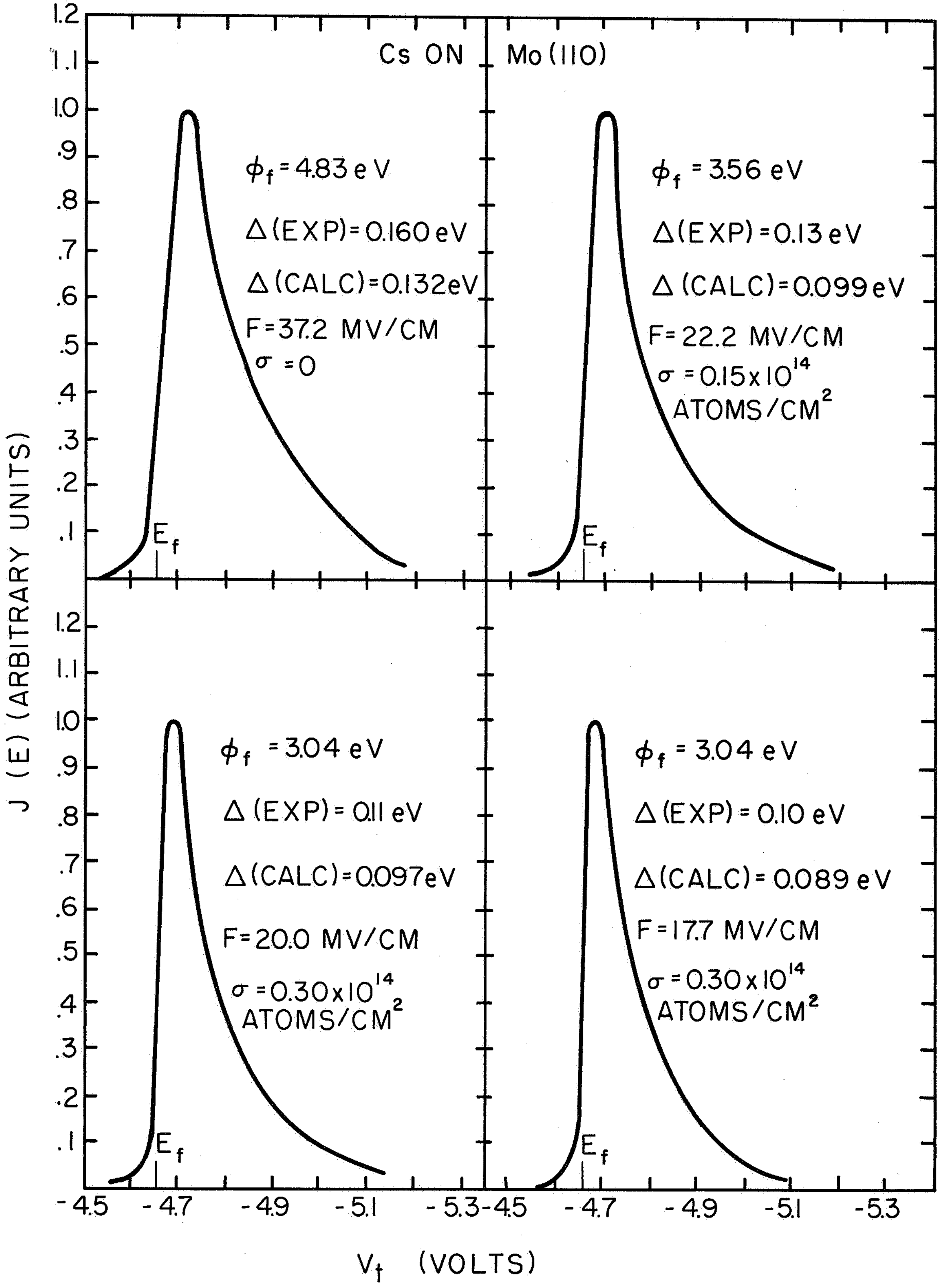

Figure 1. Experimental total energy distribution plots along the ⟨110⟩ direction of Mo at 77°K as a function of Cs coverage and applied field strengths.

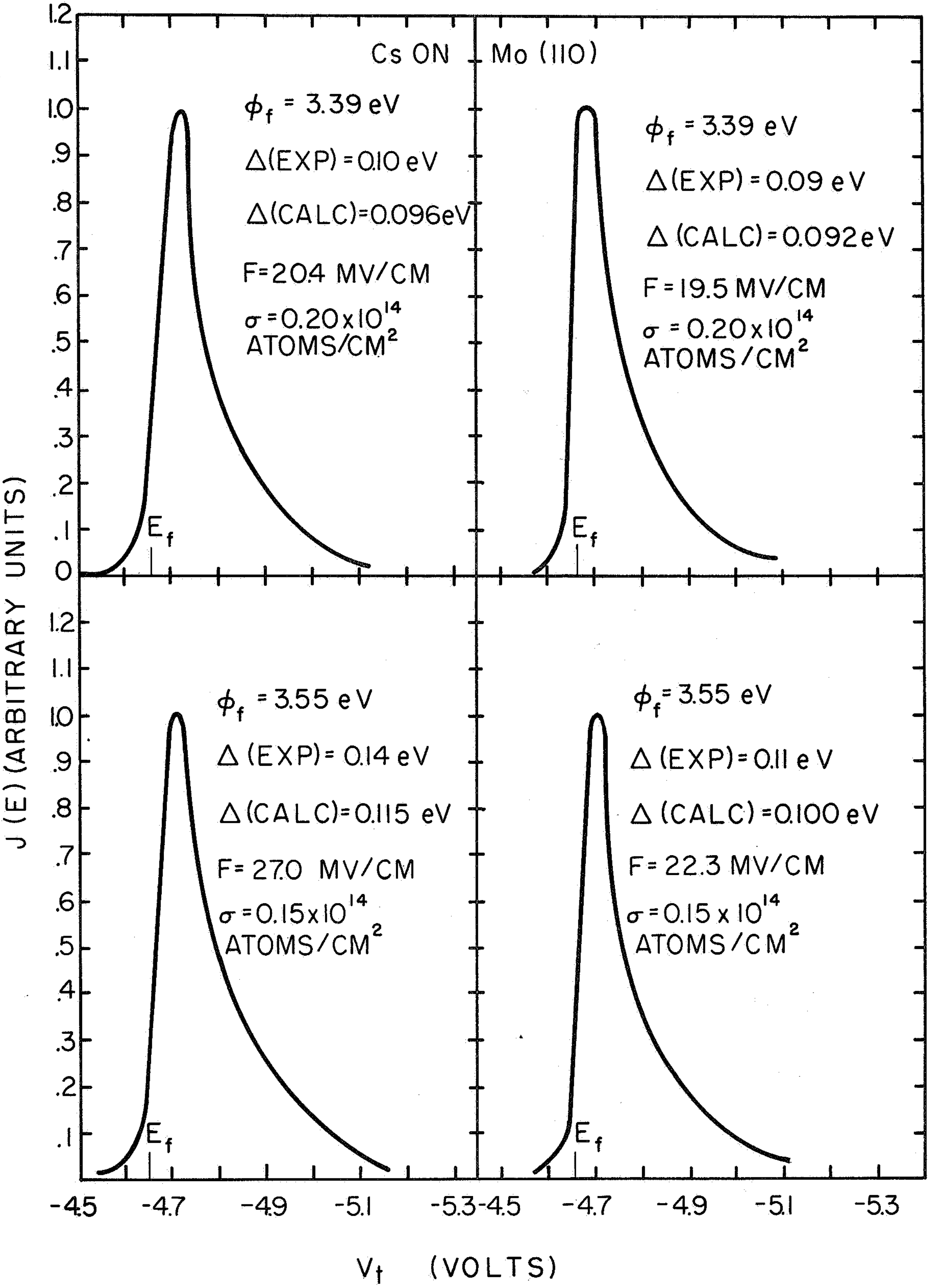

Figure 2. Experimental total energy distribution plots along the ⟨110⟩ direction of Mo at 77^{o}K as a function of Cs coverage and applied field strengths.

the ⟨110⟩ direction along with the calculated and experimental values of half-width Δ. These curves show the effect on the TED of the applied field strength, obtained through varying the anode voltage V, and the Cs coverage. Plots of the integral current according to Equation (2) of Section V are given in Figure 3 at various Cs coverages for the ⟨110⟩ direction.

TABLE I

Summary of Results for Cs on Mo (110)

$\bar{\phi}$ (eV)	ϕ_f (eV)	ϕ_e (eV)	log A_f/A_o	B
4.20	4.81	5.12	0	0
3.34	3.56	3.97	1.05	-1.672
3.17	3.55	3.91	0.91	-0.316
3.22	3.39	3.76	1.15	-2.636
2.85	3.04	3.35	1.22	-1.577

In our initial studies of the Mo ⟨110⟩ reported here TED measurements were performed with Cs coverages such that the work function approximately equaled the adsorbate ionization potential; this allows the adsorbate valence level to coincide roughly with the Fermi level which in turn leads to the greatest emission enhancement according to D and A.[1] The results of the TED measurements given in Figures 1-3 for Cs on Mo ⟨110⟩ show no major discrepancy from the FN model. The slightly larger values of Δ (exp) may be attributed to resolution limitations of the analyzer. Interestingly, the values of ϕ_e continues to be 0.4 eV larger than ϕ_f not only for clean Mo ⟨110⟩, but throughout the coverage range of Cs. It is worth pointing out that the ⟨110⟩ work function in this coverage range is comparable with the nearby surrounding planes, hence, patch field corrections[5] should be of little consequence.

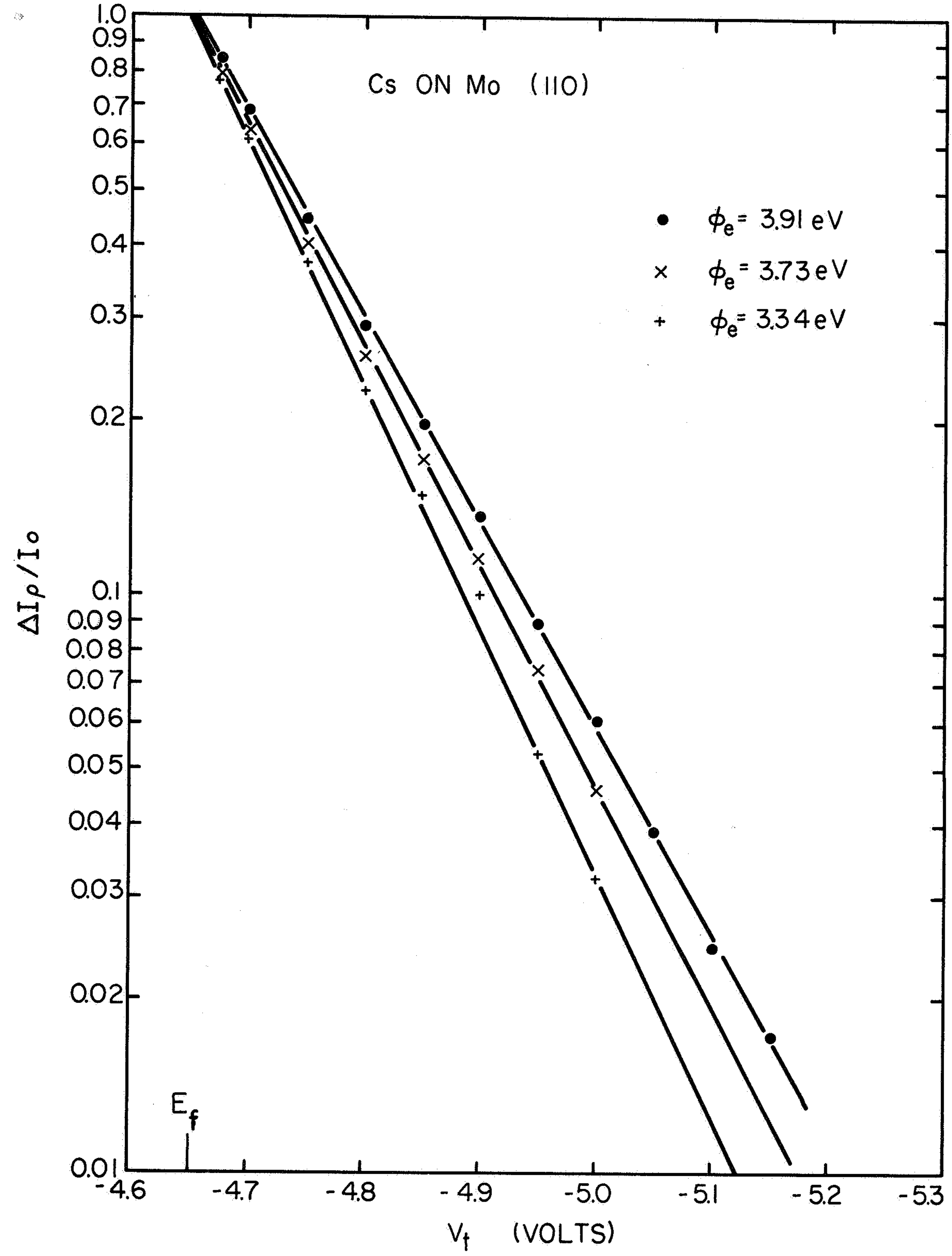

Figure 3. Typical results of retarding plots of the integral field emission current plotted according to Equation (2) of Section V. The data is from the ⟨110⟩ direction of a cesiated Mo emitter at 77°K. The data is from the ⟨110⟩ direction of a cesiated Mo emitter at 77°K.

Table II gives results similar to Table I for the $\langle 112 \rangle$ and $\langle 100 \rangle$ directions of Mo. The beam deflection required for the $\langle 112 \rangle$ results was sufficiently large to perturb the TED results, hence only the TED results for the $\langle 100 \rangle$ direction are given in Figure 4. The relative reduction in the lower energy peak can be attributed to the much lower field strength required for the low work function surface. As noted in Section V, lower field strengths favor stronger emission from the upper Δ_7 band (see Figure 7 of Section V). The fact that modifications to the $\langle 100 \rangle$ TED can be reasonably accounted for by the external changes in work function and applied field provides further evidence that the double peaks are due to bulk rather than surface phenomenon.

TABLE II

Summary of Results for Cs on the (112) and (100) Planes of Mo.

Mo $\langle 112 \rangle$

$\bar{\phi}$ (eV)	ϕ_f (eV)	log A_f/A_o	B
4.33	4.20	0	0
3.98	3.80	-1.225	-0.745
2.74	2.80	-2.665	-1.933
2.00	2.06	-0.556	0.769
1.86	2.06	-0.978	0.488
1.92	1.86	-0.662	0.745

Mo $\langle 100 \rangle$

$\bar{\phi}$ (eV)	ϕ_f (eV)	log A_f/A_o	B
4.41	4.20	0	0
4.24	3.80	-0.566	-0.483
1.95	2.06	-5.272	-3.878
1.65	2.06	-6.436	-4.748
1.86	1.66	-5.894	-4.178

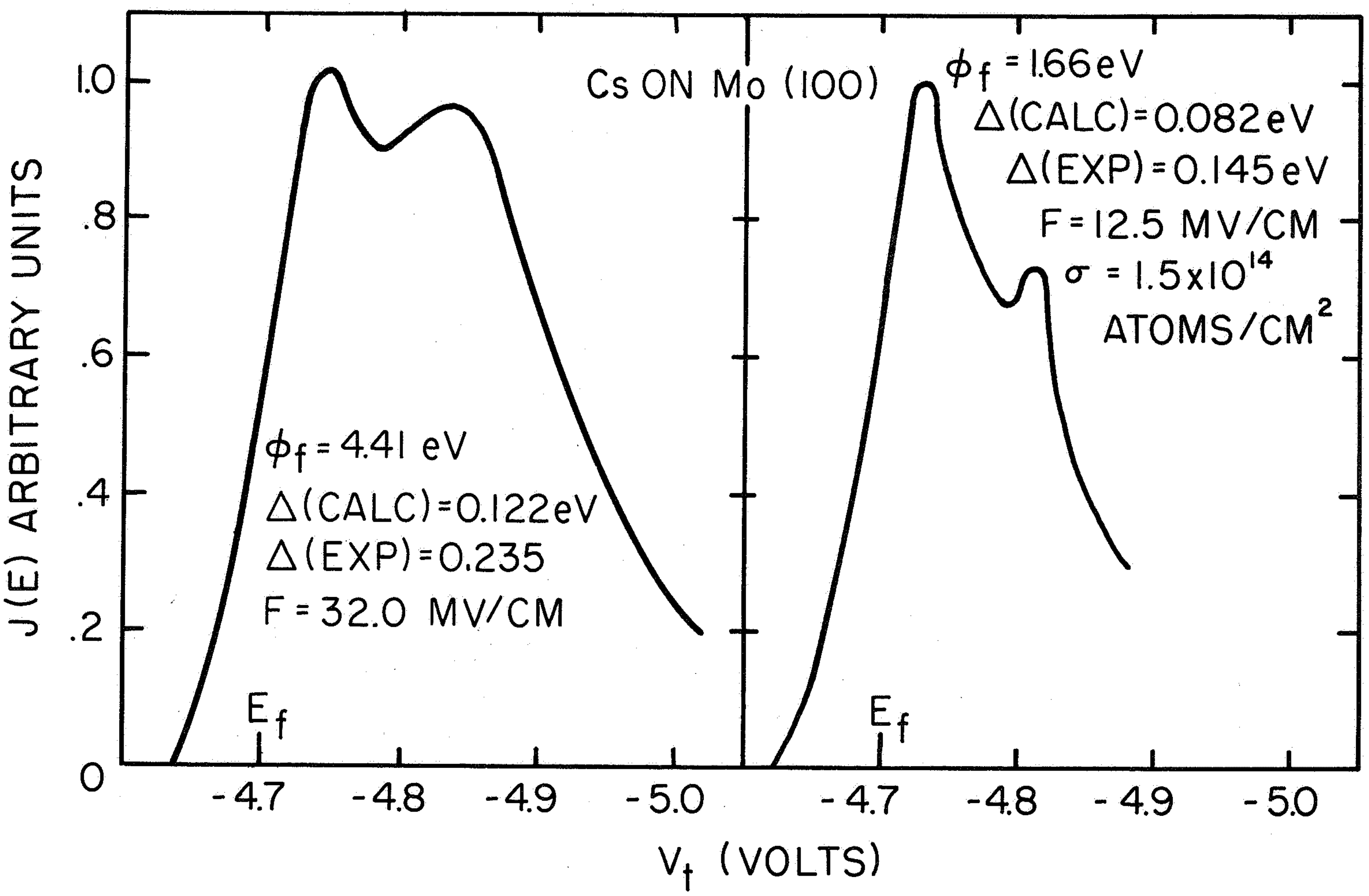

Figure 4. Experimental total energy distribution plots along the ⟨100⟩ direction of Mo at 77°K as a function of Cs coverage.

The effect of Cs on the TED and I(V) characteristics for the ⟨110⟩ direction of W is shown in Figures 5 and 6 plus Table III. Although the experimental half-widths are somewhat larger than theory throughout the coverage range, no peaks or strong deviations from the exponential decrease in J(E) can be observed. [illegible] ([illegible]) [illegible] be observed. The discrepancy between Δ (exp) and Δ (calc) is probably real and may stem from bulk properties inasmuch as it occurs with clean W.

TABLE III

Summary of Results for Cs on the (110) Plane of W.

σ (x 10^{14} atoms/cm^2)	ϕ_f (eV)	log A_f/A_o	B
0	5.82	0	0
0.52	3.79	-0.041	0.571
1.37	1.76	-3.003	-1.008
1.39	1.73	-0.875	1.158
1.62	1.52	-0.996	1.308
2.35	1.67	-1.004	1.104
2.50	1.84	-1.045	0.864
2.56	1.96	-1.571	0.199
2.62	2.05	-1.696	-0.006
2.70	2.22	-1.170	0.418

If all changes in the intercept of the FN plots are accountable by the FN theory, the value of log A_f/A_o, which is calculated according to the method described elsewhere[6], should be zero. Thus, we see from Tables 1-3 that log A_f/A_o varies from +1, at low coverages on the (110) of Mo to -6 for the (100) plane of Mo. Except for the (100) of Mo, the values of log A_f/A_o are slightly negative throughout most of the coverage range.

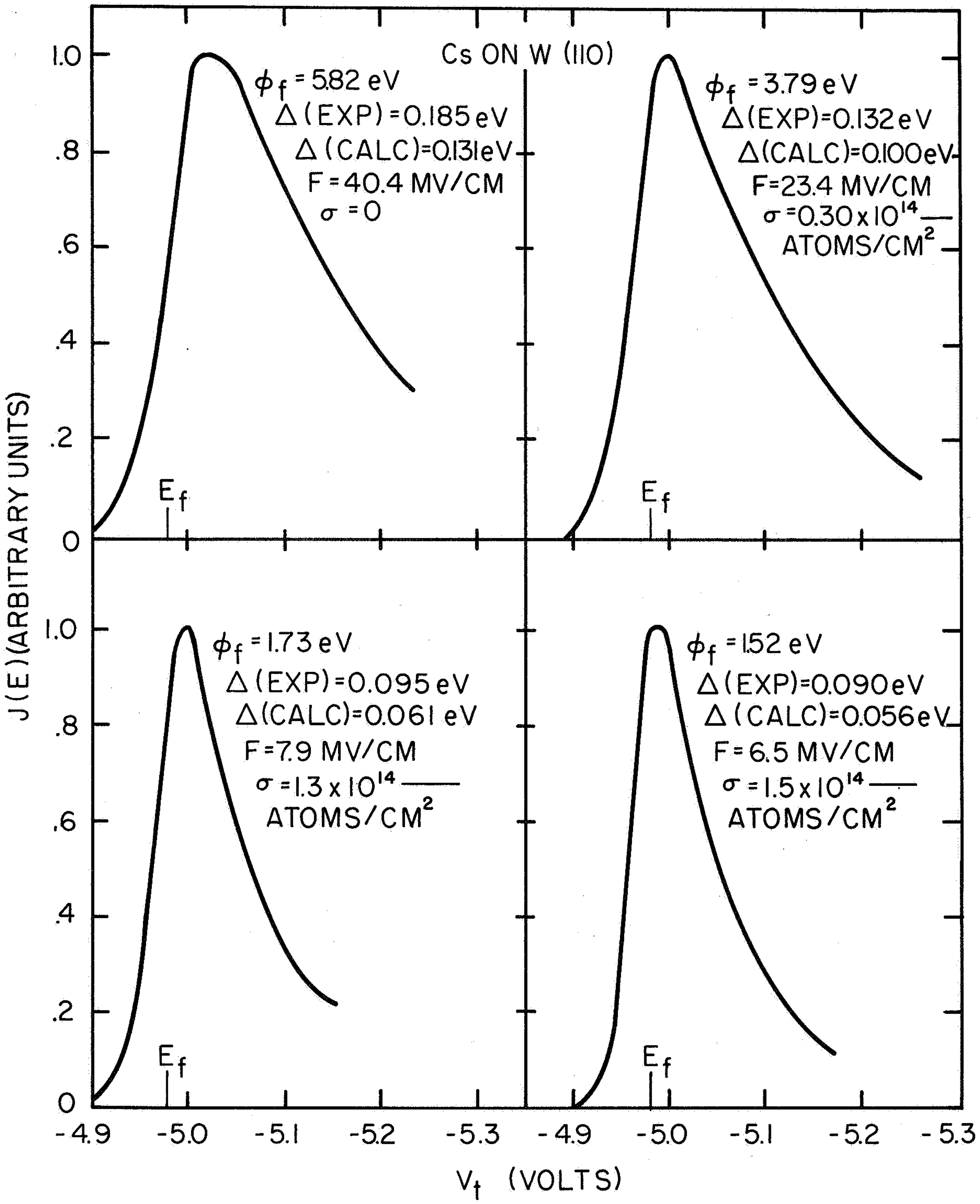

Figure 5. Experimental total energy distribution plots along the ⟨110⟩ direction of W at 77°K as a function of Cs coverage and applied field strengths.

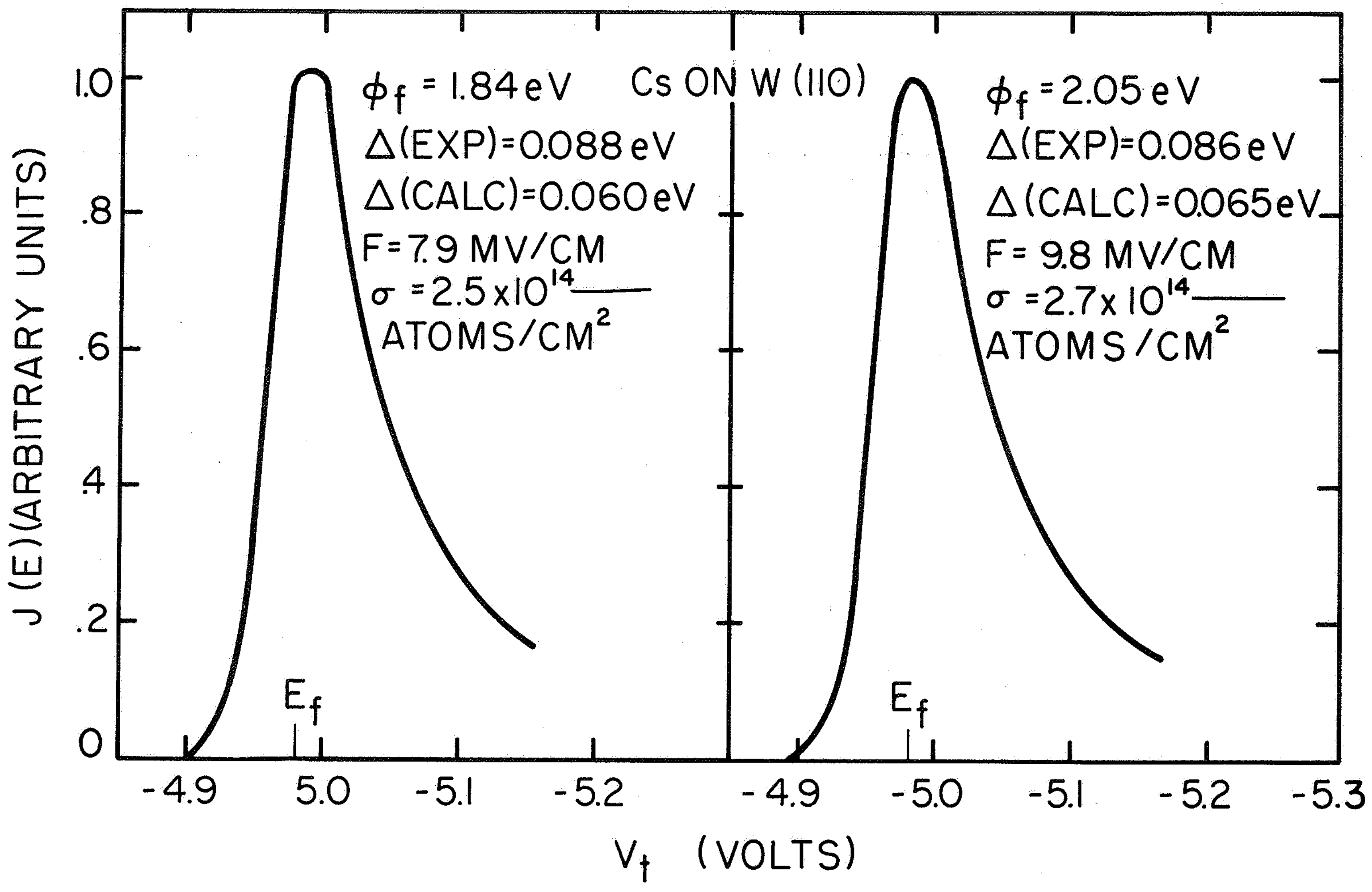

Figure 6. Experimental total energy distribution plots along the ⟨110⟩ direction of W at 77°K as a function of Cs coverage and applied field strengths.

If the deviations in log A_f/A_o from 0 are ascribed to polarization of the adlayer by the applied field, then[2]

$$\log A_f/A_o = -26.4 \times 10^7 \phi^{1/2} \pi \alpha \sigma, \qquad (1)$$

where α is the adatom polarizability in cm^3 and σ the coverage in atoms/cm^2. This formulation of the polarization effect cannot account for the small positive values of log A_f/A_o observed for the Mo $\langle 110 \rangle$ results. On the other hand, values of α calculated by Equation (1) for the Mo $\langle 112 \rangle$ and W $\langle 110 \rangle$ results are in the reasonable range 5 to 20 A^3. The large negative values of log A_f/A_o for the Mo $\langle 100 \rangle$ direction lead to excessively large values of α, thereby suggesting that the polarization model is inadequate for this plane.

CONCLUSIONS

Except for the low coverage Mo $\langle 110 \rangle$ results, enhancement of the emission as predicted by the D and A theory for metallic adsorption is not observed in these results. In fact, all other directions show a decrease in the log A_f term. In addition, no obvious alterations of the TED curves are observed throughout the coverage range of Cs. It thus appears that the D and A theory does not adequately describe the emission changes due to metallic adsorption. The polarization model gives sensible results except at low coverages and on the $\langle 100 \rangle$ plane of Mo. The latter may be due in part to the serious deviation from the FN model along the $\langle 100 \rangle$ direction.

It is clear that results from other adsorbates would be desirable before a final conclusion as to the relative merits of the D and A theory or the polarization model can be made. Combining TED and I(V) data from single crystal plane adsorption appears to be a promising approach to follow in order to test various theoretical descriptions of the field emission process through adsorbed layers.

REFERENCES

1. C. B. Duke and M. E. Alferieff, J. Chem. Phys. 46, 923 (1967).
2. L. Schmidt and R. Gomer, J. Chem. Phys. 42, 3573 (1965).
3. A van Oostrom, Philips Res. Rept. Supplement, (Netherlands) No. 11, 102 (1966).
4. R. E. Weber and L. F. Cordes, Proceedings of the 25th Annual Conference on Physical Electronics, (Massachusetts Institute of Technology, Cambridge,Mass. , 1965) p. 378.
5. R. D. Young and H. E. Clark, Phys. Rev. Letters 17, 351 (1966).
6. F. M. Charbonnier and E. E. Martin, J. Appl. Appl. Phys. 33, 1897 (1962).

LIST OF ILLUSTRATIONS

SECTION VI

FINAL DISTRIBUTION LIST

Contract NASw 1516

NASA Headquarters Washington, D. C. 20546	
Attn: Dr. R. R. Nash - Code RRM	4
G. Pfannebecker - Code RNT	1
T. Tsacoumis - Code REG	1
Scientific and Technical Information Facility Attn: NASA Representative Post Office Box 5700 Bethesda, Maryland 20014	2
NASA Lewis Research Center Cleveland, Ohio 44135	
Attn: Dr. R. Breitweiser, Section 2131	1
Dr. R. A. Lad, Section 2330	1
J. Ferrante, Section 9711	1
D. L. Lockwood, Section 9711	1
Dr. J. F. Morris, Section 1951	1
Dr. H. Schwartz, Section 9213	1
Dr. L. Tower, Section 2132	1
NASA Marshall Space Flight Center Huntsville, Alabama Attn: Dr. I. Dalins, Code R-RP-N	1
NASA Electronic Research Center Cambridge, Massachusetts Attn: Dr. M. S. Macrakis, Code CT	1
U.S. Naval Ordnance Test Station Physics Division, Michaelson Laboratory China Lake, California 93556 Attn: Dr. E. Bower, Head Crystal Physics Branch	1

National Bureau of Standards
Atomic Physics Division
Washington, D. C. 20546
Attn: Dr. R. D. Young
Electron Physics Section 1

Professor Robert Gomer
Institute for the Study of Metals
University of Chicago
Chicago, Illinois 60637 1

Professor W. L. Boeck
Department of Physics
Niagara University
Niagara University, New York 14109 1

U. S. Atomic Energy Commission
Division of Research
Washington, D. C. 20546
Attn: Dr. A. R. Van Dyken
Director for Chemical Programs 1